ENCODING OF MOTOR BEHAVIORS BY CORTICAL NEURONAL NETWORKS

by

Ryan J. Smith

A dissertation submitted to The Johns Hopkins University in conformity with the requirements for the degree of Doctor of Philosophy.

Baltimore, Maryland

February, 2016

Abstract

Performance of motor behavior requires complex coordination of neural activity across diverse regions of cortex at multiples scales. At the level of coordination across large areas of cortex, this activity is thought to be related to similarly broad concepts of movement from goal identification to motor planning to generation of motor commands. At smaller scales on the level of local populations of individual neurons in motor and premotor cortex, we observe complex non-stationary firing patterns that appear to be related to the movement itself. Our understanding of the details of this relationship are incomplete, however. Earlier work by the community largely focused on the analysis of individual units in isolation. Technological advances and changes in experimental paradigms have led to the simultaneous recording of hundreds of neurons simultaneously. Approaches to analysis must also adapt and embrace a shift in focus from the behavior of individual neurons to the interactions of the population as a whole.

This work presents a number of techniques developed to address challenges and opportunities associated with the simultaneous recordings of large populations of neu-

ABSTRACT

rons. The first part of this thesis demonstrates that information related to reaching and grasping is encoded dynamically within an ensemble of neurons in the motor and premotor cortices. Second, a semi-supervised approach is developed to identify co-modulated communities of neurons within the population ensemble for use in motor decoding and broader exploratory analysis. Finally, this work details a model for representing task-relevant information encoded in the structure of task-specific networks formed by functionally connected networks of neurons. This work makes several significant contributions to understanding and modeling the interactions of ensembles of neurons during the performance of motor behaviors and represents important steps toward better utilizing a growing number of simultaneously recorded neurons.

Primary Reader: Dr. Nitish V. Thakor, Ph.D.

Secondary Reader: Dr. Alcimar B. Soares, Ph.D.

Acknowledgments

I would like to thank my advisor and other members of my thesis committee. My advisor, Nitish Thakor, gave me the freedom to pursue my many academic and non-academic interests and had the patience to support me through my development over my many years in his lab. Alcimar Soares served as my unofficial co-advisor and I am grateful to him for his mentorship and friendship. This work simply would not be possible without the work of Marc Schieber and his many students at the University of Rochester who have put in untold hours performing the experiments and data collection that enable the analysis and exploration contained within this document. Sri Sarma provided me with my first introduction to point processes and also served as a valuable source of feedback and inspiration on approaches to analysis.

My time in Dr. Thakor's lab has afforded me the opportunity to interact with many talented individuals who all contributed immensely to my development over the years as well as provided much needed companionship. When I first joined the lab, a number of senior lab members both paved the way for this present work and also served as peer mentors. Among these labmates, I would particularly like to acknowl-

edge Soumyadipta Acharya, Vikram Aggarwal, Mohsen Mollazadeh, and Francesco Tenore. Then there are those members of the lab I view as my contemporaries, friends, and comrades-in-arms: Heather Benz, Matt Fifer, Guy Hotson, Geoffrey Newman, Kyle Rupp, and Rezina Siddique. I thank them all for their friendship, support, and thoughtful insight these many years. Many other lab members still are deserving thanks and I am grateful for the opportunity to have known and worked with them. Thank you all.

I must also thank my incredible family. I am fortunate to be a part of a family who places such great value upon education. My parents' own academic achievements were the source of my initial aspirations for higher education and it was their unwavering support and belief in me that enabled me to pursue those dreams. My closest companion, and partner, Jessi, was there by my side throughout my entire time at Johns Hopkins and supported me throughout the ordeal while enduring second-hand many of my stresses and frustrations. And though they may never read this, I would also like to thank my dogs Loki and Puca for reminding me daily that there is more to life than work.

Finally, I would like to thank: the kind administrators and staff at Johns Hopkins University, those brave students who tolerated my mentorship, the Baltimore civic hacking community, and countless others who have contributed to my personal and professional development these past years.

Dedication

This thesis is dedicated to my grandparents, William J. Smith and Cecile Smith.

Contents

List of Tables

List of Figures

Chapter 1

Overview

Cortical neurons in motor-related regions of the brain coordinate in vast networks and produce complex time-varying neural activation patterns in order to generate a wide range of movements. Understanding the nature of this coordination and activity is of significant importance to improving understanding of the brain as well as unlocking the potential for neurally-controlled prosthetic devices.

Technological improvements to recording technology have shaped our abilities to both examine neural systems as well as address hypotheses of signaling within and across cortical areas. Just over fifty years ago, experimenters were limited to recording single neurons. Today, chronically implantable microelectrode arrays allow several hundreds of neurons to be recorded simultaneously [2–4] and improvements to imaging techniques enable whole brain imaging [5]. As the number of observable signals has increased, so has the need for modeling the relationship between neural

signals and motor behavior.

More recently, brain-machine interfaces (BMIs) have motivated a need to understand the nature of how these neurons encode information on an individual and population level. The goal of this research is to develop new algorithms and approaches to investigating the representation of motor behavior by populations of neurons in motor-related regions of cortex in nonhuman primates.

1.1 Research Aims

Aim 1: Study dynamics of neuronal coding in motor-related areas of cortex as they relate to the performance of simultaneous reaching and grasping

Seeking the nature of representation of motor behaviors by neurons is of significant importance for controlling BMIs and improving out overall understanding of the brain. In this aim I explore this interaction through inspection of lower dimensional representations of neuronal population activity during to movement. Following this I explore the concept of temporal generalization of decoders to examine the dynamics of how reaching and grasping are differentially represented by the population. These approaches reveal the presence of a temporally dynamic representation of reaching and grasping by neurons in premotor and motor cortices.

Aim 2: Identify co-modulated communities of neurons using an unsupervised clus-

tering analysis

As the number of simultaneously observed neurons grows, identifying meaningful task-relevant neurons becomes increasingly important and manual inspection of individual units becomes increasingly impractical. I propose a semi-supervised approach to identifying communities of neurons that co-modulate in relation to external variables. I demonstrate that this method is useful both for exploratory analysis of neuronal functionality and for neuron selection for use in motor decoding applications.

Aim 3: Develop a neuronal encoding approach utilizing task-specific networks among neurons to decode grasp postures

Traditional models of neuronal spiking often attempt to model neuronal firing activity as being primarily related to the behavior being performed through use of a specific tuning function. This approach necessitates the specification of a tuning function and typically requires the assumption that neurons encode signals independently of one another. I propose a model for signal encoding that does not require a tuning function and assumes that signals are encoded in the network structure of a neuronal population. This model prototype is demonstrated to have several desirable properties with regards to encoding and decoding performance compared to alternative models.

1.2 Organization

In order to provide context for the current work, Chapter 2 provides background related to brain recording, BMIs and approaches to modeling neuronal signals.

My proposed algorithms and methodology were developed on data from a single experimental paradigm. Chapter 3 will describe this paradigm in detail and serve as a reference for the data used in this research.

In Chapter 4, I investigate the presence of dynamic coding in the motor and premotor cortex during performance of reaching and grasping behaviors. In particular I detail a series of methods for initial investigation into coding of behavior by population and demonstrate decoding of simultaneous reaching and grasping behaviors. These decoding techniques are then applied to better understand the dynamics of the neural code.

Building upon the decoding results from the previous chapter, Chapter 5 proposes a semi-supervised method for identifying populations of neurons that co-modulate in relation to a common external stimulus. This method is then implemented in identifying task-relevant neurons for use in decoders of reaching and grasping behavior.

In Chapter 6 I will describe the development of a novel approach to encoding and decoding population activity based on task-specific interactions among neurons. Here I hypothesize that neurons participate in functionally connected networks with structures dependent on the task being performed. I explore this hypothesis through the development of novel models of neuronal firing applied to the task of encoding

and decoding of grasping behaviors.

The concluding Chapter 7 summarizes the results and proposes future directions for additional investigation.

Chapter 2

Background and Motivation

2.1 Introduction

The principle focus of this thesis is on the exploration of how groups of neurons in motor and premotor cortices coordinate and encode information about motor behaviors. This focus closely relates to, and was initially derived from, the problems faced in the construction and operation of Brain-Machine Interfaces (BMIs). Given this relationship, this initial chapter will set the scene by describing what BMIs are, providing an overview of their history, and detailing the challenges faced in their development. Through this approach I will also introduce the concepts of neuronal encoding and decoding as well as the principle approaches to constructing models that address these concepts.

2.2 Milestones in Brain Machine Interface Development

As the name implies, brain machine interfaces (BMIs) are a means of interaction between a brain and some other external (typically electronic) device. This interface may be manifested in two different directions: through the being used to control a device or a device providing some form of input directly to the brain. These two directions of interaction are dependent upon the concepts of recording and stimulation, respectively. Recording simply requires some method of obtaining a read-out of brain activity which may then be acted upon. Stimulation involves supplying some sort of input directly to the brain, often in the form of applied electrical current. Although a BMI may be capable of both recording and stimulation, this is currently rare in practice and the BMIs of interest in the context of this work are largely BMIs that record only. However, the absence of direct stimulation does not necessarily imply the absence of feedback or influence on the brain.

2.2.1 Cosine Tuning and Population Vectors

To understand the present state of BMIs, some historical context is important. Perhaps the earliest BMI work can be attributed to research performed in the late 1960s by Eberhard Fetz. One early study [6] demonstrated that macaque monkeys could learn to adjust the firing rate of individual neurons if provided with audio

feedback that indicated the rate of firing. This initial work importantly illustrated the potential for willfully modulating brain activity in the presence of external feedback. While controlling the firing rate of small numbers of arbitrary neurons certainly has validity in BMI, this concept may not scale to the control of complex devices. Later studies sought to analyze the relationship between neural firing and motor behaviors. If this relationship could be understood or approximated, a BMI user's movement intentions may be read directly from the brain and manifested in the control of prosthetic device.

In 1982, a study by Georgopoulos, et al. [7] identified neurons in the motor cortex that reliably varied their firing rate depending on the reach angle of a monkey performing a two-dimensional reach task. Many of the cells demonstrated a maximal firing rate related to some preferred direction of arm movement. This firing rate tended to fall off predictably as a function of deviation from the preferred direction with cells firing minimally when the arm moved in the opposite direction. The researchers observed that the relation between firing rate and reach angle could be approximated by the cosine of the angle between a neuron's preferred direction and the actual movement direction. With this cosine tuning function, there was now a basis for predicting the direction of limb movement based only on observed neuronal spiking. Though there was now a means to find a meaningful behavioral signal encoded by single neurons, the firing of individual neurons is especially unpredictable and the signal-to-noise ratio is generally poor as a result.

The same group later built upon the cosine tuning model by examining the collective tuning properties of a population of neurons. In [8], the group reported that reach direction appeared to be simultaneously encoded in the firing rates of many neurons in a population. A model known as the *population vector* was proposed. Under the population vector model, each neuron could be thought of as having a vector pointing in its preferred direction of arm movement. The difference between the neurons present firing rate and its maximal firing rate provided the magnitude of this vector. If the firing activity of many such cells in a population could be observed simultaneously, these vectors could all be added together resulting in a single combined estimate of reach angle. This so called "population vector" set the stage for making more accurate predictions of arm movements in a shorter period of time by leveraging the power of a population of neurons and overcoming some of the noise issues associated with using only a single neuron.

2.2.2 Open Loop Control of BMIs

Not long after the pioneering work by Georgopolous and others, the first motor BMIs were developed. Motor BMIs are generally any BMI that uses the subject's brain activity to control some motor behavior; often manifested through the movement of a virtual cursor or a physical robotic limb. Many of the earliest motor BMIs were performed in an open loop paradigm. Open loop decoding implies that a device is being controlled without providing the user with feedback regarding the outcomes

of neural control. Providing feedback to the user may allow improved control but may also cause a BMI to fail if the relationship between physical activity and brain activity was learned during actual movement. Feedback may cause the observed observed brain activity to behave differently than when actual physical behavior was performed. This may cause the BMI to under perform due to a mismatch between the model and actual brain activity. Open loop paradigms attempt to avoid this issue by withholding feedback about neural control.

In one of the earliest BMI experiments by Chapin et al. [9], researchers demonstrated real time neural control of a one-dimensional robotic arm in rats using a population of primary motor cortex neurons. The relation between neural activity and physical activity was learned from trials in which rats physically pressed a lever to control an arm and receive a reward. On trials where neural control was used to control the arm, the rats still physically depressed the lever. In later similar experiments by Wessberg et al. [10], monkeys were trained to control a one-dimensional robotic limb using a joystick. Researchers found they could predict the intended movement of the robotic limb from simultaneously recorded brain activity from motor and parietal regions of cortex. This activity was decoded and used to control the limb while the monkey moved a disconnected joystick. In both these studies, the BMI was considered to be controlled in an open-loop paradigm and the animals were generally not made aware of the use of neural control as opposed to control via lever or joystick. Despite the open loop paradigm, researchers readily demonstrated the

ability to extract task-relevant motor intention from the brain.

2.2.3 Closed Loop Control of BMIs

The next significant milestones in the evolution of BMI came through the demonstration of closed loop control. Closed loop control implies that the feedback loop has been closed and the BMI user is able to directly observe the effects of BMI control. This distinction is especially important as providing feedback may actually perturb the underlying neural activity causing the decoder to perform more poorly than expected [11, 12]. Additionally, closed loop control provides the user with the opportunity to correct for mistakes by the decoder [13] and to adapt to the decoder over time [14].

In one of the earliest closed loop studies by Serruya et al. [15], a monkey was trained to move a cursor on a computer screen with a joystick while neural activity was recorded from neurons in primary motor cortex. Researchers learned a linear mapping was learned between the cursor movement and brain activity. The researchers then had the monkey continue the experiment while intermittently alternating between joystick control of the cursor and brain control of the cursor. Researchers learned that not only did the monkey successfully completed trials with brain control, but periodically completed trials without moving the joystick at all.

In another study, Taylor et al. [16] demonstrated closed-loop three-dimensional end point control in primates. Similar to other studies, researchers initially al-

lowed the primate to control the limb via a joystick while recording neuronal activity through electrode arrays. Researchers compared decoding via open-loop and closed-loop paradigms and found that closed-loop control resulted in more successful trials than open-loop. Additionally researchers noted that the directional tuning properties of cells involved in the task appeared to change and the monkeys showed signs of adaptation by improving their performance in offline-control over a period of 20 to 40 days.

One of the next milestones came through simultaneous control of several variables through a closed-loop BMI. In [17], Carmena et al. demonstrated that a monkey could simultaneously control reach direction, reach velocity, and grip force. This simultaneous control was demonstrated through the performance of a closed-loop BMI task that required the monkey to control a virtual cursor's two-dimensional position as well as its size in order to match a target cursor. In addition to successfully demonstrating simultaneous control, researchers observed neurons changing their firing properties depending on whether physical or neural control was used.

Another milestone in BMI control was achieved recently in a study by Ifft et. al [3]. Researchers demonstrated the capability of a monkey to use a BMI to control two limbs independently and simultaneously in a virtual environment. An integral part of this accomplishment was the ability to simultaneously record from nearly 500 neurons in multiple distinct brain regions. In addition to this bimanual control, researchers also observed adaptation as well as apparently different representation for

simultaneous bimanual control versus unilateral control.

2.2.4 BMIs in Humans

Beyond closed loop control in non-human primates, the next significant milestones in the development of neuronal-based BMIs involved the control of BMIs by humans. In human subjects, typically a distinction is made based on the recording technology, i.e. electroencephalography (EEG), electrocorticography (ECoG), functional magnetic resonance imaging (fMRI), and implanted microelectrode arrays. While BMI control in humans was demonstrated earlier by non-invasive EEG and less-invasive ECoG, BMIs controlled by spiking activity recorded from microelectrode arrays have generally shown superior performance in typical BMI tasks at the cost of being most invasive with regards to the recording methodology.

In one of the earliest applications of neuronal-based BMI control in humans, Hochberg et al. [18] demonstrated closed loop control of a prosthetic by a human with tetraplegia using neuronal recordings from primary motor cortex. In this study, an adult man with complete spinal cord injury at C4 demonstrated two-dimensional cursor control using approximately 50 to 60 neurons in a given session. Unlike earlier studies in monkeys, the subject was not able to participate in an initial training phase that relied upon explicit physical movement of a limb. Instead, the subject imagined movements in response to researcher instructions. This study demonstrated that even imagined motor behavior could be used to learn and control a BMI.

One concern with BMIs dependent on implanted microarrays is whether the device will work over a period of several years. A significant milestone in this regard came from further studies by the Donoghue group [19]. Similar to the previously mentioned human study, this study used the same recording technology and investigated whether long-term control of BMIs was possible following chronic implantation of an electrode array. Remarkably, in this work a tetraplegic human subject demonstrated control of a point and click interface 1000 days after the array had been implanted.

Following the progression of BMI control observed earlier with monkeys, additional milestones in human BMI control were marked by an increase in the number of signals recorded as well as the number of degrees of freedom controlled. In work by Collinger et al. [20], researchers implanted two 96-channel microelectrode arrays in an adult human with tetraplegia. The subject demonstrated the ability to move a robotic limb within two days and ably demonstrated control over seven degrees of freedom in a number of reach and grasp tasks after 13 weeks of training.

2.3 Overview of Cortical Anatomy

At their core, BMIs for motor control depend on measuring changes in brain activity. The task at the heart of successful BMI operation is that of identifying user intent at the level of neuronal signaling and then translating that intent into external behaviors. Understanding the overall organization of the brain and the functionality

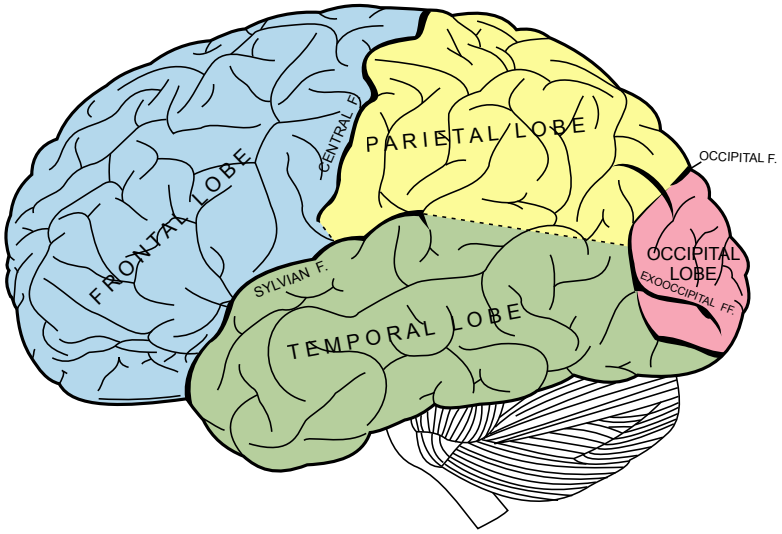

Figure 2.1: Depiction of human brain with lobes highlighted. The cerebral cortex has four principal anatomical lobes: frontal, parietal, temporal, and occiptal. These lobes are functionally associated with movement, sensation, speech, and vision, respectively. Image source: commons.wikimedia.org

of the various subdivisions informs researchers where electrodes should be placed as well as the concepts that are encoded in a specific brain region. Here, a general overview of cortical anatomy provides some context to the relationship between spatial and functional organization in the brain.

Generally when referring to neuronal-based BMIs used for motor control, recordings are produced from neurons in the cerebral cortex. The cerebral cortex is the outer layer of the brain and most recently evolved region. The cerebral cortex may be divided into four lobes as shown in Fig. 2.1: frontal, parietal, temporal and occipital. While these are primarily anatomical classifications, each lobe is generally associated with certain principle functions. The frontal lobe is associated with control of movement, motor planning, short-term memory, and motivation. The parietal lobe

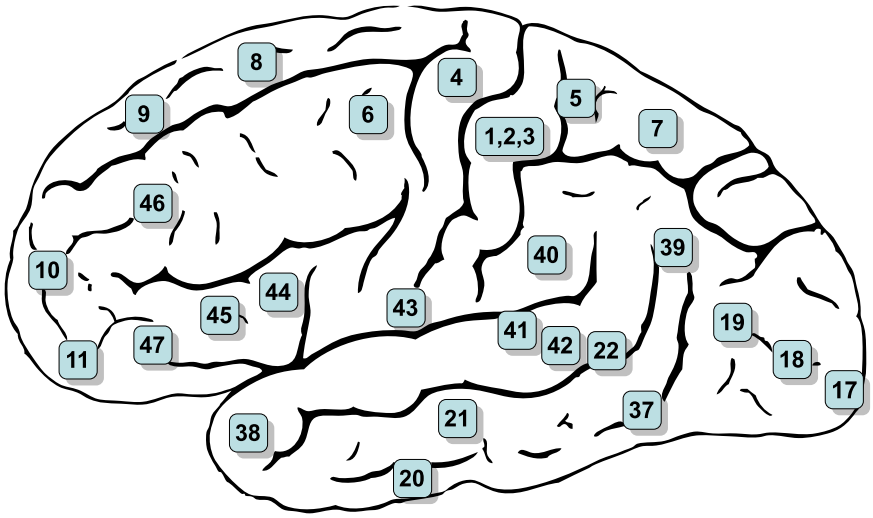

Figure 2.2: Sagittal depiction of human brain with subset of Brodmann areas indicated numerically. Brodmann areas are one means of anatomical reference for the human brain based on histology studies by Korbinian Brodmann. In BMI work, Brodmann areas 4 and 6 are of special interest since these correspond to the primary motor cortex and premotor cortex, which are both principally involved in production of movement. Image source: commons.wikimedia.org

is associated with integration of sensory information and plays an important role in the feedback loop during movement. The temporal lobe is generally deemed responsible for production of speech and language comprehension. Finally, the occipital lobe is responsible for vision. These regions clearly form very broad anatomical divisions of the brain and similarly each have functional roles that are broad in scope.

The link between anatomical and functional subdivisions continues at finer scales within individual lobes. Specific sub-regions are often identified as shown in Fig. 2.2 using a naming system referred to as Brodmann areas [21]. For BMIs used in motor controls, a number of these anatomical structures are of particular interest: primary motor cortex (M1), premotor cortex (PM), supplementary motor area (SMA), and

posterior parietal cortex (PP). Though the exact function of these regions is unknown, certain roles and responsibilities of these areas have been identified. The primary motor cortex (Brodmann area 4) is believed to be responsible for generating the motor commands that are transferred through the spinal cord to generate movement. The premotor cortex and supplementary motor areas (Brodmann area 6) are involved in planning and initiating movement. The posterior parietal cortex (Brodmann area 7) is considered to be responsible for sensorimotor integration and plays a role in movement planning [22]. Each of these regions may be suitable for recordings for use in motor BMIs but may encode different aspects of movement production. For the purposes of this work, however, the motor cortex and premotor cortex are of greater interest.

Within the motor cortex and premotor cortex there is still further evidence of functional subdivision. In a seminal study by Penfield and Boldrey [23], electrical stimulation was applied to points throughout sensorimotor cortices and noted resulting movement or sensation resulting from the stimulation. The study revealed the presence of a functionally divided somatotopy where stimulation to physically proximal areas in the cortex resulted in sensation or movement in similar regions of the body. This research later led to the development of Penfield's homunculus model [24] that mapped the somatotopy between the motor cortex and external anatomy. Similar somatotopy was similarly discovered in the brains of nonhuman primates [25]. A diagram of this broad somatotopy is shown in Fig. 2.3. Maps such as these are

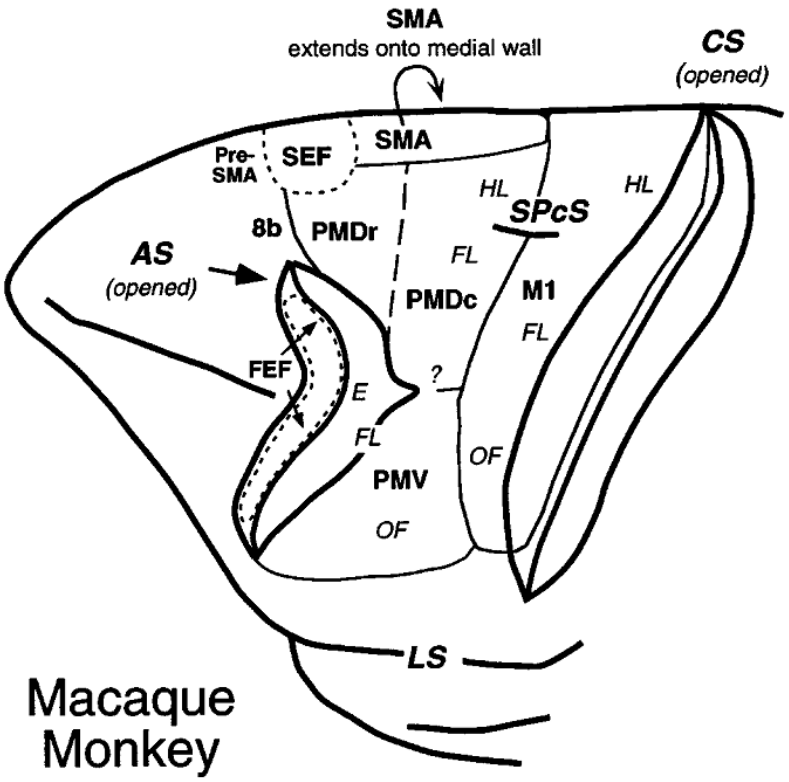

Figure 2.3: Lateral view of frontal lobe of macaque monkey indicating anatomical landmarks and putative regions of gross movement representation. Regions of movement representation are indicated for orbitofacial (OF), forelimb (FL), hindlimb (HL), eye (E). Indicated anatomical landmarks include central sulcus (CS), primary motor cortex (M1), ventral and dorsal premotor cortex (PMV, PMD), supplementary motor area (SMA), superior precentral sulcus (SPcS), arcuate sulcus (AS) and lateral sulcus (LS). Adapted from [1].

critical during the planning of electrode implantation.

Complex reaching and grasping behaviors involve recruitment and coordination of structures in many separate regions of cortex. Naturally the aforementioned regions of cortex do not act in isolation but coordinate information through various cortical circuits during the production of movement [26–28]. In the performance of reaching and grasping, references are commonly made to two specific pathways. The dorsolat-

eral pathway, thought to be involved in grasping, connects the anterior intraparietal sulcus (AIP) to ventral premotor cortex (PMv) which projects to primary motor cortex (M1) [29]. The second pathway, the dorsomedial pathway, is generally thought to be heavily responsible for reaching motions. The dorsomedial pathway involves projections from medial intraparietal sulcus (MIP) to area V6a then to dorsal premotor cortex (PMd) then to M1. Though these two pathways were originally thought to separately encode reach and grasp, more recently this distinction has become less clear. The dorsomedial pathway in particular may also have an additional role in coordinating reach and grasp [26, 30].

Knowledge of the overarching functional anatomy of the brain is vital for successful development of BMIs. Keeping in mind that BMIs are about decoding intention from brain signals, it is helpful to have a sense for how intention is represented in each particular area of cortex. Recordings from parietal cortex may represent information about the target of a particular reach. Meanwhile recordings from motor cortex may represent the specific commands necessary to activate muscles and produce the reach. Understanding the overall function of these regions is only the beginning of the challenge, however. Understanding which general concepts are encoded by a particular part of the cortex is not the same as understanding *how* those concepts are encoded.

2.4 The Role of Recording Technologies

Recording of brain activity has been performed with a number of different methods. These many approaches are often described in terms of a trade-off between physical invasiveness, temporal resolution, and spatial resolution. Commonly used *noninvasive* methods include functional magnetic resonance imaging (fMRI), magnetoencephalography (MEG), electroencephalography (EEG), and functional near-infrared spectroscopy (fNIRS). Invasive methods include electocorticography (ECoG) and penetrating microelectrode recordings. The noninvasive methods each suffer from significant drawbacks such as enormous recording equipment (fMRI and MEG), poor temporal resolution (fMRI), poor spatial resolution (MEG, EEG, fNIRS), and low signal to noise ratio (fNIRS, EEG). ECoG provides a compromise in many of these regards with temporal resolution comparable to EEG with higher spatial resolution and improved signal to noise ratio. This improvement in recording quality with ECoG comes at the cost of requiring an array of electrodes to be implanted on the surface of the brain. Penetrating microelectrode recordings operate at the finest spatial and temporal resolution. Microelectrodes are commonly used to record the activity of individual neurons and can operate at temporal resolutions suitable for capturing individual neuronal action potentials. However, this approach is considered the most invasive as the microelectrodes are inserted into the cortex itself.

The evolution of neuronal-based BMIs is intertwined with the evolution of microelectrode recording technologies. Glass micropipette electrodes were integral to

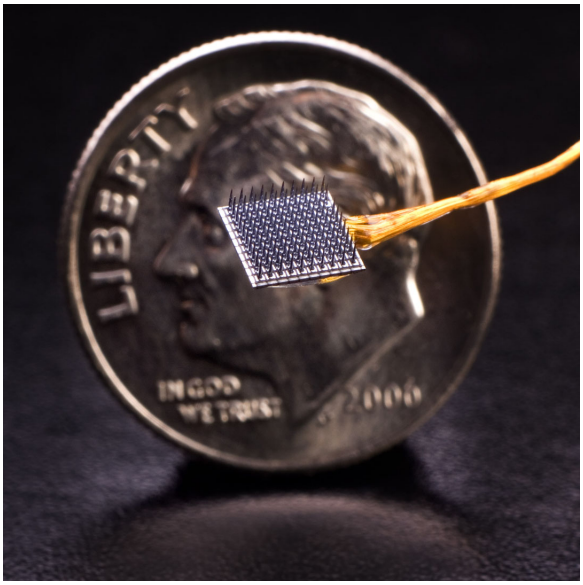

Figure 2.4: Example microelectrode array. Improvements to hardware have resulted in electrode arrays with smaller footprints and densely packed grids of electrodes. Present and ongoing developments to recording technology are driving evolution in techniques used for analyzing neuronal recordings. The array shown here has a 4 mm $\times$ 4 mm footprint and contains 100 microelectrodes. Image credit Matthew McKee/BrainGate Collaboration.

the development of the voltage clamp technique [31] by Hodgkin and Huxley which provided insight into the behavior of ion channels in neurons. Eventually, development of tungsten microelectrodes [32] and precision microposition devices [33] enabled studies that required long repeated recordings from single units. These technologies played a critical role in early work that contributed to the understanding of behavior of neurons in striate cortex in response to visual stimuli [34]. While tungsten microelectrodes made single unit recording more accessible, experimenters typically only recorded from one to ten neurons simultaneously. Continued development eventually resulted in the creation of chronically implantable high density microelectrode arrays [35]. Microelectrode arrays such as the one shown in Fig. 2.4 could be em-

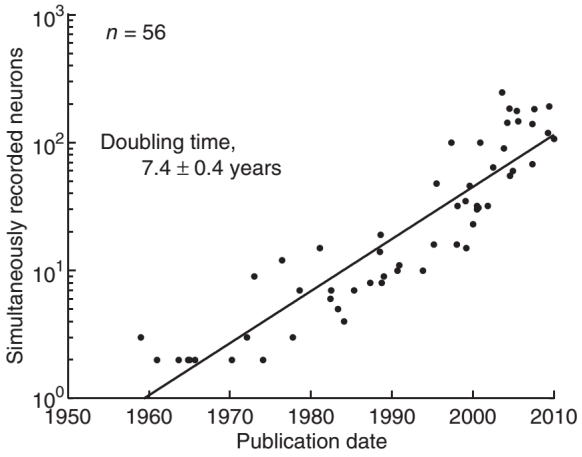

Figure 2.5: Number of simultaneously recorded neurons over time. Since the earliest experiments, the number of simultaneously recorded neurons has increased at a rate approximating Moore's law. Today, experiments regularly record from several hundreds of individual neurons simultaneously. Reproduced from [2].

ployed to record from over a hundred neurons simultaneously. Today, experiments commonly involve recordings from multiple implant multiple microelectrode arrays for simultaneous recordings [3, 36, 37].

One of the direct effects of technological advancement with regards to recording can be seen in Fig. 2.5 reproduced from work by Stevenson and Kording [2]. Much like the Moore's law commonly applied to the doubling rate of transistors in integrated circuits, the number of simultaneously recorded neurons appears to have its own doubling rate of roughly seven years. Increasing numbers of neurons include several positive effects such as wider varieties of neurons observed, richer information derived from simultaneous interactions, and decreased emphasis on precise selection of recording locations. On the other hand, as more neurons are observed simultaneously, recorded spiking activity approaches the ominous realm of *big data*. Larger

and richer datasets require that models operating on this data must increasingly deal with big data problems such as increases in computation time and the curse of dimensionality. Understanding general anatomy informs where signals should be recorded and recording technology dictates the volume and types of data available. The next obstacle that must be dealt with in this sequence is deciding how this data should be represented and capitalized upon.

2.5 Simulated Spiking

Prior to deeper discussions regarding modeling of neuronal activity, an initial simulated example may help to convey some of the basic issues at hand. One of the problems with recording from individual neurons is that the firing of cortical neurons is often noisy. Though the individual action potentials from a given neuron may be considered identical, the timing between spikes is highly variable. It has been observed that cortical neurons rarely produce identical sequences of spikes even in response to repeated presentations of a stimulus [38] or of repetitions of an identical behavior. This irregularity in spike timing has given rise to the hypothesis that many neurons represent information in the overall rate of spiking rather than in the specific timing of spiking. This model is referred to as rate coding.

Under the model of rate coding, the low signal to noise ratio of neuronal spiking can still be problematic. In the example shown in Fig. 2.6, firing was simulated

from a single neuron over a period of 1000 ms. This neuron was simulated to have an underlying actual firing rate that oscillated between 15 Hz and 55 Hz. Despite this underlying rate, spiking is still the result of a noisy random process. From looking at the generated spike train alone in the top panel of Fig. 2.6, oscillating behavior is not readily apparent. As a second step, a smooth underlying firing rate was approximated by convolving the simulated spike train with a gaussian kernel with 25 ms standard deviation resulting in the smoothed rate shown in the middle of Fig. 2.6. Even after smoothing, most would agree that there is not clear evidence of oscillatory activity. Given the observation of this single trial, it would be difficult to say anything substantive about this neuron beyond that the neuron appears to have an average firing rate of about 35 Hz.

In practice, the issue of neuronal noise is commonly overcome through repetition. Fig. 2.7 shows a simulation in which over 200 repetitions of 1000 ms trials were drawn from the same unit shown in Fig. 2.6. Each trial was influenced by the same random processes observed previously. In aggregate, both the raster of spikes over all trials in Fig. 2.7a and the raster of smoothed firing rates in Fig. 2.7b more readily show the presence of oscillatory firing activity. Aggregating information across these many trials either through binning as in Fig. 2.7a or point-wise averaging as in Fig. 2.7b recovers a firing rate that closely matches the one that generated the spikes in the first place.

To relate this example to the problem of representation, let us imagine that these

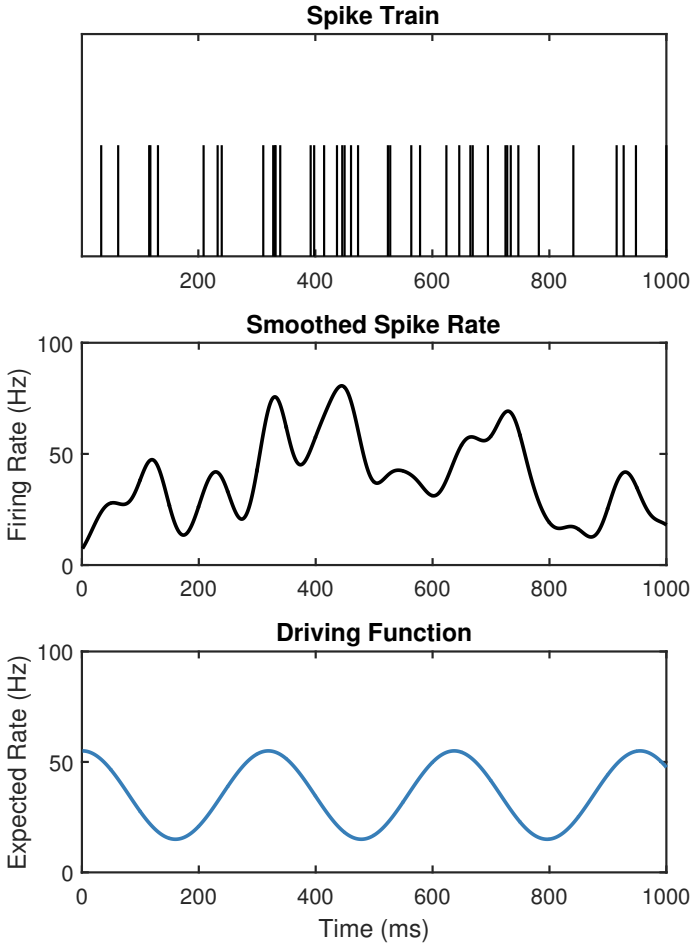

Figure 2.6: Example of rate coding with simulated spike train and estimated firing rate generated by a noisy driving function. An example of a simulated spike train (top) observed over a 1-second period generated by a time-varying driving function (bottom). Spike trains are often smoothed with a kernel function (middle) to attempt to better recover the underlying firing rate. The low signal-to-noise ratio of spiking often results in single-trial firing rate estimates that only roughly approximate the true underlying function.

recordings were made from a neuron in a rat while the each trial requires the rat to run along some track and that this neuron is tuned to vary its firing rate in response to the rats position on the track. The problem of representation requires us to find an explanation for the neuron's spiking activity while keeping in mind that we do not

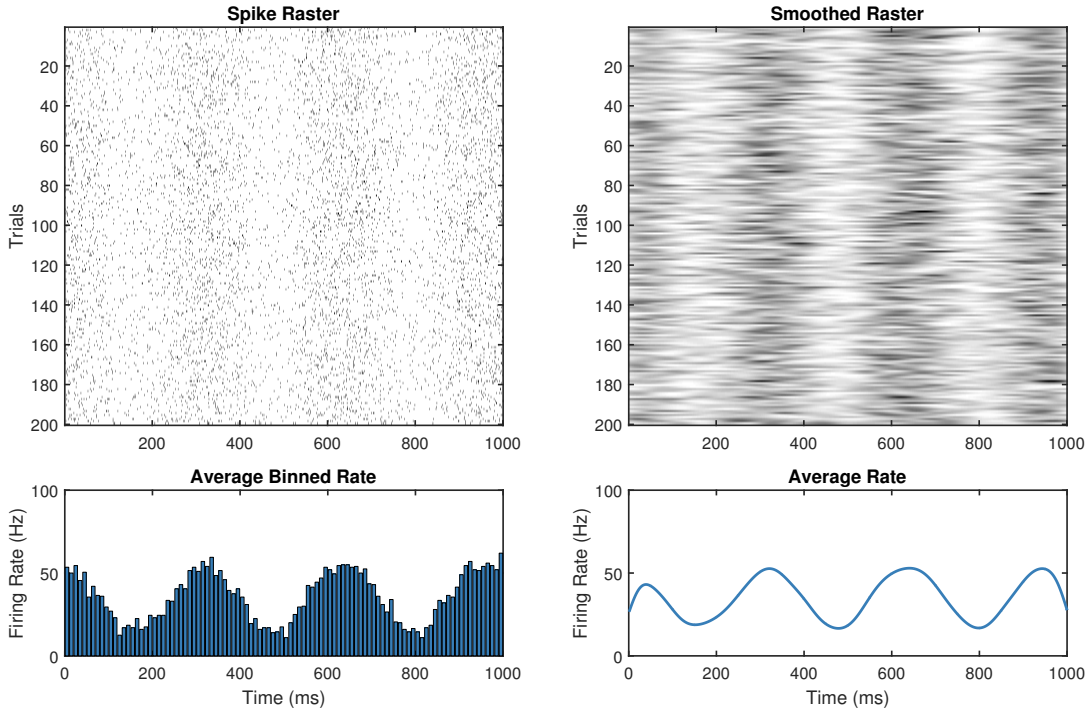

Figure 2.7: Spiking patterns become clearer through observation of multiple trials. These examples build upon the single trial shown in Fig. 2.6. Several hundred repetitions of the same trial were simulated and both individual spikes (a, top) and smoothed firing rate estimates (b, top) were observed. By counting the average number of spikes within each time bin (a, bottom) or calculating the average firing rate observed at each time across all trials (b, bottom) reveals an estimated firing rate much closer to the true underlying rate that generated the activity.

actually know the true underlying driving function in Fig. 2.6. We may approach an initial solution to this by observing that the trial-averaged spiking seen in Fig. 2.7 appears to oscillate with some regular frequency. We may then correlate this signal with some other observed signal such as the rat's overall movement speed to observe whether or not there appears to be a connection.

2.6 Encoding and Decoding

Two important concepts to understand when discussing models relating brain activity to behavior or external stimuli are encoding and decoding. In general, *encoding* describes the manner in which the brain represents some signal of interest. By contrast, *decoding* describes the act of attempting to read out the behavior or stimulus associated with some observed brain activity. These concepts of encoding and decoding can also be described from a modeling standpoint. An *encoding model* is a mathematical function that takes a behavior or stimulus as input and provides the expected associated brain activity as an output. A *decoding model* is a function that takes brain activity as input and provides the expected behavior or stimulus as an output.

Though the problems of encoding and decoding are inverses of one another, the models themselves are not necessarily invertible and research is often focused on one objective or the other. In the case of modeling the interaction between the brain and motor behavior, the quality of an encoding model is measured by how closely the predicted brain activity matches the observed brain activity associated with the performance of a known behavior. The quality of a decoding model is measured by the similarity between the behavior or stimulus predicted by the model compared to the actual behavior that gave rise to the brain activity provided as input to the model.

Because of the difference in objective measures, researchers must often choose to

place emphasis on either encoding or decoding. From the standpoint of constructing models for use in BMIs for motor control, decoding performance is typically perceived as being of greater importance. After all, the problem underlying motor prosthetic control is that of extracting behavioral intention from brain signals. A successful decoding model may lead to highly intuitive, accurate, and precise control of a computer cursor or prosthetic limb. Meanwhile, from the perspective of understanding the brain, encoding performance is often of greater concern. Encoding models allow researchers to assemble hypothetical models of brain activity and observe the extent to which these models actually seem to describe the observed activity. A successful encoding model may provide significant insights leading to further experimentation.

2.7 Encoding Models

Neuronal encoding models are simply models that attempt to relate the spiking behavior of a neuron to one or more variables of interest. Encoding models take a wide range of forms depending on their context and desired application. The Hodgkin-Huxley model of spiking [31] for example, considers factors at a sub-millisecond scale and attempts to describe the probability of a neuron spiking based on the activity of individual ion channels. At a slightly larger time and spatial scale, so-called point process encoding models [39,40] attempt to predict the occurrence of individual spikes and at a timescale of 1 to 5 ms. In comparison to ion channel models, these point

process models tend to focus on extracellular factors such as the spiking of nearby neurons. At a still larger scale, firing rate models attempt to predict the overall average firing rate of neuron, typically on a timescale of 25 ms to 500 ms. These models tend to base predictions of spiking on concepts such sensory stimulation or motor behavior.

Of the previous models, encoding models that attempt to explain spiking over broader time scales have traditionally been more popular. As in the example shown in Fig. 2.6, these models assume that the observed spiking is the manifestation of some variable process that encodes information through variations in overall firing rate. The seminal example here is the cosine tuning model introduced by Georgopolous et al. [7] that related the firing rate of a neuron to the difference in the direction of arm movement versus the neuron's preferred direction. More generally, this encoding model is solved through ordinary linear regression. In this model, the firing rate of a neuron is expressed as some linear combination of a number of variables of interest. The cosine tuning model can be shown to be a special case of this where firing is expressed as a linear function of the arm's instantaneous velocity through space.

Recently, point process models [39, 40] have grown in popularity. In contrast to the rate-based model, these models do not apply any smoothing to the observed firing. Instead, these models view the neuron as having an underlying instantaneous probability of spiking and liken the observation of a spike train to the outcome of a sequence of coin flips. The more important difference is that of time-scale. Point pro-

cess models can often incorporate the influence of certain intrinsic neuronal properties such as refractoriness, bursting, or whether other neurons have fired recently [40–42]. Smoothed rate-based models often cannot account for these effects because they occur at too fine a temporal resolution and are lost in the smoothing process.

George Box famously wrote, "...all models are wrong, but some are useful." Neuronal encoding models are no exception. There is significant uncertainty and disagreement in the manner in which neurons actually encode motor behavior. As stated in [43], "The activity of motor cortical neurons has been related to almost every tested parameter including isometric force, muscle activity, joint torques, joint angles, changes in joint angles, and even the serial order of movements." A number of studies have attempted to address, for example, whether neurons in motor cortex individually encode single variables or instead encode multiple variables either in sequence or simultaneously [43–45]. From the standpoint of modeling, this raises questions with regards to the variables that should be included in the model and whether the model should be stationary or time-varying. From the standpoint of interpretation, encoding models for motor behavior are often met with significant skepticism due to the similar goodness-of-fit of so many different models applied to the same data.

Encoding models extend beyond the scale of individual neurons as well. Many efforts are focused on how various signals are encoded by populations of neurons. Individual neurons are highly variable in their behavior and in the presence of identical

repetitions of a single stimulus are unlikely to ever respond in precisely the same way. Thus many studies insist that attention should be applied to how populations of neurons interact together in order to more reliably represent variables of interest [46, 47]. The population vector model [8] provides one seminal example of modeling the encoding of a stimulus by a population of neurons. Though individually, each neuron of a group encodes a noisy estimate of the direction of reach, when the individual estimates are combined by averaging, a more accurate and precise estimate is achieved. Population coding is one proposed way of addressing the examples shown in Fig. 2.6 and Fig. 2.7. In lieu of repeating a process many times over to average the response of a single neuron, the cortex likely relies on entire populations of neurons encoding the same variable to reduce noise.

While it is still unclear whether individual neurons encode single or multiple variables, populations of neurons recorded from the same electrode array may encode several variables simultaneously. In an experiment involving reaches around obstacles, [48] found that an ensemble of neurons in primate dorsal premotor cortex (PMd) encoded representations of the direction of hand movement, the direction of the target relative to the current position as well as the location of the target. Additionally, the strength of these individual representations was found to vary depending on whether or not an obstacle was present. In another study, Shanechi et al. [49] found that a population of neurons in the premotor cortex of a rhesus monkey encode information about multiple cued targets simultaneously. Experimenters were able to predict both

the first and second targets the monkey would reach toward before the reach had been made.

2.8 Decoding Models

Within the context of BMI, the ultimate goal is often to modulate brain activity to control a prosthetic limb or a mouse cursor in order to achieve a desired purpose. Because of this specific objective, the encoding problem is often treated as being of secondary importance compared to the problem of signal reconstruction or decoding. The extent to which a particular encoding model accurately represents the neuron's behavior is a secondary concern to how well the model can be used to control an external device. In many cases where decoding performance is the priority, encoding models may not be used at all and instead the behavior may be treated as the output of some black box into which the time-varying firing rates of neurons are providing input.

Before advancing into further discussions regarding decoding, it is important to point out that the generally the problem of decoding is typically addressed in one of two ways: *classification* or *regression*. Within the context of BMIs, classification is the task of attempting to assign a particular sequence of brain activity as belonging to one of a number of finite groups or classes. Classification use cases within BMIs include: choosing a letter of the alphabet to type, deciding whether to move a mouse

cursor left or right, or determining which of a finite set of grasps a user wants to perform with a prosthetic hand [50]. By contrast, regression is typically concerned with trying to predict one or more continuous-valued variables. Examples of this within the context of BMIs may include: determining the speed and direction to move a cursor in a 2d plane, predicting how far to open or close a prosthetic hand, attempting to reconstruct an image that someone is viewing [51]. In many cases, either approach may offer a suitable solution, though one may be slightly preferable to the other.

As the previous few examples suggest, neural decoding is a broad concept with many possible applications. Within the context of this work however, the application of decoding to the cases of reaching and grasping is of particular interest. These actions in particular were among the first problems to be addressed by BMIs and are perhaps the most practical uses of BMI for a paralyzed individual beyond control of a computer cursor or wheelchair.

2.8.1 Decoding Reach

Some of the earliest decoding tasks in BMI work involved decoding of reaching movements. The ideal case would be to use brain signals to provide biomimetic control of a robotic limb. Brain signals could be used to control each of the joint angles of the limb independently to allow for total control of the limb in a naturalistic fashion. This particular goal is ambitious, however, when one considers the number of degrees of

freedom that may be utilized in naturalistic reaching. One state-of-the-art prosthetic limb, the Modular Prosthetic Limb by the Johns Hopkins Applied Physics Lab, is capable of moving with 26 degrees of freedom. How to extend the natural performance of the intact human body to such a limb is difficult since the manner of control applied by the central nervous system to manipulate the hand is still unclear [52,53]. Another limitation appears when we consider that the human brain contains approximately 100 billion neurons. While not all of these are dedicated to control of a single limb, there are still several orders of magnitude more neurons involved in this task than the several hundred that researchers can simultaneously record from today. According to [54], even if our recording capabilities increase similar to Moore's law, with a doubling of the number of neurons every 7 years, we still will not reach 100 billion simultaneously recorded neurons for 220 years. Facing this reality, the problem of decoding reach from brain signals is often simplified significantly.

One simplification comes from broadly thinking of reaching as a matter of moving our hand to some arbitrary point in space, this line of thinking leads to modeling reaching using a regression-based approach. Under this view, the task of decoding is reduced to continually estimating the intended instantaneous hand (or cursor) position or velocity. This task was initially approached through linear estimation methods such as the population vector algorithm or linear regression [16, 17, 55, 56]. Beyond the initial linear method, a number of non-linear regression techniques were evaluated including neural networks [10, 57] and particle filters [58]. However, the

Kalman Filter approach has become the *de facto* standard for regression of reach due to its intrinsic ability to smooth estimates of position and velocity across multiple samples [3, 59–61]. More recently, so-called point process filters [62–64] have seen some popularity as they offer properties similar to the Kalman Filter while allowing spiking to be modeled as a point process. While the regression approach to reaching has seen promising results, further simplifications are possible and may be preferable.

One further simplification is to assume that reaches can only be performed to a small but distinct number of locations. In this paradigm, a classification approach can be taken to determine which location a user intends to reach or which of a finite subset of directions a user intends to reach in [57, 65–71]. Additionally, this may not be a simplification but a necessity based on where signals are recorded. Recordings from parietal regions of cortex, for example, may encode information about the objective of movement rather than an explicit motor plan of how to reach that objective [22,72–74]. The drawback of this approach is often the lack of generalization. If the classifier is trained to identify intention to reach some finite set of locations, the user is limited to selecting from only those locations. Intention to reach to novel locations generally cannot be accommodated under this approach.

A third approach to decoding reach blends the classification and regression approaches in a method often called goal-directed reaching. Despite the prevalence of the Kalman Filter, pure regression performances often leave much to be desired. For instance, neurons in M1 appear to strongly encode information about instantaneous

reaching direction while speed is less strongly encoded [75]. This commonly results in effects in cursor control experiments where the cursor overshoots the target or never entirely becomes stationary. Meanwhile classification approaches often do not allow for variations in reaching speed or overall trajectory. One approach that has emerged to treating these effect is the combination of reach regression with information about the objective of the reach [74, 76–79]. This approach also lends itself to hierarchical control where information about the objective of reach may be obtained from PM or PPC prior to reaching [78] or to hybrid control where environmental sensors such as tracking of eye gaze may help identify reach targets [80].

2.8.2 Decoding Grasp

Much like decoding of reach, there are several different approaches to decoding of hand posture with varying degrees of fidelity to naturalistic grasp. The human hand is capable of many complex postures. The joints of the hand and wrist allow for potentially 27 degrees of freedom (DoF) of movement. In reality, mechanical coupling by tendons and muscles [81] reduces the true number of degrees of freedom substantially. However, the resulting space of potential hand postures is still high dimensional in comparison to the 6 degrees of freedom that describe the general location and orientation of the hand in space.

Decoding of hand posture or grasp in order to achieve the most naturalistic postures often results in the problem being treated as one of regression. In this paradigm,

the joint angles of the hand and wrist are seen as continuous variables to be regressed from spiking activity. Each joint angle may be decoded individually [82]. However, in naturalistic movement the hand does not use all degrees of freedom equally; there are a finite number of hand postures that are regularly used by primates. From a BMI standpoint, researchers have attempted to find a set of synergies or lower dimensional spaces that capture hand movement [53, 83–85].

In the same way that decoding of reach can be simplified by limiting the number of possible reach locations, decoding of hand posture can be simplified by limiting the problem to selection from among a finite number of grasps. A number of classification approaches have been applied to this task including linear discriminant analysis [36, 86], naive bayes classifiers [87, 88], support vector machines [69, 89, 90] and various other non-parametric approaches [91]. One approach that preserves the possibility of more complex hand postures is decoding the activation of individual fingers [50, 92].

2.8.3 Decoding Simultaneous Reach and Grasp

Though many studies treat decoding of reaching and grasping separately, naturalistic reaching and grasping requires coordination of the two. A number of studies have incorporated the two to varying degrees. Typically reaching is controlled through a regression approach and grasping is limited to a binary hand open/close postures or regression of grasp aperture. An early example of simultaneous decoding of reaching and grasping by Carmena et al [17] required monkeys to control the location and size

of a virtual cursor through a BMI that had previously been trained on wrist velocity and grip force. Another previously mentioned study by Velliste [56], required a monkey to use a BMI to control a physical robotic limb to reach to a piece of food, then grasp it and return. Other experiments by the Donoghue group [93,94] demonstrated simultaneous offline decoding of reach and grasp using data from an experiment that required a monkey to reach out and grab a swinging object. Similar studies have been performed with human subjects using a BMI to control cursor position and clicking in virtual reality [19] or using a BMI to control the reaching and grasping of a robotic limb [20, 86].

2.9 Summary

This chapter attempted to provide a broad overview and introduction to many of the concepts involved in working with BMIs. Though this work is focused more on encoding and decoding than on the implementation of these models in a BMI, the concepts generally go hand in hand. Whether the intention is to control a BMI or perform exploratory brain research, the concepts of cortical anatomy, recording technology, and modeling methodologies are all interlinked. While each topic is worthy of independent research in its own right, the following chapters will largely focus on the modeling aspect. In particular these chapters detail a number of methods suitable for dealing with encoding and decoding while keeping in mind the trend toward

simultaneous recordings from ever larger populations of neurons.

Chapter 3

Experimental Protocol

3.1 Introduction & Background

The work in this thesis depends upon data from an experimental protocol conducted on non-human primates in the lab of Dr. Marc Schieber at the University of Rochester. Since data from this experiment will be re-used throughout this work, an early description of the experiment seems prudent. Here we present the experimental procedure, the methodology of neurophysiological recordings, and a number of figures and tables that may serve as a reference for further chapters.

The experimental procedures and signal acquisition described in this chapter were fully performed by Dr. Schieber and the members of his lab at the University of Rochester. All procedures involving nonhuman primates were approved by the University Committee on Animal Resources at the University of Rochester.

3.2 Experimental Procedure

Two male rhesus monkeys (*monkey L* and *monkey X*) were trained to perform a center-out reach, grasp, and manipulate task. The monkey was seated in a primate chair and restrained such that the task was performed only with the right hand and arm. The monkey interacted with an experimental apparatus similar to that depicted in Fig. 3.1A. Four peripheral objects and a central home object were mounted on individual rods extending outward from a vertical plane in front of the monkey. The peripheral objects were arranged along a coplanar arc centered on a central home object. The arc had a radius of 13 cm and each peripheral object was separated by 45° along the arc. The home object was positioned approximately 32 cm in front of the monkey's right shoulder.

The peripheral objects consisted of 4 unique forms: sphere, coaxial cylinder (pull), perpendicular cylinder (mallet) and push button (push). Each object also had a specific manipulation associated with it. The coaxial and perpendicular cylinders could be pulled toward the monkey against a small spring load, the sphere could be rotated, and the push button could be pressed.

A trial began when the monkey grasped and pulled the home object approximately 1 cm toward itself against a small spring load. This initiated a variable hold period requiring the monkey to maintain its pull on the home object for a random duration from 1,000 to 1,500 ms for monkey X and 1,500 to 2,000 ms for monkey L. Following the initial hold period, a blue LED was illuminated next to one of the four peripheral

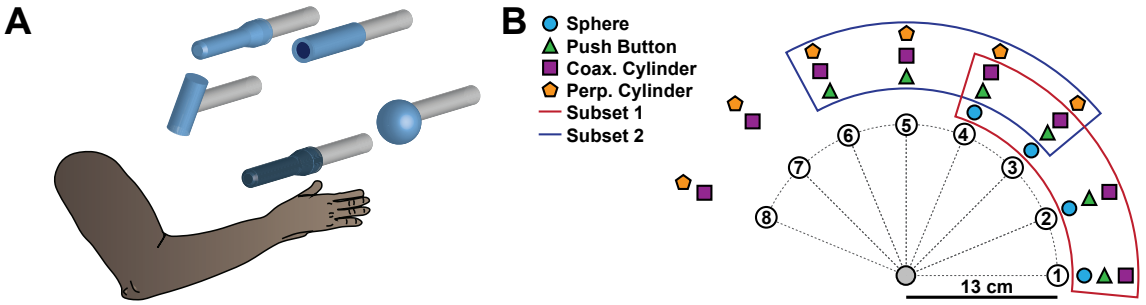

Figure 3.1: Experimental apparatus (A) and analyzed experimental conditions (B). Trials consisted of cued reach, grasp and manipulate behaviors from a home object (indicated with darker shading) to one of four objects located at 45 degree intervals along an arc centered on the home object. Moving clockwise along the arc, the objects were: perpindicular cylinder, coaxial cylinder, push button and sphere. The apparatus could be rotated and allowed for objects to be presented at 8 possible locations. During a single experimental session, trials were performed at a total of 24 unique object-location combinations. We subdivided these conditions into 2 sets for analysis (Subset 1 and Subset 2, as indicated). Subsets were constructed to include 3 objects presented at each of 4 locations. In this figure, objects are denoted by shapes and possible positions are indicated by number. The apparatus setting depicted in (A) shows the objects in positions 2, 4, 6 and 8.

objects. This cued the monkey to release the home object and to reach, grasp and manipulate the indicated object. Successful manipulation of the indicated object resulted in the closure of a microswitch. This illuminated a green LED next to the object indicating successful manipulation and initiating a final hold period. The final hold period required the object manipulation to be maintained for 1,000 ms. Completion of the final hold resulted in a successful trial; the blue and green LEDs were turned off and the monkey received a liquid reward. Failure to complete any portion of this sequence resulted in a failed trial and no reward.

The mounting rods were attached to a mechanical apparatus that allowed rotation about the central object. This apparatus could be rotated to any of 8 discrete zones

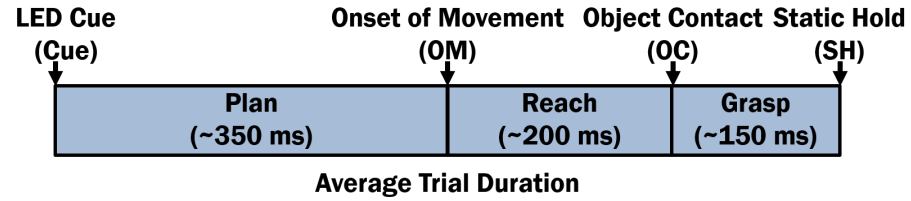

Figure 3.2: Average time course of a typical trial. Event markers of interest such as onset of movement (OM), object contact (OC) and static hold (SH) are indicated. Successful trials required the monkey to maintain the static hold for an additional 1000 ms (not shown).

separated by a rotation of 22.5°. Peripheral objects maintained their ordering along the arc and adjacent peripheral objects were always separated by 45°. For example, in one zone, the four objects would be located at 0°, 45°, 90° and 135°. An adjacent configuration would reposition the objects at 22.5°, 67.5°, 112.5° and 157.5°.

The experiment was self-paced and the monkey voluntarily initiated each trial by pulling on the central (home) object. Trials were performed in blocks consisting of approximately 10 reaches per object with the apparatus fixed in one zone. Following each block, the apparatus would be rotated to a new zone in pseudorandom fashion. Within a block, trials were cued in pseudorandom order except for in the event of failed trials. Following a failed trial, the next trial would be cued to repeat the same object and location. Failed trials were not included in this analysis. Trials were limited to objects located in the range of 0° to 157.5°. As a result, trial blocks could consist of cued reaches to 2, 3 or 4 objects depending on the rotation of the apparatus. These tested conditions are shown in Fig. 3.1B and summarized along with number of trials at each condition in Table 3.1.

Table 3.1: Trial Counts At Each Object & Location For Monkey X (Monkey L)

	0°	22.5°	45°	67.5°	90°	112.5°	**Total**
Sphere	34 (30)	33 (30)	39 (27)	24 (29)	–	–	130 (119)
Push	28 (25)	26 (26)	29 (27)	30 (26)	37 (27)	29 (29)	179 (160)
Pull	33 (29)	33 (30)	33 (29)	35 (29)	33 (29)	31 (31)	198 (177)
Mallet	–	–	25 (28)	29 (29)	31 (29)	34 (31)	119 (117)
Total	95 (84)	92 (86)	126 (114)	118 (113)	101 (85)	94 (91)	626 (573)

Critical time points in each trial were measured via the experimental apparatus to provide precise measurements of several experimental epochs. Cue presentation (Cue) is meant as the time when the LED was first ignited next to the target peripheral object. Onset of movement (OM) indicates the time the monkey released the central home object and was determined initially by accelerometers placed in the central object and verified by post-experimental analysis of motion recordings. Object contact (OH) corresponded to the initial contact of the monkey with one of the peripheral objects and was determined according to recordings made from accelerometers in each of the peripheral objects. Switch closure (SC) corresponds to the completion of object manipulation as determined by closure of a microswitch located on the target peripheral object.

The epoch from cue presentation to onset of movement is referred to as planning epoch and the duration of this epoch may be referred to as reaction time. The ensuing epoch from onset of movement to object contact is labeled as the reach epoch and the duration is referred to as the reaching time. The epoch from object contact to switch closure consists of the period in which the monkey was manipulating the object

Table 3.2: Average and standard deviation experimental epoch durations for each monkey

		Monkey X		
Object	Trials	Reaction Time	Reach Time	Switch Time
Sphere	130	0.43 ± 0.07	0.17 ± 0.02	0.16 ± 0.07
Push	179	0.42 ± 0.07	0.27 ± 0.08	0.33 ± 0.17
Coax. Cyl.	272	0.38 ± 0.07	0.17 ± 0.04	0.15 ± 0.04
Perp. Cyl.	185	0.38 ± 0.05	0.18 ± 0.04	0.15 ± 0.04
		Monkey L		
Object	Trials	Reaction Time	Reach Time	Switch Time
Sphere	119	0.32 ± 0.07	0.18 ± 0.03	0.13 ± 0.11
Push	160	0.32 ± 0.06	0.29 ± 0.09	0.15 ± 0.13
Coax. Cyl.	237	0.31 ± 0.04	0.20 ± 0.05	0.15 ± 0.08
Perp. Cyl.	176	0.31 ± 0.03	0.15 ± 0.03	0.07 ± 0.06

and is referred to as the grasping epoch. Finally, after switch closure, the monkey maintained his final grasp posture in an epoch referred to as static hold.

3.3 Electrophysiology

Each monkey was chronically implanted with multiple floating microelectrode arrays (FMAs) (MicroProbes for Life Science, Inc). Each FMA consisted of 16 recording microelectrodes arranged in a 4 x 4 grid. Microelectrodes within each FMA were of variable length ranging from 1.0 to 6.0 mm. Recordings were made simultaneously from 8 separate FMAs during performance of the task.

In each monkey, recordings were made from arrays implanted in putative primary motor cortex (M1) and premotor cortex (PM) regions of the left hemisphere. In the sessions examined in this study, recordings were made from 6 FMAs in M1 and 2

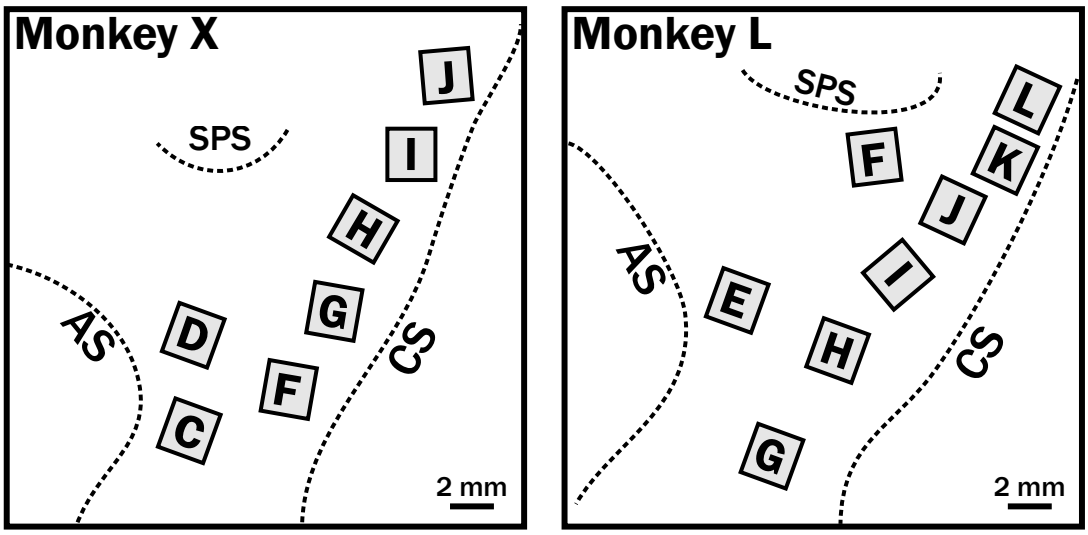

Figure 3.3: Location of implanted arrays in Monkey X and Monkey L. Each monkey was implanted with 8 electrode arrays. Each array consisting of 4×4 grid of electrodes. Arrays were implanted in putative forelimb regions of the motor cortex consistent with known anatomical landmarks. Array E in Monkey X is not shown since reliable spiking activity was not observed from this array in the examined sessions.

FMAs in PM. Approximate positions of these FMAs are depicted in Fig. 3.3. Specifically, the M1 arrays in each monkey were implanted anterior to the central sulcus and positioned to record from varying depths down the anterior bank of the central sulcus as well as from the crown of the precentral gyrus. The M1 arrays spanned the entire upper forelimb representation as verified by intracortical microstimulation. In each monkey, two FMAs were implanted posterior to the genu of the arcuate sulcus and lateral to the superior precentral gyrus in the ventral premotor area. Additional details regarding implantation are available in [36].

Analog neural recordings were taken from a total of 16 channels per array for a total of 128 channels per monkey. Neural activity was recorded with a Plexon Multi-

Table 3.3: Number of identified spiking units per array for each monkey including definite single units, probable single units, and multi units

Monkey X			Monkey L		
Array	Loc.	Count	Array	Loc.	Count
E	M1	0	G	M1	19
F	M1	2	H	M1	15
G	M1	11	I	M1	15
H	M1	8	J	M1	17
I	M1	26	K	M1	20
J	M1	16	L	M1	12
C	PMv	14	E	PMd	2
D	PMv	35	F	PMd	4
Total		**112**			**104**

Acquisition Processor (Plexon, Dallas, TX). Spike snippets from each channel were extracted online using Plexon Sort Client software (Plexon, Dallas, TX) with channel gains and thresholds set by the experimenter. Offline spike sorting was performed using Plexon Offline Sorter (Plexon, Dallas, TX). Principal component analysis was used to project waveform features into a low dimensional representation. Unit waveform centers were manually identified by visualizing raw waveforms and clusters in principal component space. Automated spike sorting was applied by assigning waveforms to the nearest cluster.

Following spike sorting, spike trains were characterized based upon the signal to noise ratio (SNR) and inter-spike intervals (ISIs). Signals were classified as definite single units if the SNR was greater than 3.0 and there were no ISIs of less than 1 ms. Signals were classified as probable single units if the SNR was greater than 2.5 and at least 90% of ISIs were greater than 1 ms. Other units were classified as multiunit recordings. These procedures are in line with metrics recommended in [95]. In the

analyses presented in this document, we do not distinguish between single unit and multi-unit activity. This lack of distinction between signal types is expected to have little impact on the analyses.

Empirically, trial averaged responses of neurons tended to show significant variation in firing rate due to the grasp being performed as well as the location of the object. Inspection of condition-specific peristimulus time histograms of the various spiking units revealed units with varying degrees of object-only or location-only tuning as well as several units with notable interaction effects between the conditions. The spiking activity and task-specific average firing rate for an individual unit is shown in Fig. 3.4.

3.4 Summary

The experiment described here provides a rich data set suitable for many analytical approaches. These procedures improve upon earlier similar experiments performed by Dr. Schieber's group at the University of Rochester [36, 82] by incorporating a means of dissociating reach location from object shape. A thoughtfully designed experimental apparatus and trial structure allows for precise identification of several behaviorally relevant events such as onset of movement and object contact. Simultaneous recordings from multiple electrode arrays enable examination of the interaction of neuronal activity across multiple spatial and temporal scales. While the number of

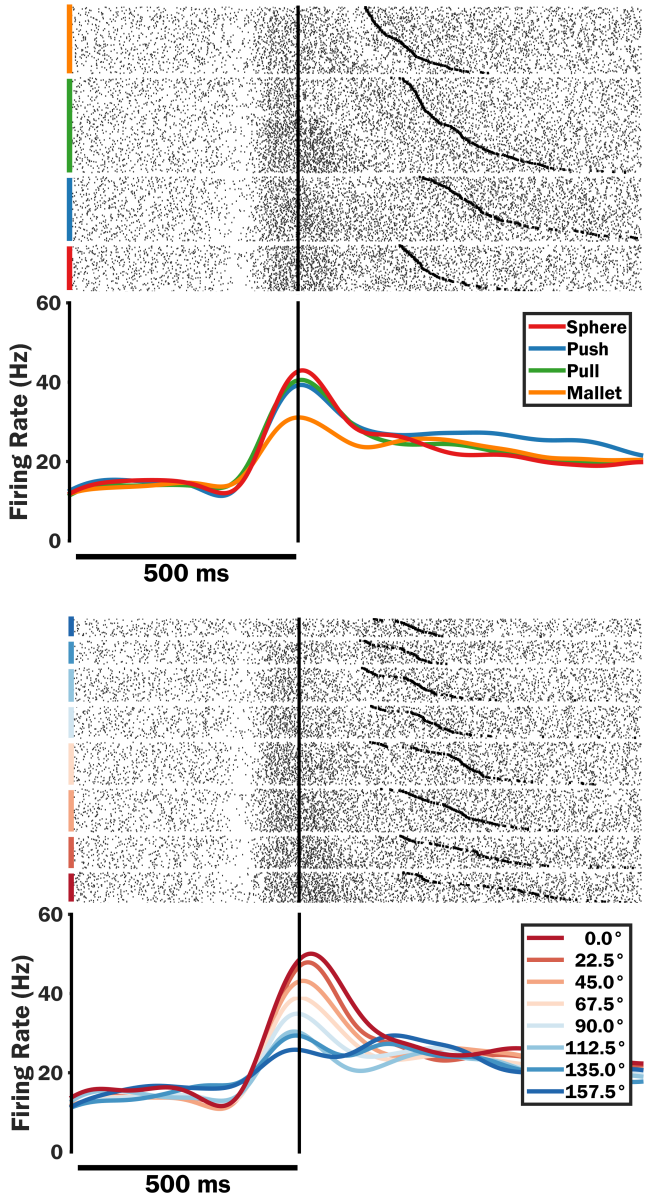

Figure 3.4: Spike rasters and trial averaged firing rates from all trials for an individual unit from Monkey L grouped by grasp (top panel) and reach (bottom panel) conditions. Trials were aligned to the onset of movement (thick vertical line) and order within task conditions by increasing trial duration. Times of completion of object manipulation in each trial are indicated with thick black marks. Spike trains were smoothed with a Gaussian kernel with standard deviation of 50 ms before averaging.

identified spiking units was typically on the order of one hundred, analysis techniques developed to deal with this cardinality of neurons should largely be relevant for several hundreds of neurons or more. Data gathered from this experiment in the following chapters will be applied to the task of investigating the dynamics of neural coding, identification of neuronal functionality by unsupervised clustering, and task-specific networks of functionally connected spiking units.

Chapter 4

Exploring Dynamic Motor Code

4.1 Introduction & Background

The response to stimulus and production of movement requires coordination across multiple regions of the brain, each with a distinct role to play in the process. In the example of producing a reaching behavior, separate regions of the brain are believed to engage dynamically in the tasks of identifying an objective, preparing a motor plan, producing the signals required to execute that plan, integrating sensory information to provide feedback, and making continuous adjustments to the process to account for noise and changes in the external environment [96]. However, this dynamical interaction is not restricted to larger brain regions.

The firing activity of neurons in motor cortex and premotor cortex has been observed to vary with time both in preparation of performing a movement [57, 97, 98]

as well as during the movement itself. The variation of this firing activity is of great interest. Repeated variations in firing rate of a single neuron over repetitions of a trial may provide clues as to the types of information represented by the neuron, such as limb kinematics or the eventual goal of a reaching motion. At the level of a population of neurons, systematic variations in population firing activity across experimental conditions may enable the decoding or read-out of the motor behavior being performed.

Decoding is commonly applied to neural signals with the intent of controlling a BCI. Decoding can serve a more general purpose by attempting to measure the information content in a set of neural signals as well as the stability of a particular representation [99]. More commonly within the motor BCI framework, population dynamics are often marginalized by averaging firing rate over entire trials or time periods of several hundred milliseconds. Information about a stimulus or behavior may involve coordination of an entire ensemble or population of neurons [100]. Additionally, individual neurons have been shown to have significant time-varying activity not readily explained by a extrinsic task-relevant covariates [43–45, 73, 101–104]. Individual units may further vary the parameters that are encoded depending on the task [48] or the presence of prior information [71].

In decoding motor behavior, regression-based approaches to decoding can account for some temporal variation in population activity by associating the time-varying firing rates with one or more time-varying kinematic parameters. Classification tech-

niques, meanwhile, typically model neural population activity as evolving through some number of discrete states using finite state machines [67] or hidden markov models [105, 106]. Insight into spatial and temporal evolution of discriminable neural activity can be assessed by evaluating classifier performance based on signals limited to a particular window of time [36] or a particular subset of all available signals [36, 69, 94, 107].

In this chapter we apply dimensionality reduction and classification techniques to signals from motor and premotor cortex in order to investigate the dynamics of the neural population during production of reach and grasp motions.

4.2 Methods

4.2.1 Experimental Protocol

The experimental protocol used here was the same as that described in Chapter 3. Briefly, two rhesus macaques participated in a motor experiment involving cued reach to grasp and manipulate trials beginning from a central object and ending at one of four peripheral objects positioned at one of eight possible locations. In total, 24 experimental conditions were evaluated. Electrophysiological recordings were made from eight intracortical floating microelectrode arrays implanted in M1 and PM areas of each monkey. Each array consisted of a 4 x 4 square grid of 16 recording electrodes of varying lengths. Recordings from each channel were processed to isolate neuronal

spiking activity as described in Chapter 3.

4.2.2 Feature Extraction and Time Rescaling

For this work, we assumed the observed neurons encoded information through rate coding. In each trial, spike times for each unit were converted to binary spike trains with sampling rate of 1 kHz. These binary spike sequences were convolved with a 50 ms wide boxcar kernel to provide an estimate of firing rate. This technique of generating smoothed firing rate estimates by convolution with a gaussian or boxcar kernel is commonly applied in the literature [82, 88, 93, 108]. The width of these smoothing functions commonly range from 50 ms to 200 ms or more depending on the intended application. In BCI applications the choice of kernel width reflects a trade-off between responsiveness and smoothness [13,108], while in other applications the width reflects inherent time-scale of neural activity of interest.

Trials exhibited differences in average duration related both to object type as well as location. Differences in trial duration can complicate multi-trial analysis due to misalignment of key events. In order to ameliorate difficulties due to variation in trial lengths, we applied a time normalization technique to smoothed firing rates for each trial. Linear interpolation was used to resample each experimental epoch to be the same number of samples across trials. Three epochs were identified: cue presentation to onset of movement, onset of movement to object contact, and object contact to static hold. Linear interpolation was applied to resample each interval to

a number of equally spaced samples matching the number of samples corresponding to the interval's global average at a sample rate of 1 kHz. Since this interpolation is performed after the estimation of firing rates, the magnitude of each unit's firing does not change, though the overall time course may become compressed or dilated.

For example, the global average duration for the OM to OC epoch was approximately 200 milliseconds or 200 samples at 1 kHz. In each trial, the smoothed firing rate samples corresponding this epoch were linearly interpolated to 200 samples. While this results in some dilation or compression of time across trials, the percentage of time elapsed between experimental events is preserved. In this case, 50 samples from the rescaled trials during epoch will always correspond to 25% of the time elapsed between onset of movement and object contact, regardless of the original duration.

4.2.3 Visualization and Comparison of Neural Trajectories

To visualize the dynamics of the ensemble during reaching and grasping, we apply a two-step dimensionality reduction procedure similar to that described in [108, 109]. Spiking activity was converted to smoothed firing rate estimates as described previously. Each unit's smoothed firing rate was standardized by mean centering and scaling according to its standard deviation. Each trial's standardized neuronal activity was then time-rescaled as previously described to a vector of length n. This

time-rescaled activity from each of p spiking units during the i^{th} trial was gathered into a $n \times p$ matrix $\mathbf{X}_i$. This matrix represents the time-varying trajectory of the neural population in p-dimensional space over the course of a single trial.

Average task-specific population trajectories can be produced by first gathering all the matrices for each of the trials in one or more experimental conditions, then averaging each cell of $\mathbf{X}$ along the collected trials. We performed this procedure for trials in each of the 24 experimental conditions observed during the experiment, where the expected population activity for the i^{th} experimental condition $\mathbb{E}\left[\mathbf{X}^{(i)}\right]$ is denoted $\mathbf{S}^{(i)}$. These trajectories were compared pairwise on a sample-by-sample basis according to average euclidean distance in the high-dimensional space

$$d(\mathbf{S}^{(i)}, \mathbf{S}^{(j)}) = \frac{1}{n} \sum_{k=1}^{n} ||\mathbf{s}_k^{(i)} - \mathbf{s}_k^{(j)}||_2 \tag{4.1}$$

where $\mathbf{s}_k^{(i)}$ is the k^{th} row of the matrix $\mathbf{S}^{(i)}$, or the k^th sample of the time-rescaled population activity averaged across all trials within condition i. This gives us the average point-wise distance between any pair of average population trajectories $\mathbf{S}^{(i)}$ and $\mathbf{S}^{(j)}$. The interpretation of these distances are straightforward: pairs of trajectories with smaller distances tend to be more similar than pairs of trajectories with larger distances. The pairwise distances were evaluated for each pair i, j of 24 conditions and assembled into a 24×24 distance matrix $\mathbf{D}$.

We can then visualize a lower dimensional representation of these trajectories through a procedure known as multidimensional scaling (MDS) [110]. In short, mul-

tidimensional scaling is a dimensionality reduction procedure that attempts to find an arrangement of points in low-dimensional space that preserves the inter-point distances observed in the original space. For example, consider the case of being provided a 10×10 matrix of inter-city distances between 10 major cities in the United States, but not the actual names or locations of those cities. MDS can attempt to produce a 10×2 dimensional matrix describing the locations of a set of 10 points in 2-dimensional space that roughly preserves the original distance matrix. These points can then be used to visualize the approximate relative positions of each of the 10 cities in a 2-dimensional map. Here we use apply MDS to our matrix $\mathbf{D}$ to attempt to find an arrangement of points in 2-dimensional space that preserves the original pairwise distances. We will use this approach to better understand the overall behavior of the population trajectory across each of the 24 conditions.

While the MDS allows us to visually understand the relationship between population trajectories on average, the approach averages out temporal variation. Ideally we would like to be able to observe how population trajectories tend to evolve over time. To reduce the dimensionality of the high-dimensional averaged trajectories while preserving the temporal structure, we apply Principal Components Analysis (PCA). Though there are many approaches to dimensionality reduction for spiking activity (see [111] for a review), PCA is fast, effective, and widely used for investigating simple differences between differences in trial-averaged activity.

PCA is a procedure that finds a linear transformation matrix in order to find a set

of orthogonal vectors that capture the directions of the greatest variance of samples in the matrix. Given an $n - by - p$ matrix $\mathbf{X}$ where each row is an observation and each column is a feature, PCA can be performed by standardizing the columns of $\mathbf{X}$ then performing the singular value decomposition (SVD) of the resulting standardized matrix. The SVD procedure finds a decomposition of $\mathbf{X}$:

$$\mathbf{X} = \mathbf{U}\mathbf{\Sigma}\mathbf{V}^T \tag{4.2}$$

where $\mathbf{U}$ is a $n \times p$ matrix of left singular vectors, $\mathbf{V}$ is a $p \times p$ matrix of right singular vectors, and Σ is a diagonal $p \times p$ matrix of singular values corresponding to the square root of the eigenvalues of $\mathbf{X}$. The entries of $\mathbf{U}$ and $\mathbf{V}$ correspond to the eigenvectors of $\mathbf{X}\mathbf{X}^T$ and $\mathbf{X}^T\mathbf{X}$. The principal components of $\mathbf{X}$ are given by the columns of $\mathbf{U}\mathbf{\Sigma}$ and dimensionality reduction can be performed by keeping the first $k < p$ principal components.

For each monkey, we performed PCA on the data collected in three different ways: object-specific trajectories, location-specific trajectories, and combined object-location specific trajectories. As an example, the find reduced dimensions of object specific trajectories, we grouped the time-rescaled population activity $\mathbf{X}_i^{(obj_1)}$ for the first object type. We then calculated the average of these matrices, $\mathbf{S}^{(obj_1)}$. This process was repeated for each of the remaining three object types. We then vertically concatenated these matrices into a $4n \times p$ matrix:

$$\mathbf{S}^{(obj)} = \left[\mathbf{S}^{(obj_1)}; \mathbf{S}^{(obj_2)}; \mathbf{S}^{(obj_3)}; \mathbf{S}^{(obj_4)}\right] \tag{4.3}$$

PCA was performed on the resulting stacked matrix. The first 3 principal components were retained and the corresponding average reduced-dimensional trajectory matrices (now each $n \times 3$) were unstacked. The resulting matrices then represented a projection of each of the object-specific average population vectors into 3-dimensional space. This same procedure was repeated for the 8 reach locations as well as for the 24 total experimental conditions.

4.2.4 Static vs. Dynamic Decoding Performance

We are interested in further investigating the dynamics of coding of reach and grasp through an analysis based in population decoding. To achieve this, we chose to model and classify firing rates using a Linear Discriminant Analysis (LDA) classifier. LDA is a widely used classifier commonly applied in population decoding of neural signals [36, 82, 99]. LDA is favored for its simplicity, minimal computational requirements, and overall performance in classification tasks [112].

LDA is a generative classifier that models samples of the neural data during performance of a particular class as independent draws from a multivariate gaussian distribution with a class-specific mean, μ_c, and a common covariance matrix that is shared across all classes, $\Sigma_c = \Sigma$. From these assumptions, the likelihood of a single

observation x under any class-specific distribution is defined as:

$$p(x,\theta) = |2\pi\Sigma|^{-\frac{1}{2}} \exp\left[-\tfrac{1}{2}(x-\mu_c)^T\Sigma^{-1}(x-\mu_c)\right] \tag{4.4}$$

The probability that the sample was drawn from a particular class can then be evaluated from Bayes Rule:

$$p(y=c|x) = \frac{p(y=c)p(x|y=c)}{\sum_{c'} p(y=c')p(x|y=c')} \tag{4.5}$$

Thus under the assumptions made by the LDA model, the posterior distribution can be estimated as:

$$p(y=c|x,\theta) = \frac{|2\pi\Sigma|^{-\frac{1}{2}} \exp\left[-\tfrac{1}{2}(x-\mu_c)^T\Sigma^{-1}(x-\mu_c)\right]}{\sum_{c'} |2\pi\Sigma|^{-\frac{1}{2}} \exp\left[-\tfrac{1}{2}(x-\mu'_c)^T\Sigma^{-1}(x-\mu'_c)\right]} \tag{4.6}$$

This expression can be reduced to:

$$p(y=c|x,\theta) = \exp\left[\mu_c\Sigma^{-1}x - \tfrac{1}{2}\mu_c\Sigma^{-1}\mu_c + \log\pi_c\right] \exp\left[-\tfrac{1}{2}x\Sigma^{-1}x\right] \tag{4.7}$$

Model training corresponds to identifying the means for each class and estimating the pooled covariance matrix. Once a model has been fit, classification can be performed by evaluating the posterior probability of a new data point under each of the class conditional distributions. The data point can then be labeled as being a member of the class corresponding to the highest posterior probability. The name

LDA is derived from the fact that decision boundaries between a pair of classes are simple hyperplanes.

For our case, we treat each observation of the population activity in some particular bin as a single observation of a p-dimensional feature. We took two different approaches to classifying data from a particular bin, however. A single classifier was trained on data from all of the discretized bins in all of the trials from the training set. We call this classifier the *global* or *static* classifier as it reflects the assumption that the population activity is relatively stationary over the entire trial duration. In addition, this classifier learns a boundary optimized for separating data aggregated over the entire trial and will thus tend to ignore localized variations.

Multiple *local* classifiers were trained to evaluate the possibility of a dynamic neural code. Each local classifier was trained on data from a single discretized time bin from all of the trials in the training set. In other words, given m instances of $n \times p$ single trial population activity $\mathbf{X}^{(1)}$, $\mathbf{X}^{(2)}$, ... $\mathbf{X}^{(m)}$, we trained n separate classifiers, each trained on data from a single row of each of the m population activity matrices.

If the underlying code is static, the classification performance of any local classifier on data from any point during a trial should be similar. That is, a classifier trained on data from a specific point in time should have roughly equal chance of correctly classifying data from any point during the trial, regardless of time. If instead the population activity is dynamic over the course of a trial, we would expect to observe a change in classification accuracy as some function of the time difference between the

training bin and evaluation bin. In general, we would expect performance to fall off as the temporal difference between training time and evaluation time increases. As described in [113], a monotonic decrease in performance need not always be the case, such as in the presence of oscillatory systems. Evaluating classification performance in this way will provide an indirect view of temporal variations in the representation of behavior-specific population spiking activity.

The global classifier as well as each of the local classifiers were then evaluated on data from all discretized time bins in the testing set. Decoding metrics were indexed according to the time bin the test data was drawn from.

4.2.4.1 Temporal Generalization

In the event that a neural code is changing dynamically and utilizing different elements of the population over time, a classifier trained on data from one point during a trial may not generalize well to data from other points during a trial. This general concept is known as temporal generalization [113]. Temporal generalization is a property of the classifier itself and not necessarily a property of the brain. However, the choice of classifier represents an assumed model of coding utilized by the brain and allows us to better consider whether this proposed coding scheme is static or dynamic.

Temporal generalization was examined by evaluating performance of each of the local classifiers against data from all time bins. Performance by the local classifier

trained on data from time bin i and evaluated on test data from time bin j was aggregated for all values i and j to form a temporal generalization matrix, $\mathbf{G}$. The entries along the main diagonal of this matrix, $\mathbf{G}(i, j)$ for $i = j$, should reflect optimal decoding performance. This is because the main diagonal represents evaluation of data on a classifier trained under similar, if not identical, conditions. Meanwhile, entries off of the main diagonal indicate temporal generalization. As the magnitude of the difference between i and j increases, we would generally expect classification performance to decrease in the event of a dynamic neural code. This is because data from time bin j may no longer be representative of the underlying neural conditions that were present during the period i in which the classifier was trained. The temporal generalization matrix avails itself to empirical inspection where various patterns may reveal insights into the underlying neural code [113]. The global classifier does not lend itself to evaluation for temporal generalization because it was trained on data from all time bins.

The extent of temporal generalization was quantified by measuring the half-bandwidth of generalization performance. Specifically the half-bandwidth was identified as the duration between peak classification performance and the first time point in which this performance fell to $1/\sqrt{2}$ of its maximal value.

4.2.4.2 Crossvalidation

A stratified 5-fold crossvalidation approach was applied to divide entire trials into training and testing sets to ensure a reasonable approximation of generalization performance. Within each fold, 20% of trials were assigned to the test set. The remaining trials were allocated to the training set. Across all folds, each trial appeared in the test set exactly once. A stratified approach was applied to ensure that the relative proportions of experimental conditions were preserved. That is, the testing set and training set each contained approximately the same distribution of trials corresponding to each class as was present in the full dataset.

4.2.5 Temporal Recruitment of Neurons

In the event temporal generalization is evaluated and the underlying neural population is observed to have a dynamic representation of behavior, we would like to attempt to understand how and where this information is distributed over time.

In [99], researchers proposed a method of identifying neurons engagement at different points in a task. Their method consisted in evaluating the difference in average firing rate for a neuron across two conditions, a measure similar to modulation or tuning depth [17]. This time-series was taken as an estimate separability, or the degree to which a particular neuron's activity changes across differences in the experimental condition. This separability measure was then compared with the temporal general-

ization performance of a population classifier trained at a specific time bin. If the two time-series were significantly correlated, the neuron was accepted as being engaged in the task at that particular time bin.

Here we apply a similar technique. The difference in firing rate method does not directly extend to the case of more than two classes. As a surrogate measure of the degree of differential representation of signals by each neuron, we repeat the earlier procedure of training and evaluating LDA classifiers at each time bin. The time-rescaled activity from each unit was binned and used individually to train a single classifier for each time bin. This classifier was then evaluated on samples from the same time bin from trials in the test set. We substitute the instantaneous classification accuracy as a measure of separability.

Pearson's correlation was measured between each neuron's time-series of classification accuracy with the time-series of temporal generalization of the population classifier trained at a particular time bin. If this correlation was statistically significant ($p < 0.0001$), the unit was taken to be a significant contributor to the population classifier trained in that time bin. As such, the unit was labeled as being significantly engaged in the representation of the task at this point in time.

4.3 Results

Neural units with average firing rates less than 3 Hz were excluded from the analysis. This resulted in inclusion 58 of 112 units in Monkey X and 74 of 104 units in Monkey L. The initial reach to grasp experiment consisted of 24 unique reach and grasp combinations. All 24 of these conditions were included in the initial analysis, but only a subset of these trials were included in the classification analysis. Conditions used for classification were limited to trials to the sphere, push button, and coaxial cylinder at locations 1, 2, 3, and 4. This combination of trials is denoted as Subset 1 in 3.1B. This selection was made to ensure that each object and location included in the subset were examined in all possible combinations so as to minimize bias of the classifier.

Spike trains from these trials were converted to firing rate estimates by convolution with a boxcar kernel with a width of 100 ms. For each monkey, data from all trials was temporally rescaled to be of uniform length with an approximately 1 kHz sampling rate.

The time course of the firing rates for each trial were interpolated in order to standardize trials to be of equal duration. Three intervals were identified: reaction time (Cue to OM), reach time (OM to OC), manipulation time (OC to SC). The average duration of these intervals for each monkey are detailed in Chapter 3. In addition to these intervals, an additional 250 ms following switch closure were included for each trial. This final epoch was included as a representative sample of the static

hold period which lasted a full 1000 ms.

As a result of this time rescaling, trials for monkey X were rescaled to a total of 967 samples and trials for monkey L were rescaled to 846 samples. The mean and standard error of trial length distortion (absolute difference in number of samples between original and time-rescaled trials) was 136 ± 5.4 samples for monkey X and 110 ± 4.4 samples for monkey L. The magnitude of the firing rate estimates was not standardized or rescaled. Rescaled firing rates were downsampled from 1 kHz to 100 Hz such that samples reflected a sliding 100 ms window with a 10 ms slide size.

4.3.1 Empirical Analysis of Population Dynamics

Spiking activity from all units in a particular trial were combined into a single matrix representative of the neural trajectory through high dimensional space during that trial. To better visualize these matrices, trials within experimental conditions were combined and average to form an average neural trajectory. PCA was performed on concatenated versions of these trajectories and the top 3 principal components were visualized in three-dimensional space.

Inspection of low dimensional representations of neural trajectories yielded several insights that were consistent across both monkeys. PCA was performed separately on neural trajectories grouped by object type as well as trajectories grouped by reach location. The averaged object-specific and location-specific trajectories are shown in principal component space in 4.1. The first three principal components of object

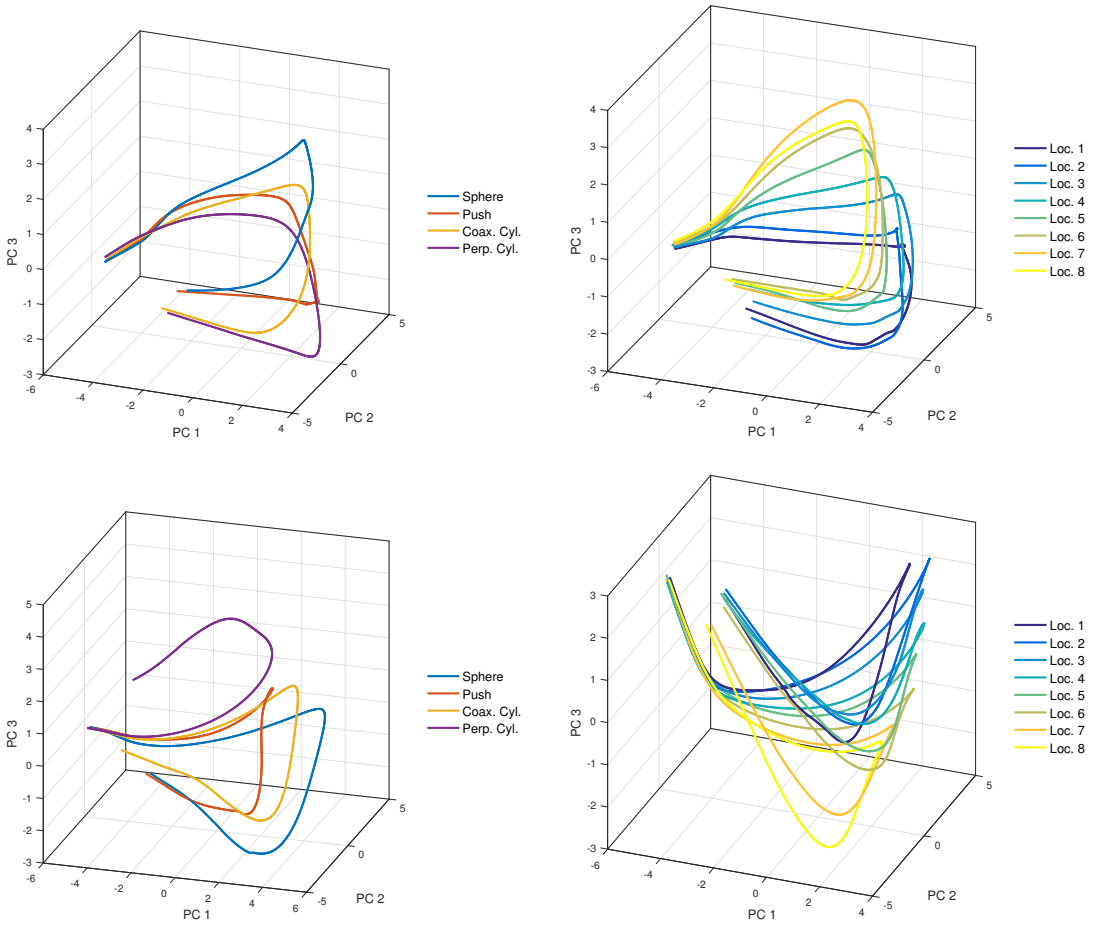

Figure 4.1: Visualization of neural trajectories for reaching and grasping in lower dimensional space. Dimensionality reduction techniques (principal component analysis) were applied to time normalized population activity during simultaneous reaching and grasping. Trial-averaged responses to different object types (left panels) and reach locations (right panels) are shown for Monkey X (top panels) and Monkey L (bottom panels).

specific trajectories accounted for 71% and 72% of the variance in monkeys X and L, respectively. The first three components of location specific trajectories accounted for 68% and 76% of the variance.

Both grasp-specific and object-specific trajectories exhibited a cyclical shape originating from a common point corresponding to cue presentation. In general trajec-

tories appear to diverge as they travel away from the origin then converge as the loop returns toward the origin. That is to say the pairwise distance between any pair of trajectories appears to achieve a maximum sometime during the middle of the trajectory before declining.

Trajectories corresponding to reaches to different locations appear to vary smoothly through the low directional space. For example, the trajectory corresponding to location 2 appears to be closer in space to the trajectory for location 1 than the trajectory for location 8. Object-specific trajectories appear to have similar topology overall but also appear to be better separate than location-specific trajectories.

PCA was then performed on the mean trajectories of all 24 experimental conditions and the resultant PCs were visualized as in 4.2. Though all 24 trials are shown in the figure, trajectories are colored according to object shape. The first three components here accounted for 57% and 59% of the variance in monkeys X and L.

Simultaneous inspection of mean neural trajectories for all experimental conditions appear to show that in the lower dimensional space, neural trajectories for different grasps are better separated than trajectories for different reaches to locations. In this low dimensional space, we see that trajectories appear to cluster by grasp first and then show differentiation based on reach location within the broader grasp cluster. The trajectories collectively appear to simultaneously exhibit the qualities shown in the reach-specific and object-specific trajectories in Fig. 4.1.

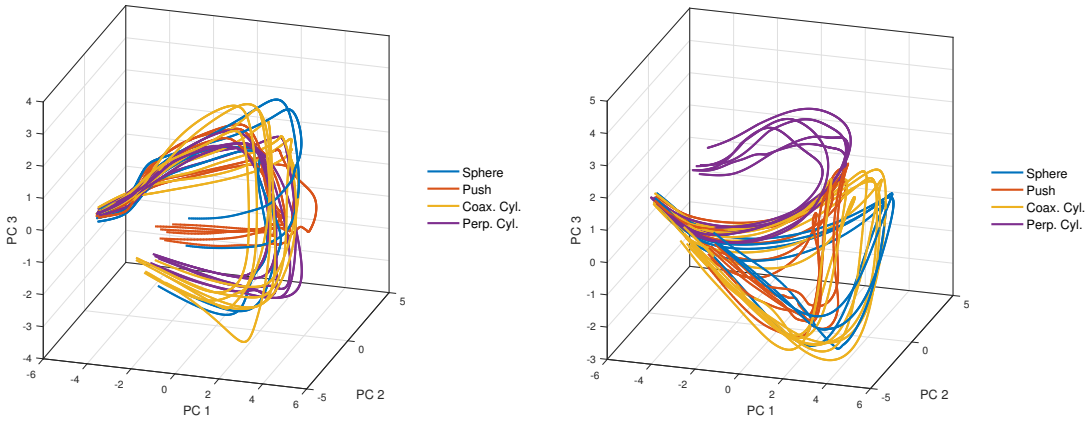

Figure 4.2: Visualization of neural trajectories for reaching and grasping across all experimental conditions shown in lower dimensional space. Dimensionality reduction techniques (PCA) were applied to time normalized population activity during simultaneous reaching and grasping. Trial-averaged responses to all experimental conditions are shown for Monkey X (left) and Monkey L (right). Traces have been colored by grasp type to illustrate clustering among grasps.

To further examine the differences between condition-specific trajectories, we examined the pairwise distance between the condition-specific average trajectories. These distance were combined to form a distance matrix for each monkey shown in 4.3. Distances were calculated according the the average pointwise euclidean distance over time under the assumption that trajectories moved through space at the same velocity.

The distance matrices largely appear to confirm what we empirically observed in the reduced dimension visualizations. The neural trajectories between trials to the same object at two adjacent locations tended to be more similar than trajectories between trials to two different objects at the same location. There does, however seem to be a relationship among reach locations preserved across objects. For example, push button trials at location 1 (experimental condition 5 in Fig. 4.3) are more

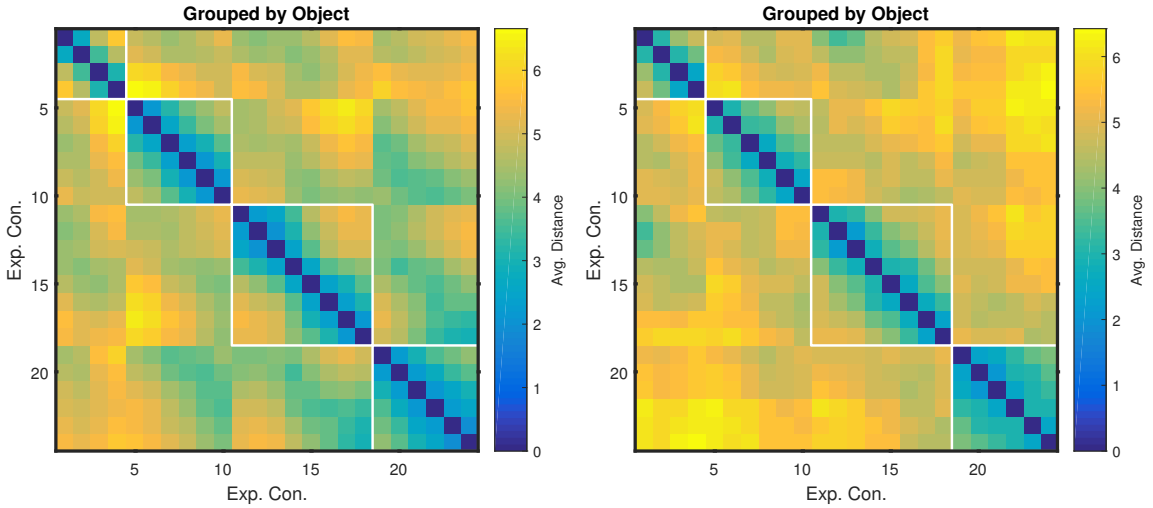

Figure 4.3: Pairwise distance of averaged neural trajectories for each of the 24 experimental conditions in Monkey X (left) and Monkey L (right). Conditions are presented in order of object and location. Here, condition 1 corresponds to the sphere at 0^0 where condition 2 is sphere at 22.5^0. Condition 5 is push button at 0^0 and condition 10 is push button at 135^0. Neural trajectories for a particular object tend to be close together though there appears to be a monotonically increasing distance between trajectories as a function of distance. Trajectories for a single object at two adjacent locations tend to be closer than trajectories for different objects at the same location.

similar to coaxial cylinder trials at location 1 (experimental condition 11) than they are to coaxial cylinder trials at any other location (experimental conditions 12-18).

As a final visualization of the population activity, the average pairwise trajectory distance matrix was reduced to two dimensional space using multidimensional scaling (MDS). The result of this operation is shown in Figure 4.4. A good quality of fit was ensured by examining the correlation between the original pairwise distances and the pairwise distances of the coordinates resulting in the MDS space. In Monkey X (Monkey L) these distances had a Pearson's r value of 0.88 (0.86). These values indicate that the visualization is a relatively good low dimensional representation of

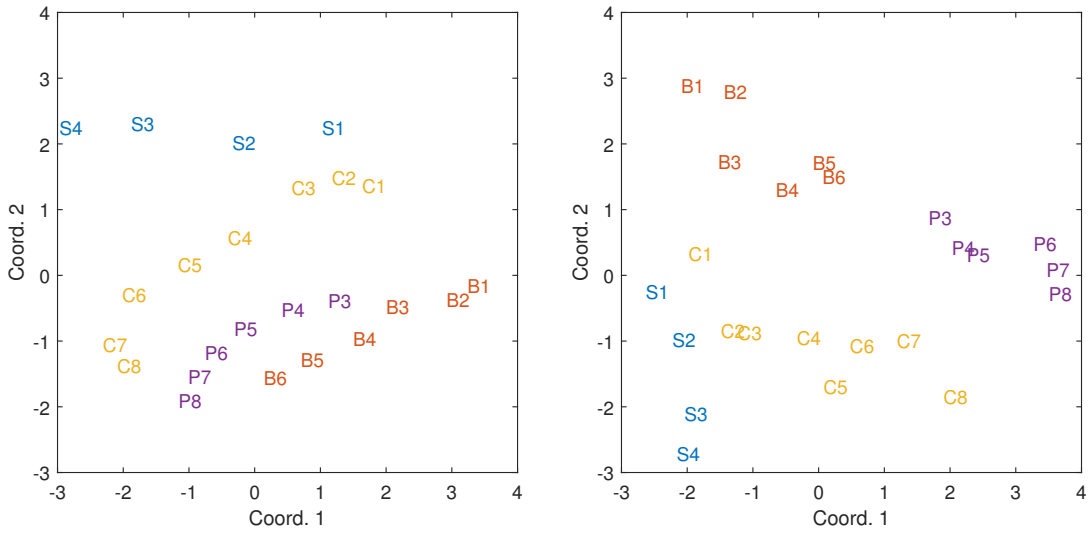

Figure 4.4: Multidimensional scaling of average neural trajectories for Monkey X (left) and Monkey L (right). A 2-dimensional representation of average neural trajectories was found through multidimensional scaling. Each of the points corresponds to a different experimental condition representing a combination of an object (S = sphere, B = push button, C = coax. cyl., P = perp. cyl) and a location (1-8).

the data.

The reduced dimensional representation produced by MDS confirms largely what was observed in the visualizations produced by PCA. Experimental conditions appear largely to be grouped primarily by grasp type and then secondarily by reach location. We also see that the smooth relationship of distance between reach trajectories is generally preserved in each of the grasp specific clusters. MDS also confirms that reaches to one location are largely similar across objects. For example, in both monkeys we see in Fig. 4.4 that reaches to the same location are generally close together despite being primarily clustered by object.

4.3.2 Classification by Neural Populations

The previous visualization of the averaged neural trajectories appear to indicate the presence of a substantial degree of structure and separability suggesting that both classification of reach and grasp should be possible. We examined two different paradigms for classification of population activity:

1. Global classification: A single classifier is trained on data from all time bins. Performance is then evaluated with data from all time bins.

2. Local classification: Multiple classifiers are trained, each one using data exclusively from a single time bin. Performance for each classifier is evaluated data from the bin it was trained on.

As we are using simple LDA classifiers, the difference in performance between global and local classifiers may be seen as an indicator of the complexity of the boundary between neural trajectories of different conditions. In general, we would expect the local classifiers to have better performance than the global classifier. This is because the local classifiers are better able to fit localized trends in the data than a single global classifier. One exception to this is that local classifiers may have poorer performance than the global classifier in situations where the local classifier overfits the training data due to insufficient data for reasonable parameter estimates. A large difference between the local and global classifier performance would suggest boundaries are highly nonlinear, whereas small distance would indicate the boundaries

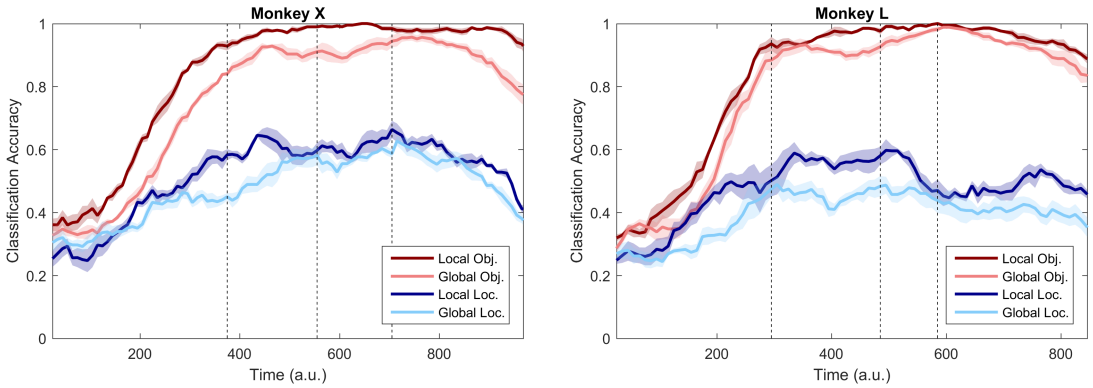

Figure 4.5: Classification accuracy of object and location decoding for each monkey. Dashed vertical lines correspond to average time-rescaled occurrences of movement onset, object contact and switch closure. Performance is shown for local classifiers, which were trained and evaluated on data from the same time bin, and global classifiers, which were trained on data from the entire trial and evaluated on data from each time bin.

between classes are not changing substantially over time.

For each monkey, classification was performed independently for decoding object and location. The performance of these classifiers is shown in Fig. 4.5. Three objects and four locations were assessed resulting in chance classification accuracy of 33% and 25%, respectively. Several trends were evident and consistent across both monkeys. Classification of grasp performed significantly better than classification of location. Local classifiers had better classification accuracy than the global classifier. On a point-by-point basis, local classifiers tended to outperform global classifiers.

Object decoding was assessed in terms of classification accuracy. Monkey X achieved a maximum classification accuracy of $100\% \pm 0$ for local classifiers and $95.7\% \pm 1.1\%$ for the global classifier. Monkey L achieved a maximum classification accuracy of $100\% \pm 0$ for local classifiers and $98.8\% \pm 0.3\%$ for the global classifier.

Location decoding was similarly assessed in terms of classification accuracy. Monkey X achieved a maximum location classification accuracy of $66.3\% \pm 2.8\%$ for local classifiers and $62.7\% \pm 1.5\%$ for the global classifier. Monkey L achieved a maximum location classification accuracy of $59.7\% \pm 3.5\%$ for local classifiers and $48.9\% \pm 24\%$ for the global classifier. Differences in maximum classification accuracy for both object and location were significant in Monkey L (paired t-test, $p < 0.05$) but not Monkey X.

Classification accuracy alone does not provide the full picture of decoding performance for decoding location. In further assessing the performance of location decoding, we analyzed performance in terms of a cost function. A simple linear cost function was chosen. If the classifier correctly classified the location, there were 0 units of cost incurred. If the classifier incorrectly chose an adjacent location, 1 unit of cost was incurred. Classifying to the next location even further out incurred 2 units of cost and so on. This difference in evaluations was necessary as we would generally consider a near miss during a reach to be better than missing by an especially large margin. In the space of grasping, if an incorrect class of grasp is performed, it is difficult to generally quantify just how close the incorrect grasp was to the intended grasp.

Monkey X achieved a minimum mean cost of 0.40 ± 0.04 for the local location classifiers and 0.43 ± 0.02 for the global location classifier. Monkey L achieved a minimum mean cost of 0.44 ± 0.04 for the local location classifiers and 0.58 ± 0.04 for

the global location classifier. This difference in location decoding performance was not significant in monkey X but was significant in monkey L ($p < 0.05$).

4.3.3 Temporal Generalization

We observed in the previous section that local classifiers did outperform global classifiers, though the effect size seemed somewhat small. To better understand the nature of the dynamics in the population code, we examined the concept of temporal generalization. Analysis of temporal generalization makes use of the local classifiers trained on data from a single time bin. Each classifier's performance is then evaluated on data from all other time bins. Unlike the previous section, we are interested in observing how performance falls off as data is provided from temporally distant regions. For the purposes of analysis of temporal generalization, classification performance was of grasping was measured in terms of classification accuracy while classification performance of grasping was measured in terms of the previously mentioned average linear cost.

Temporal generalization metrics were arranged into generalization matrices as shown in Fig. 4.6, where the main diagonal reflects the optimal performance of a classifier evaluated on data from the same time bin it was trained on. This performance is identical to the *local* performance shown in Fig. 4.5. The off-diagonal elements are more of interest, however. Elements above the diagonal represent performance on time bins later than when the classifier was trained. Similarly, elements

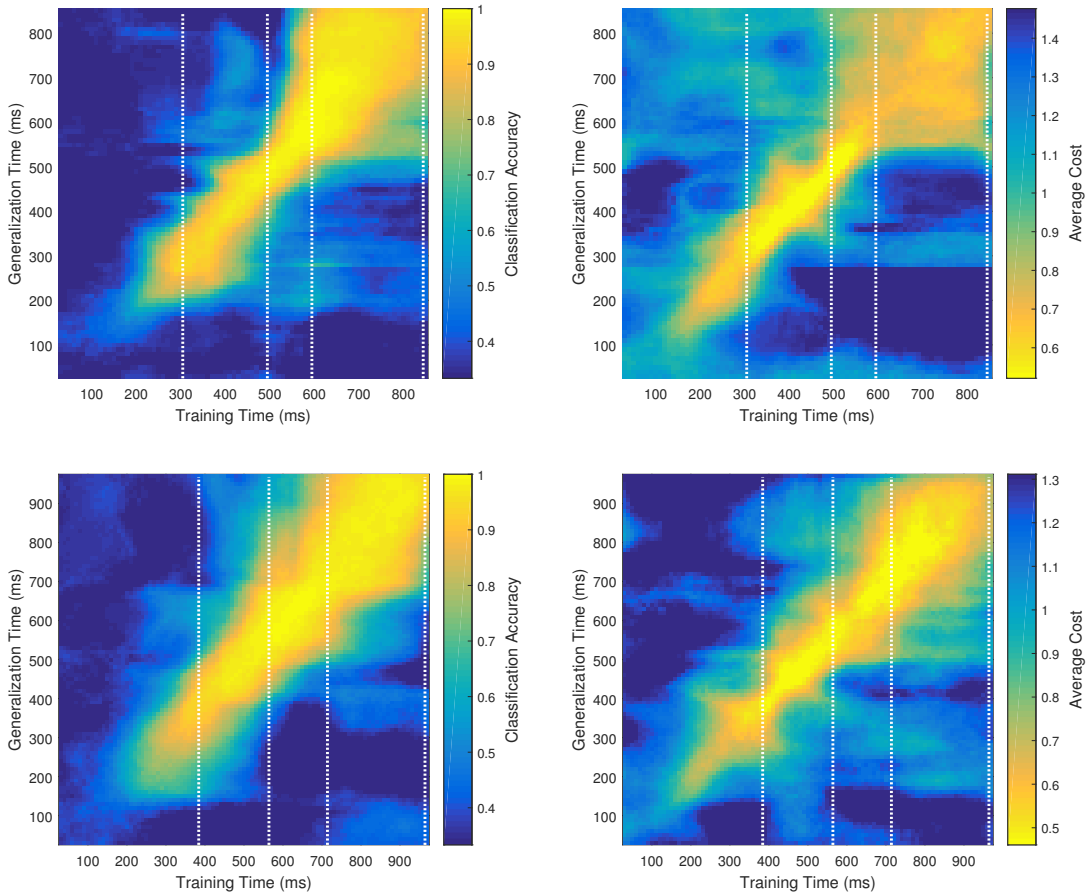

Figure 4.6: Generalization matrix for classification of grasp shape (left) and reach location (right) in monkey L (top) and monkey X (bottom). Each column of this matrix indicates the classification accuracy of an LDA classifier trained in one time period when this classifier is evaluated on data from all time periods. The main diagonal indicates optimal classification performance while the off-diagonal region indicates generalization performance across time. The three vertical lines correspond to the average times of onset of movement, object contact, and switch closure. The pattern here suggests information about grasp becomes available just before onset of movement and is dynamically represented before switch closure. After switch closure there is evidence of the emergence of a more stable code.

below the diagonal represent performance on time bins prior to the training of the classifier.

The temporal generalization matrices exhibited several trends common to both

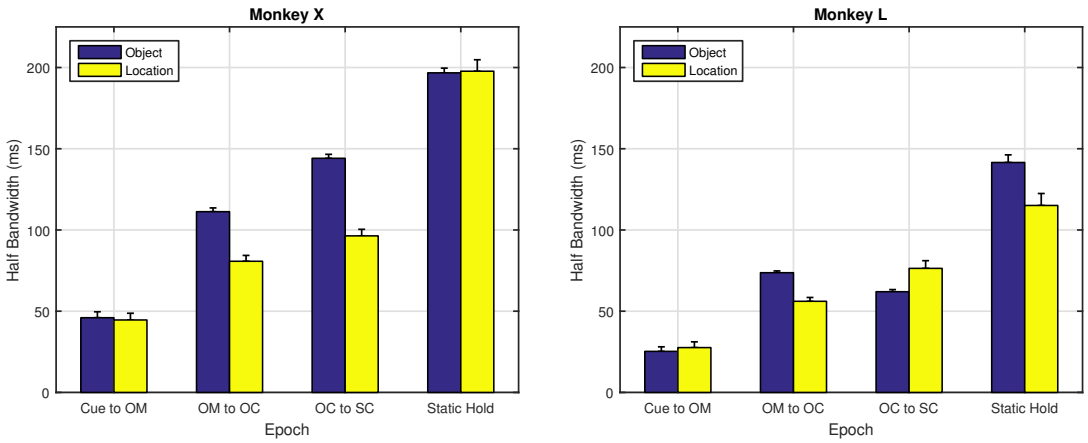

Figure 4.7: Half bandwidth of temporal generalization performance for both monkeys in each experimnental epoch. Half bandwidth here indicates the average time for a specific classifier's performance to decline from peak accuracy to 70.1% of peak accuracy. Half bandwidth was used because the rolloff was not always symmetric and bandwidth was taken as the minimum time elapsed on either side of the peak. Each bar represents the average half bandwidth within the epoch and error bars indicate standard error.

monkeys. In general, for both reach and grasp decoding, the generalization matrices showed a banded structure that began just prior to onset of movement and continued throughout the remainder of the trial. The width of this band may be thought of as an approximation to the temporal relevance of the population code at any point in time. Specifically the bandwidth can be thought of as the range over which the classification rules learned in that instant are still relevant. We observed that, relatively speaking, the bandwidth was smallest prior to movement and gradually broadened over the remainder of the movement. The average bandwidth during each experimental epoch is shown in Fig. 4.7.

The bandwidth broadened substantially during the static hold period indicating that the degree of change of the population dynamics had reduced and a more stable

code was present. This narrow banded structure broadens significantly after switch closure, indicating that the encoding of reach and grasp is more stable during this period. Additionally, taken in consideration with the results shown in Fig. 4.5 and Fig. 4.1, this period also exhibits a slow decline in classification performance that appears to correspond to a gradual decline in the separability of the class-conditional signals. This suggests that population activity appears to slowly converge toward a baseline state.

4.3.4 Individual Unit Performance

In order to examine dynamic coding at the scale of individual units, we evaluated the grasp classification performance of each unit individually. For each unit, separate LDA classifiers were trained for each time bin. Five fold cross-validation was applied and performance was evaluated on data from the holdout set from the same bin the classifier was trained on. Classification was measured in a manner identical to the optimal local classifier performance from previous sections.

The results of this classification analysis are shown in Fig. 4.8. In both monkeys, the time course of classification accuracy for individual units showed unimodal characteristics. Individual units also showed a wide range of preferred times, with most having peak classification performance sometime after the onset of movement. When considering the population-averaged individual unit classification performance, monkey X showed peak performance between switch closure and static hold while monkey

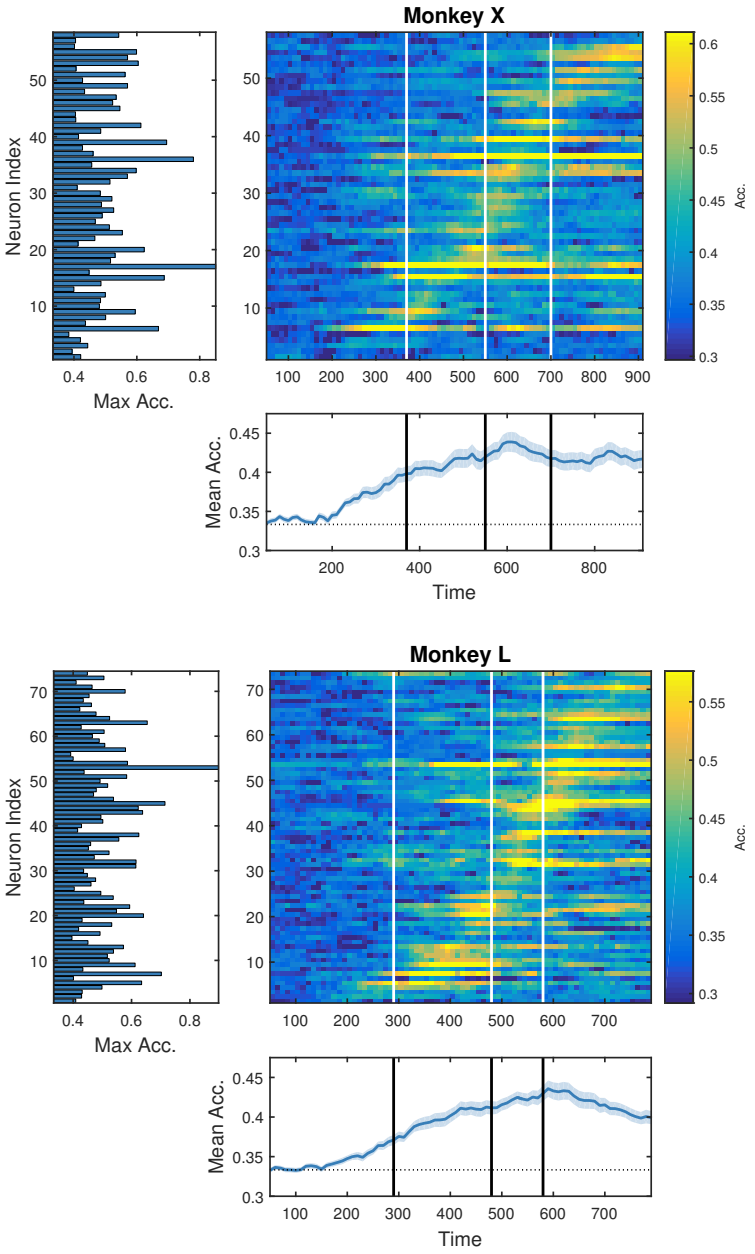

Figure 4.8: Individual unit classification performance for both monkeys on object classification. Each plot shows performance of classifier trained on individual unit. Units were sorted by order of peak accuracy (upper right). The average individual unit performance (shaded region ± standard error) is shown below. Left panel indicates maximum classification accuracy for each of the units.

L had peak performance shortly after switch closure.

While units did generally indicate a range of preferred times for maximal classification performance, there was substantial variation in the maximal classification accuracy as seen in the left panels of Fig. 4.8. The period of relevance for each unit also showed variation in that many units appear to have object-specific firing rate variation in small time windows while others demonstrate largely separable activity over longer periods. This variation is easily observed in the upper right panel of Fig. 4.8.

4.4 Discussion

In this chapter we applied several methods to examining the nature of neuronal population activity by spiking units in motor cortex and primary motor cortex during performance of a reach to grasp and manipulate task. We created smoothed estimates of firing rates that were temporally normalized to attempt to align event markers across trials and allow for comparisons across experimental conditions. These aligned trajectories were then used to examine lower dimensional projections of task-specific population activity. Classification analysis was performed to assess the presence of discriminative activity within the population as well as the temporal stability of this code at a population level. Finally classification analysis was performed at the level of individual units to gain further insight into the nature of the time varying population

code.

4.4.1 Dimensionality Reduction

Population trajectories observed in lower dimensional space are consistent with those seen previously in similar works [91, 108, 111, 114, 115]. The average trajectories for different experimental conditions exhibit apparent smooth structure in low dimensional space and appear to be largely monophasic in the first three principal components. Empirical analysis of the PCs along with dimensionality reduction through multidimensional scaling suggest a hierarchical structure to the trajectories primarily along grasp type and secondarily along reach location. In a recent study [116], a similar smooth variation in firing patterns in low dimensional space was observed for center-out reaches to different directions.

This separation observed in low dimensional space was reflected by the performance of population classifiers for reach and grasp. Classifiers readily achieved near-perfect classification of object type while having difficulties decoding reach location. This suggests that while there is apparent structure across trial averaged population trajectories, the signal to noise ratio across individual trials may be low. Another explanation could be that the observed units were more primarily involved in coding behavior related to the hand and wrist. An analysis of the separability of location based on joint angle in [117] indicated that much of the discriminating information about reach location was contained in shoulder angles as opposed to joint angles of

the hand and wrist.

4.4.2 Population Coding

Population performance was compared for global linear classifiers as well as sequences of linear classifiers. The sequence of piecewise linear classifiers approximates the behavior of a more complex non-linear classifier. Differences in performance between global and local classifiers could indicate significant deviations from linear separability and justify the use of more complex decoding approaches. In the case of Monkey L, local classifiers appear to result in slightly improved overall classification performance of both reaching and grasping. Monkey X showed little to no difference in decoding performance for the local versus global classifier. These results are not especially surprising given inspection of task-specific trajectories in Fig. 4.1, which seem to indicate that trajectories may generally be well separated by a hyperplane. Perhaps more revealing is that local classifiers did not dramatically improve decoding of reach location, again suggesting that classification performance is limited by noise or feature representation rather than the flexibility of the classifier.

Analysis of population coding by temporal generalization matrices indicated the presence of a dynamic code throughout much of the movement. Prior to the static hold period, locally trained population classifiers tended to be relevant only for 100-200 ms as shown in Fig. 4.7. A more stable code appeared to emerge during the static hold period, corresponding to a general abatement of kinematic activity. This stable

code appeared to begin just prior to switch closure and largely considered throughout the 250 ms of static hold period that was included in the analysis. This observation is similar to findings of another study that observed slowing of neural dynamics in motor cortex during the hold period of a center-out reach task [115].

4.4.3 Individual Unit Relevance

The dynamics expressed in the analysis of population classification suggest that individual units are relevant to the task for only brief periods of time. To investigate this further we examined the temporal patterns of classification performance by each of the individual units. We observed that many units appeared to provide discriminative information related to object type for only a brief period during each trial. Individual neurons exhibited a wide range of classification performance as shown in Fig. 4.8. There did not appear to be a clear relationship between the time offset of temporal relevance and overall maximum classification performance at the single unit level. While most units exhibited temporally localized discriminative information, some units in both monkeys were relevant over a more broad period of time. These units also appeared to have better discrimination performance overall.

This sequential activity has been observed in other domains and could potentially be explained as the activation of sequences of cell assemblies [118]. Similar sequences of activation have been observed in other brain areas including hippocampus [119], prefrontal cortex [120,121], and parietal cortex [99,122]. Within motor areas, however,

this sequential activity could also potentially be tied to the kinematics of the monkey performing the task [117].

The analysis of dynamics in this chapter provided some insight into the complex nature of coding of behaviors by neurons in the motor and premotor cortices. Neurons did not all contribute information about behavior equally or at the same time. With larger numbers of recorded neurons, there may be a need to select and decode using only the most relevant neurons in a population. The next chapter will address this issue along with providing another method for exploration of neuronal interactions within a population.

Chapter 5

Finding Co-modulated Communities of Neurons

5.1 Introduction & Background

When working with spiking data in the brain, we are interested in finding natural structure within the firing patterns of individual units as well as common structure across units. Researchers may be interested in finding cell assemblies that are broadly characterized as groups of neurons with similar firing properties [118, 123–127]. According to Donald Hebb [123], these assemblies were correlated with repeated co-activation or synchronous firing of neurons. This concept is remembered in the well known mnemonic: "Cells that fire together, wire together." Clustering techniques have previously been demonstrated as effective means for finding patterns of neu-

ronal activity in single unit and multi unit responses [128–130]. Similar approaches have been developed for detecting cell assemblies based on similar firing activity across units [126, 131–133].

Neurons may form other functional groups, however, that do not necessarily have correlated firing rates. In the motor cortex, neural activity has been shown to correlate to a number of external covariates including reach direction, hand position, joint angles, and muscle activity. Generating movement of the limb to reach for and grasp an object requires these external covariates to be coordinated. Though the exact means of how this is achieved at the cortical level is still unclear, evidence of coordinated physical behavior has been observed through movement synergies [53, 134, 135], muscle synergies [136, 137], evocation of complex multi-joint movements from stimulation [138, 139], and muscle synergies [140, 141].

Though physical activity may be coordinated, randomly sampled neurons involved in producing this coordinated activity may not necessarily have correlated firing activity. In general, the specific coding properties of a given neuron are unknown. Neurons may not be tuned to a single parameter or function, and neurons within a small volume may have heterogeneous firing properties [43, 44, 142]. Multiple neurons may be involved in control of the same limb but may each contribute differently. Additioanlly, neurons that are tuned to represent a given signal are not necessarily tuned linearly and may dramatically change their firing properties in association with small changes of the encoded signal [143]. A number of unsupervised methods are

useful for exploring the relationship between the neural activity and a behavior or stimulus [91, 116, 140, 144, 145].

In this chapter we develop a clustering-based method for identifying task-relevant neurons and co-modulated communities of neurons. We use cluster analysis to create partitions of single trial activity within individual spiking units. Partitions are chosen such that they are maximally similar to the natural variation across trials resulting from experimental design. A partition similarity measure is then applied to assess each unit's suitability for use in a classifier. Partitions are compared across neurons to identify groups of neurons with firing patterns that tend to modulate in response to a common external variable. This approach allows us to identify units that may somehow interact functionally to produce a behavior while not necessarily having similar firing properties.

5.2 Methods

As in the previous chapter, we base our analysis on data collected from two rhesus macaques performing a simultaneous reach to grasp and manipulate task. Array implantation, signal acquisition, spike sorting, and experimental procedure are all as reported in Chapter 3. Briefly, in each monkey, single unit and multi unit spiking was recorded from floating microelectrode arrays implanted in ventral premotor cortex and motor cortex.

Spike times were first converted to binary spike trains with a sampling rate of 1 kHz. These spike trains were convolved with a boxcar function (width = 100ms) to produce an estimate of each unit's firing rate.

5.2.1 Time Rescaling

Firing rate estimates for each unit and each trial were temporally rescaled in order to be of equal length. We identified the mean duration across all trials of each of three experimental epochs: cue presentation to onset of movement, onset of movement to object contact, and object contact to switch closure. For each unit and each trial, linear interpolation was performed to rescale the firing rate in each epoch to the length of that epoch's average duration.

We define $\mathbf{X}^{(p)}$ as a $n \times m$ matrix of firing rates from the p^{th} individual unit. Each row vector $\mathbf{x}_i$ represents the firing of the unit over the i^th trial rescaled to m discrete bins.

5.2.2 Clustering Single Unit Activity

To perform clustering, we apply the K-means algorithm to the elements of the firing rate matrix $\mathbf{X}^{(p)}$. This clustering procedure is performed separately for each unit p.

The k-means algorithm consists of assignment and update steps performed itera-

tively in a method similar to the expectation maximization algorithm. The method is initialized by specifying a number of clusters, k, and randomly assigning k m-dimensional vectors, $\boldsymbol{\mu}_1, \boldsymbol{\mu}_2, ..., \boldsymbol{\mu}_k$, to serve as initial centroids.

In the assignment step, each vector of firing rates $\mathbf{x}_i$ is assigned to the group that minimizes the distance between the firing rate vector and the group's centroid, $\boldsymbol{\mu}$, according to some distance function $d(\cdot, \cdot)$:

$$\mathbf{s}_i = \arg\min_{k'} d(\mathbf{x}_i, \boldsymbol{\mu}_{k'}) \tag{5.1}$$

where $d(\mathbf{x}_i, \boldsymbol{\mu}_{k'})$ is some appropriate distance function and $\mathbf{s}_i$ is a k-dimensional binary vector with a single non-zero element indicating the group assignment of the i^{th} vector.

This procedure is performed for all the samples such that each firing rate vector is assigned to the cluster with the nearest centroid. A new centroid is estimated for each of the k clusters according to the mean of all the vectors in that cluster:

$$\boldsymbol{\mu}_j = \frac{1}{|C_j|} \sum_{\mathbf{x}_i \in C_j} \mathbf{x}_i \tag{5.2}$$

where $|C_j|$ is the cardinality of the j^{th} cluster and the sum is over all members belonging to that cluster.

The procedure then iterates by re-assigning each datapoint to clusters based on the new centroid values followed by updating estimates of the centroids following this

assignment. The iteration continues until the sum of distances between all points and their centroids converges and there are no further changes to cluster membership.

Due to the random initialization and the possible existence of local minima in the loss function, k-means will not necessarily close to a globally optimum configuration on a single iteration. Performance of k-means is sensitive both to the number of clusters chosen as well as the initial locations of the cluster centroids. To improve performance, we choose initial centroids according to the k-means++ algorithm [146].

The choice of distance function applied by k-means can dramatically affect the results. For clustering trials from an individual unit, we use cosine distance [128,147]. Cosine distance can be defined as

$$d(\mathbf{x}_i, \mathbf{x}_j) = 1 - \frac{\mathbf{x}_i \cdot \mathbf{x}_j}{||\mathbf{x}_i|| \cdot ||\mathbf{x}_j||} \tag{5.3}$$

where $\mathbf{x}_i$ and $\mathbf{x}_j$ are equal-length vectors of binned spike counts from neuron i and neuron j respectively. As the firing rates were always non-negative, the value of the second term ranged between 0 and 1. The distance measure then was bounded between 0 when firing rate vectors were identical and 1 when they were orthogonal.

5.2.2.1 Clustering Examples

To see the potential benefit of clustering single trials, consider the toy example presented in Fig. 5.1a. In this example, 500 repeated trials of 1000 ms length were sampled from a simulated neuron. The neuron was simulated such that it had two

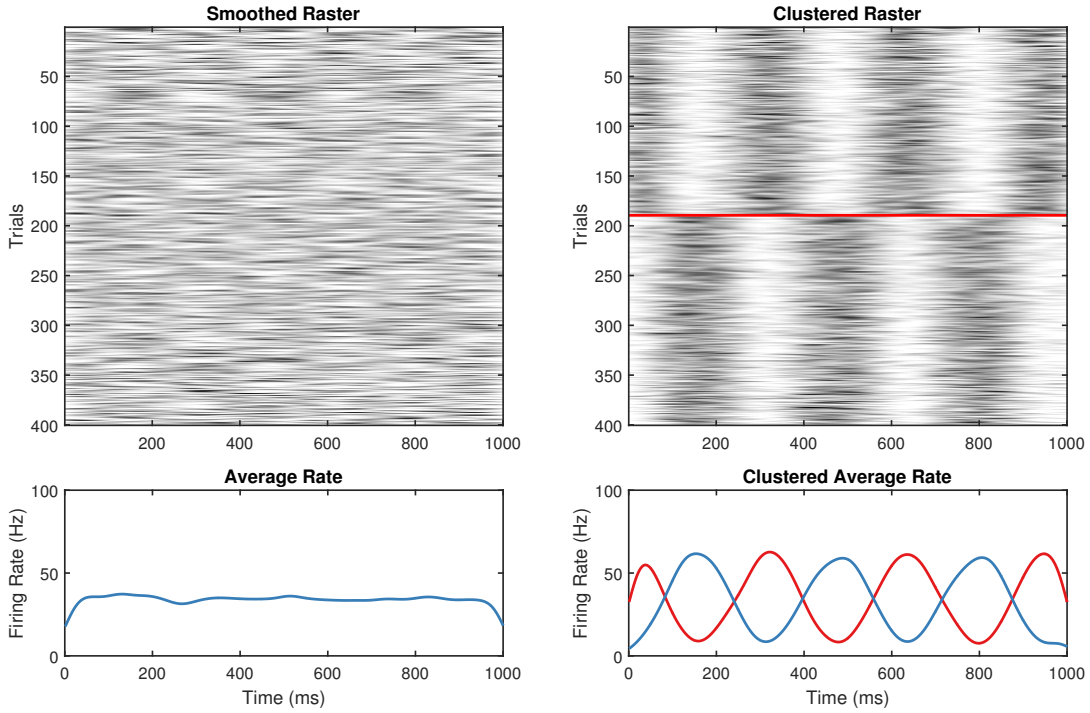

Figure 5.1: Clustering may reveal hidden structure. Here, simulated activity is shown from 500 1-second simulated trials of a neuron with constant firing activity. When trials are not grouped in any particular order (a, top), no trial-average structure is apparent (a, bottom). However, if a clustering algorithm is applied and trials are ordered by cluster (b, top), we may see apparent differences in trial-averaged activity (b, bottom).

behavioral modes. In both modes, the neuron had a sinusoidal firing rate with a fixed frequency. However, this signal was 180 degrees out of phase across the two modes. In Fig. 5.1a, we observe a simulated raster when the simulated trials are shown in the order they were produced and the neuron's mode was set randomly to one of the two states in each trial. The trial-averaged activity shown in the lower panel of Fig. 5.1a indicates the absence of any real patterned firing.

However, after applying the aforementioned clustering technique to the simulated

data with the number of clusters set to two, structure emerges. In Fig. 5.1b, the trials have been rearranged according to cluster membership and the presence of two stable oscillatory modes becomes apparent. This is confirmed by the cluster-specific trial averaged activity shown in the lower panel of Fig. 5.1b. In neuronal recording scenarios across repeated trials of varying conditions, this clustering technique may help to reveal structure that is not readily apparent from the original rasters alone.

However, as an example of the potential pitfalls associated with this clustering approach, consider the simulation shown in Fig. 5.2. In this second simulation, 500 trials of 1000 ms length were sampled from a simulated neuron. Unlike the previous example, however, the neuron only had one mode of operation. Spiking was generated with a uniform firing rate. The trial averaged firing rate shown in the lower panel of Fig. 5.2a is a good representation of this activity.

As in the previous simulation, single trial clustering was applied to this simulated activity. Here 5 clusters were chosen. Trials were grouped according to cluster assignment and visualized as in Fig. 5.2b. The clustering assignment appears to reveal significant structure indicating that this neuron had periods of phasic firing with different offsets. The differences between the cluster-specific activity are made more apparent in the cluster-averaged firing rates shown in the lower panel of 5.2b. Of course, this structure is spurious as the simulated neuron was set to spike with a constant firing rate. Trial clustering grouped trials that were similar purely by chance rather than differences in structure. This reveals one of the concerns of clustering:

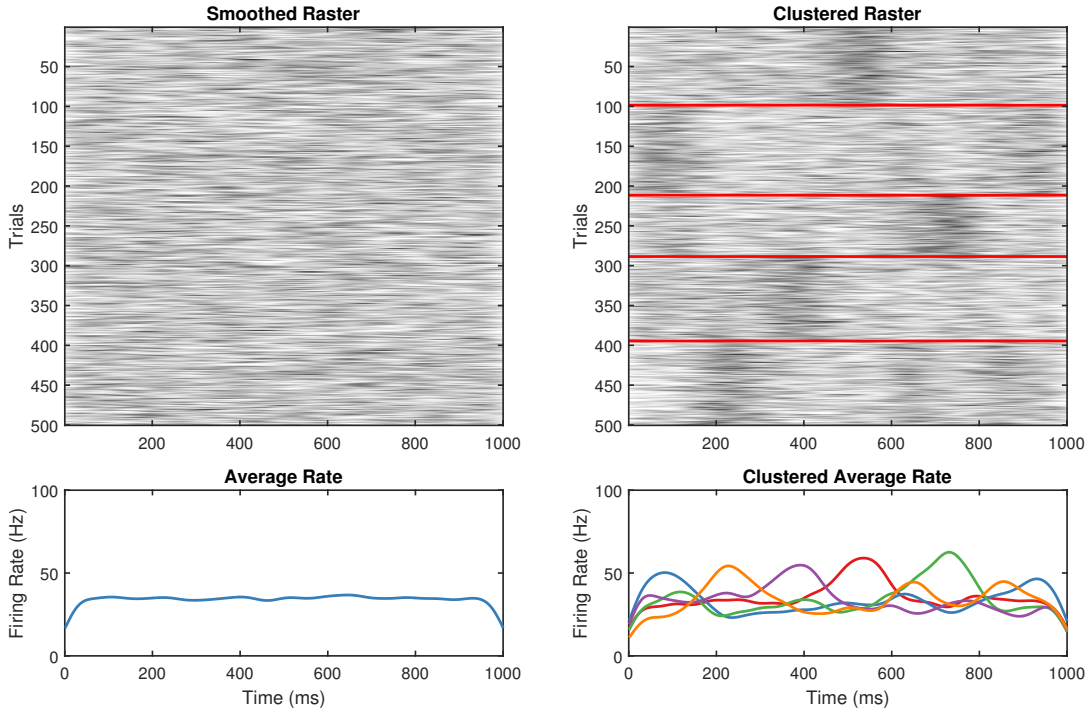

Figure 5.2: Clustering may erroneously detect structure where none exists. Here, simulated activity is shown from 500 1-second simulated trials of a neuron with constant firing activity. When trials are not grouped in any particular order (a, top), no trial-average structure is apparent (a, bottom). However, if a clustering algorithm is applied and trials are ordered by cluster (b, top), we may see apparent differences in trial-averaged activity (b, bottom). These apparent differences across clusters are not the result of structured variation but rather a byproduct of repeated random sampling.

finding structure when none actually exists. The following sections will present a potential solution to this problem by ensuring that structure found by clustering is similar to structure expected from experimental design.

5.2.2.2 Comparing Partitions

There are many ways to divide a finite set of units into groups. We define any given division of a set of units into groups as a partition. We refer to divisions within a partition as clusters or groups. Thus a number of trials may be assigned to form a coherent group and any division of all the trials into groups is referred to as a partition. In this study we will be interested in a measure of similarity between any two partitions. To quantify the consistency of group membership over task conditions, we computed the normalized mutual information (NMI) [148,149] between partitions. As the name suggests, this is simply the mutual information between two partitions that has been normalized such that it takes on values in the range of 0 to 1. Formally, mutual information between two random variables X and Y is defined as:

$$I(X;Y) = \sum_{x,y} p(x,y) \log \frac{p(x,y)}{p(x)p(y)} \tag{5.4}$$

This quantity represents the reduction in uncertainty of the value of X due to knowledge of Y [150]. This quantity is bound according to

$$0 \leq I(X;Y) \leq \min(H(X), H(Y)) \tag{5.5}$$

where $H(X)$ and $H(Y)$ are the entropy of X and Y, respectively. To facilitate more general comparison among partitions, this quantity is commonly normalized to form the normalized mutual information:

$$NMI(X,Y) = \frac{2I(X;Y)}{H(X) + H(Y)} \tag{5.6}$$

For some intuition behind this value, consider a set of items and two identical partitions of these items, $\mathcal{A}$ and $\mathcal{B}$. If we draw an item at random and are not told anything about the item other than the cluster it belongs to in partition $\mathcal{A}$, we still know with certainty the cluster it belongs to in partition $\mathcal{B}$. The NMI in this case is 1. Now imagine that we modify partition $\mathcal{B}$ by swapping a few items randomly between groups. This has introduced some uncertainty into the system. Now if we choose a random item and are told its group membership in $\mathcal{A}$, we are no longer fully certain which group that item belongs to $\mathcal{B}$. The NMI in this case is less than 1 and will continue to decrease if we continue randomly swapping items between groups in either partition. After some number of swaps, the partitions may become completely independent; knowing the group membership of a random item in $\mathcal{A}$ tells us nothing about its group membership in $\mathcal{B}$. In this instance, the NMI between $\mathcal{A}$ and $\mathcal{B}$ is 0.

To actually calculate NMI between two arbitrary partitions $\mathcal{X}$ and $\mathcal{Y}$, we create an $n_X \times n_Y$ contingency table $\mathbf{N}$, where n_X and n_Y are the number of groups in each of the partitions. Table values $\mathbf{N}(i,j)$ are set to the cardinality of the intersection of the i^{th} group in $\mathcal{X}$ with the j^{th} group in $\mathcal{Y}$. This table is then normalized such that the sum of all entries is 1. We refer to this normalized matrix as $\mathbf{P_{xy}}$. Entries of this matrix now corresponds to values of the joint probability distribution, $p(x,y)$, over cluster assignments across the two partitions. The vectors of marginal probabilities

of group membership, $\mathbf{p_x}$ and $\mathbf{p_y}$, for the two partitions are found according to the row sums and column sums of $\mathbf{P_{xy}}$, respectively.

To compute NMI, we must first use this table to calculate the mutual information, $I(X;Y)$, which can be defined as:

$$I(X;Y) = H(X) + H(Y) - H(X,Y) \tag{5.7}$$

where

$$H(X) = \sum_{i=1}^{n_X} \mathbf{p_x}(i) \log \mathbf{p_x}(i) \tag{5.8}$$

$$H(Y) = \sum_{j=1}^{n_Y} \mathbf{p_y}(j) \log \mathbf{p_y}(j) \tag{5.9}$$

$$H(X,Y) = \sum_{i=1}^{n_X} \sum_{j=1}^{n_Y} \mathbf{P_{xy}}(i,j) \log \mathbf{P_{xy}}(i,j) \tag{5.10}$$

These quantities are then plugged back into Eq. 5.6 in order to produce the estimate of NMI between partitions.

5.2.2.3 Selecting the number of clusters

In any application of k-means clustering, the number of clusters k is a free parameter that must be externally specified. Failing to evaluate the quality of fit of a particular number of clusters may result in detection of spurious clusters. In such

cases, as in the simulated data in Fig. 5.2, structure may be found in data where none actually exists. Typically, various values of k are evaluated by repeating the procedure over a range of values. The optimal number of clusters is commonly chosen as one that optimizes some heuristic, such as the silhouette value [151] or the gap statistic [152].

In this application, we have reason to believe that there will be some inherent structure in single trial clustering due to the repetition of trials within experimental conditions and the highly-trained states of the monkeys. We would expect in general that trials from a single experimental condition would have similar firing patterns and would tend to be assigned to the same cluster. With this in mind, we incorporated this expectation into our procedure for choosing k. Simply, we will choose the value k that maximizes the NMI between the clustering of single trials and the natural partition defined by experimental conditions.

For each unit, p, we varied the number of clusters, k, from 2 to 10 and performed k-means each time. We refer to the resulting partition of trials from the p^{th} unit with k clusters as $\mathcal{R}_k^{(p)}$. We created a separate fixed partition of the trials according to the known experimental conditions. Each of the location and object combinations was assigned to a separate group. Thus the experimental conditions partition divided the trials into 24 groups. We refer to this partition by experimental conditions as $\mathcal{S}$.

For each of the $\mathcal{R}_k^{(p)}$ partitions, we calculated the similarity to the experimental condition partition as $NMI(\mathcal{R}_k^{(p)}, \mathcal{S})$. However, since we are varying the value k, we

must account for a baseline similarity that may occur due to chance. We define a random partitioning of the trials into k clusters as $\mathcal{Q}_k$. Thus instead of attempting to maximize $NMI(\mathcal{R}_k^{(p)}, \mathcal{S})$ directly, we wish to choose k that maximizes the difference in similarity as compared to a random partition. We define this as:

$$\Delta NMI(\mathcal{R}_k^{(p)}, \mathcal{S}) = NMI(\mathcal{R}_k^{(p)}, \mathcal{S}) - \mathbb{E}\left[NMI(\mathcal{Q}_k, \mathcal{S})\right] \tag{5.11}$$

where $\mathbb{E}\left[NMI(\mathcal{Q}_k, \mathcal{S})\right]$ denotes the expected NMI due to a random partitioning of trials into k clusters. We approximated this baseline expectation by creating 20 random partitions for each k value and taking the average over all the resulting $NMI(\mathcal{Q}_k, \mathcal{S})$ values.

For each number of clusters k, we performed 20 repetitions of the k-means procedure and calculated the average value for $\Delta NMI(\mathcal{R}_k^p, \mathcal{S})$. This repetition is necessary since k-means is a stochastic procedure with final results dependent upon an initial random initialization. The optimal value for k corresponded to the number of clusters that had the largest average delta value. Of the 20 repetitions, we kept the partition that maximized $\Delta NMI(\mathcal{R}_k^p, \mathcal{S})$ for the optimal k value. This optimal partition for unit p is referred to as $\mathcal{R}^p$. An example of these values is shown for a single unit in Fig. 5.3.

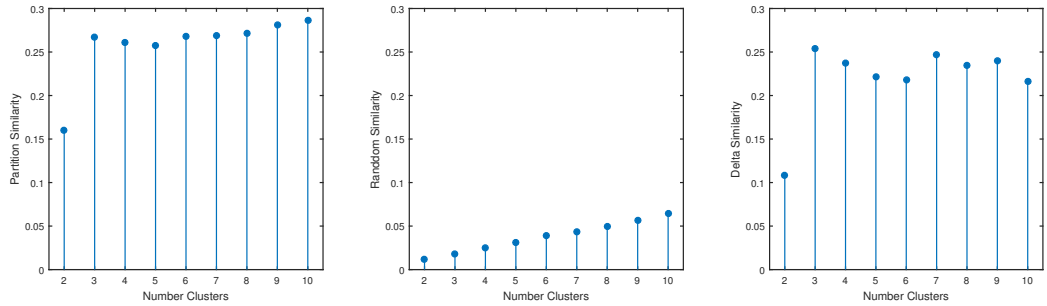

Figure 5.3: Example of cluster selection procedure. This unit from array J in monkey L shows an average initial partition similarity (left) with a maximum value at 10 clusters. However, average partition similarity due to chance (middle) increases as a function of the number of clusters. When this factor is accounted for by subtraction, a new peak is revealed in the delta similarity (right), suggesting the optimal number of clusters for this unit is 3.

5.2.2.4 Partition Similarity to Known Labels

Once the optimal partition of trials, $\mathcal{R}^p$, was found for each unit we evaluated the similarity of the partition to known experimental labels. We previously created a partition $\mathcal{S}$ that assigned each trial to one of 24 groups corresponding to the experimental condition. In addition to this, we created partitions $\mathcal{S}_{obj}$ and $\mathcal{S}_{loc}$ that partitioned trials based on the object grasped or the location of the object, respectively. We then calculated the similarity of the partition based on spiking with each of these two partitions as:

$$NMI^p_{obj} = NMI(\mathcal{R}^p, \mathcal{S}_{obj}) - \mathbb{E}\left[NMI(\mathcal{Q}^p, \mathcal{S}_{obj})\right] \tag{5.12}$$

$$NMI^p_{loc} = NMI(\mathcal{R}^p, \mathcal{S}_{loc}) - \mathbb{E}\left[NMI(\mathcal{Q}^p, \mathcal{S}_{loc})\right] \tag{5.13}$$

where $\mathcal{Q}^p$ represents a random permutation of the cluster assignments of $\mathcal{R}^p$. As in eqn. 5.11 the second term here is a correction for similarity due to chance. By creating instances of $\mathcal{Q}^p$ through permutations of the group labels in $\mathcal{R}^p$, we preserve the number of clusters as well as the cluster cardinality while largely eliminating meaning from the individual cluster assignments. The expected random similarity was estimated by evaluating the random similarity over 20 repetitions and taking the average.

Since a larger NMI value corresponds to larger concordance between a pair of partitions, we expect that units with large NMI_{obj} values have significant inherent firing rate modulation related to object type and units with large NMI_{loc} have significant inherent firing rate modulation related to reach location.

5.2.3 Classification

To evaluate the claim that NMI_{obj} and NMI_{loc} are indicative of natural task-modulation, we perform a classification analysis. Here we implement a naive bayes classifier. Naive bayes is a generative classifier that models each input feature as being independent from the other input features. More formally, for an observation of a D-dimensional feature vector $\mathbf{x}$, the joint conditional distribution over $\mathbf{x}$ given the sample was drawn from class c is:

$$p(\mathbf{x}|y=c) = \prod_{j=1}^{D} p(x_j|y=c) \tag{5.14}$$

As with many generative classification model, selection of the final class is chosen as the class that is most probable according to a posterior distribution $p(y|\mathbf{x})$. This posterior distribution can be found from the class-conditional likelihood distribution through application of Bayes Rule:

$$p(y=c|\mathbf{x}) = \frac{p(y=c)p(\mathbf{x}|y=c)}{\sum_{c'} p(y=c')p(\mathbf{x}|y=c')} \tag{5.15}$$

where $p(y=c)$ is the prior probability of class c. In our case we assume a uniform prior over all classes.

The features for our classifier are the vectors of unit-specific cluster assignments resulting from the observed firing activity of single trials. As an example, assume a partition $\mathcal{R}^{(p)}$ consisting of 4 clusters. The feature vector from a trial belonging to cluster 3 would be represented as [0, 0, 1, 0]. Given this structure, a natural choice for each unit's class conditional distribution, $p(x_j|y)$, is the categorical distribution. The categorical distribution is a generalization of the bernoulli distribution to events where one (and only one) of K outcomes is possible.

Here, the class-specific likelihood for each unit was estimated as a K-dimensional categorical distribution where K was the number of clusters in that unit's partition. Estimation of the class-specific categorical distributions for each neuron consisted of

isolating the trials for a given class (specific object or reach location) and finding the proportions of those trials that were assigned to each of the K clusters. For the i^{th} unit, the probability of observing a sample from the j^{th} cluster during the performance of condition c' was estimated as:

$$p(x_i = j|y = c') = \frac{N_{j|c'}}{N_{c'}} \tag{5.16}$$

where $N_{c'}$ is the number of trials in the training set characterized as belonging to class c' and $N_{j|c'}$ is the subset of these trials assigned j^{th} cluster for unit i.

This procedure was performed separately for each individual unit (ensemble size of 1), as well as for varying cardinalities of ensembles of units. For an ensemble of a given cardinality, units were recruited into the ensemble randomly without replacement from a pool of all the units. Each unit's probability of being selected into the ensemble was based on one of three different selection procedure according to their respective NMI_{obj} or NMI_{loc} scores:

1. Uniform selection: Units were chosen with uniform probability

2. Proportional selection: Units were chosen with probability proportional to their partition similarity score relative to the scores of the remaining members of the pool

3. Inverse proportional selection: Ensemble members were chosen with probability inversely proportional to their partition similarity score relative to the scores of

the remaining members of the pool

Classification performance was assessed by classification error. This procedure was performed both for classification of object type as well as reach location. For each ensemble cardinality we repeated the ensemble selection and classification procedure 500 times.

5.2.3.1 Clustering by Inter-unit Similarity

Following the line of reasoning that units with large NMI_{obj} values show natural modulation with changes in object type, we might further expect that pairs of units with large NMI_{obj} values would also have partitions similar to one another. We may also observe pairs of units with similar partitions that do not have significant NMI_{obj} or NMI_{loc} values. This might indicate an additional external variable not directly related to object type or location causing systematic modulation of certain units across trials.

For each pair of units i and j we define the inter-unit similarity as:

$$NMI_{unit}^{(i,j)} = NMI(\mathcal{R}^{(i)}, \mathcal{R}^{(j)}) - \mathbb{E}\left[NMI(\mathcal{Q}^{(i)}, \mathcal{Q}^{(j)})\right] \tag{5.17}$$

As before, we correct for similarity in clustering due to chance by creating multiple random permutations of $\mathcal{R}^{(i)}$ and $\mathcal{R}^{(j)}$, denoted $\mathcal{Q}^{(i)}$ and $\mathcal{Q}^{(j)}$. The observed chance similarity was again evaluated over 20 random permutations and subtracted from the

observed inter-unit similarity.

Once $NMI_{unit}^{(i,j)}$ was calculated for all pairs of units, we formed these values into a $n \times n$ matrix. Each row, i, represents the similarity of a given unit's partition, $\mathcal{R}^{(}\rangle)$, to the partitions of each of the other units. We may think of think of this matrix as consisting of n observations in n-dimensional space. We applied the k-means procedure to this matrix to evaluate the potential presence of co-modulated communities of units. Here, the number of clusters, k, was varied between 1 and 5 and the distance between samples was taken as the squared euclidean distance between vectors of NMI_{unit} values. Partition quality was assessed empirically by reordering the matrix of NMI_{unit} values according to cluster membership and inspecting the reordered matrix for apparent structure. In this context, structure would be indicated by members of a cluster having similar feature vectors. In both monkeys, clustering units by inter-unit similarity showed significant signs of over-clustering for k greater than 5 and thus higher numbers of clusters were not considered.

5.3 Results

This analysis was applied to data collected from two rhesus macaques (monkey X and monkey L) performing the reach to grasp and manipulate task described previously in Chapter 3. We included data from trials performed to each of the 24 tested experimental conditions consisting of certain combinations of reaches and grasps to

4 different objects located at 8 different locations. All 24 observed experimental conditions were included in the analysis resulting in inclusion of 690 trials for monkey L and 764 trials for monkey X.

Analysis of data from each trial was limited to the period from cue presentation to 250 ms following switch closure. All spiking units included in the analysis had an average firing rate during this period of at least 3 Hz. This resulted in inclusion of 74 units for monkey L and 58 units for monkey X.

Spike trains were converted to firing rate estimates by convolution with a gaussian kernel with standard deviation of 25 ms. For each monkey, data from all trials was temporally rescaled to be of uniform length with an approximately 1 kHz sampling rate. The rescaling procedure produced trials of 967 samples each for monkey X and 846 samples each for monkey L. The mean and standard error of trial length distortion (absolute difference in number of samples between original and time-rescaled trials) was 136 ± 5.4 samples for monkey X and 110 ± 4.4 samples for monkey L. The magnitude of the firing rate estimates was not standardized or rescaled.

5.3.1 Basic clustering results

For each unit, k-means clustering was performed on the time-rescaled firing rate vectors from each trial. Distance between trials was assessed as the cosine distance between their respective firing rate vectors. A range of values for k was tried ranging from 2 to 10 and the optimal k value was chosen following the procedure described

in the methods section. After identifying the optimal number of clusters, k', in a partition, the best instance among examined partitions with k' clusters was chosen as the partition $\mathcal{R}$ with maximal similarity to partitioning trials according to the 24 experimental conditions, $\mathcal{S}$.

Trials that did not contain any spiking activity were excluded from the single trial cluster analysis. These trials have a constant firing rate of zero and thus have an undefined cosine distance with other signals. The clustering procedure was performed using the remaining trials and excluded trials were assigned randomly to the identified clusters.

The mean number of clusters in each unit's optimal partition was 5.0 ± 0.4 in monkey X and 5.8 ± 0.3 in monkey L. The median number of clusters was 4 in monkey X and 6 in monkey L.

5.3.2 Unit-task partition similarity

After identifying the optimal partition for each unit, partition similarity was calculated between the unit's spiking-based partition and the label-based partitions $\mathcal{S}_{obj}$ and $\mathcal{S}_{loc}$. These values are shown for each unit in Fig. 5.4. Additionally the array-wise averages for $NMI(\mathcal{R}, \mathcal{S})$ are documented in Table 5.1.

Examination of these results shows several notable trends. Some of the largest overall similarity values between partitions based on spiking and experimental conditions are observed in arrays F, G, and H in monkey X and arrays H, I, and J in

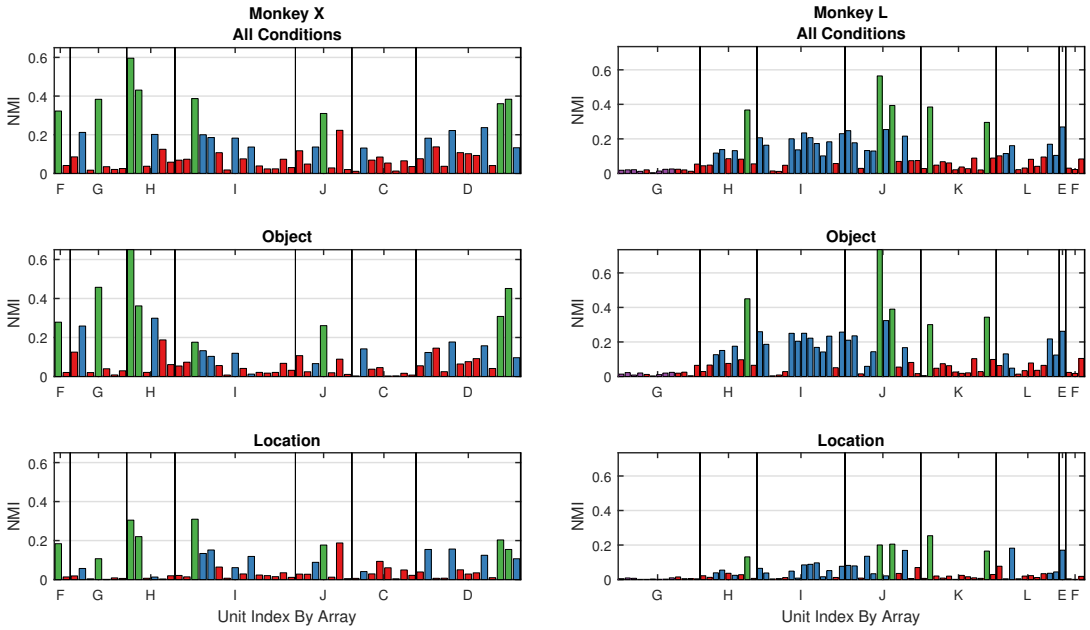

Figure 5.4: Similarity between unsupervised single trial partitions and ground truth partitions for object and location. Each bar represents a single unit and the similarity between partitions found via clustering and partitions based on object structure. Bars are grouped according to the electrode array they belonged to as described in Chapter 3. Divisions between electrode array memberships are indicated by vertical bars. Similarity between these partitions was evaluated using Normalized Mutual Information (NMI). Bars are colored according to each unit's cluster membership based on inter-unit NMI.

Table 5.1: Average unit-task partition similarity by array

Monkey X				Monkey L			
Array	Loc.	Cnt.	$NMI(\mathcal{R},\mathcal{S})$	Array	Loc.	Cnt.	$NMI(\mathcal{R},\mathcal{S})$
E	M1	0	$--\pm--$	G	M1	13	0.021 ± 0.003
F	M1	2	0.182 ± 0.141	H	M1	9	0.119 ± 0.033
G	M1	7	0.111 ± 0.052	I	M1	14	0.140 ± 0.021
H	M1	6	0.241 ± 0.092	J	M1	12	0.197 ± 0.045
I	M1	15	0.108 ± 0.026	K	M1	12	0.097 ± 0.034
J	M1	7	0.126 ± 0.041	L	M1	10	0.092 ± 0.016
C	PMv	8	0.058 ± 0.014	E	PMd	1	$0.269 \pm --$
D	PMv	13	0.162 ± 0.031	F	PMd	3	0.046 ± 0.019

monkey L. By comparing these array locations as shown in Chapter 3, these results are consistent with what we might expect to see a priori. Specifically, these arrays just

medial of the superior precentral sulcus seem to show significant modulation related to reach and grasp. Additionally, we see that NMI_{obj} is generally larger than NMI_{loc} suggesting that most of the observed neurons are likely to be more strongly tuned for variations in object type than they are tuned for variations in reach location.

5.3.3 Classification performance

We examined whether the unit-task partition similarity measures could be useful in informing feature selection for classification tasks. To evaluate this we constructed naive Bayes classifiers using randomly chosen ensembles of units. For each ensemble size we performed 500 repetitions for each of three different ensemble selection strategies. The results of the classification analysis are shown in Fig. 5.5.

We observe from these results that our intuition was correct and preferentially choosing neurons with high unit-task similarity values results in improved classification performance versus random selection. Additionally we observed that intentionally selecting units with low unit-task similarity values resulted in classification performance worse than classifiers consisting of units chosen at random. This result further emphasizes the suitability of this approach for feature selection. These trends persisted across classification of both object type and reach location in datasets from both monkeys.

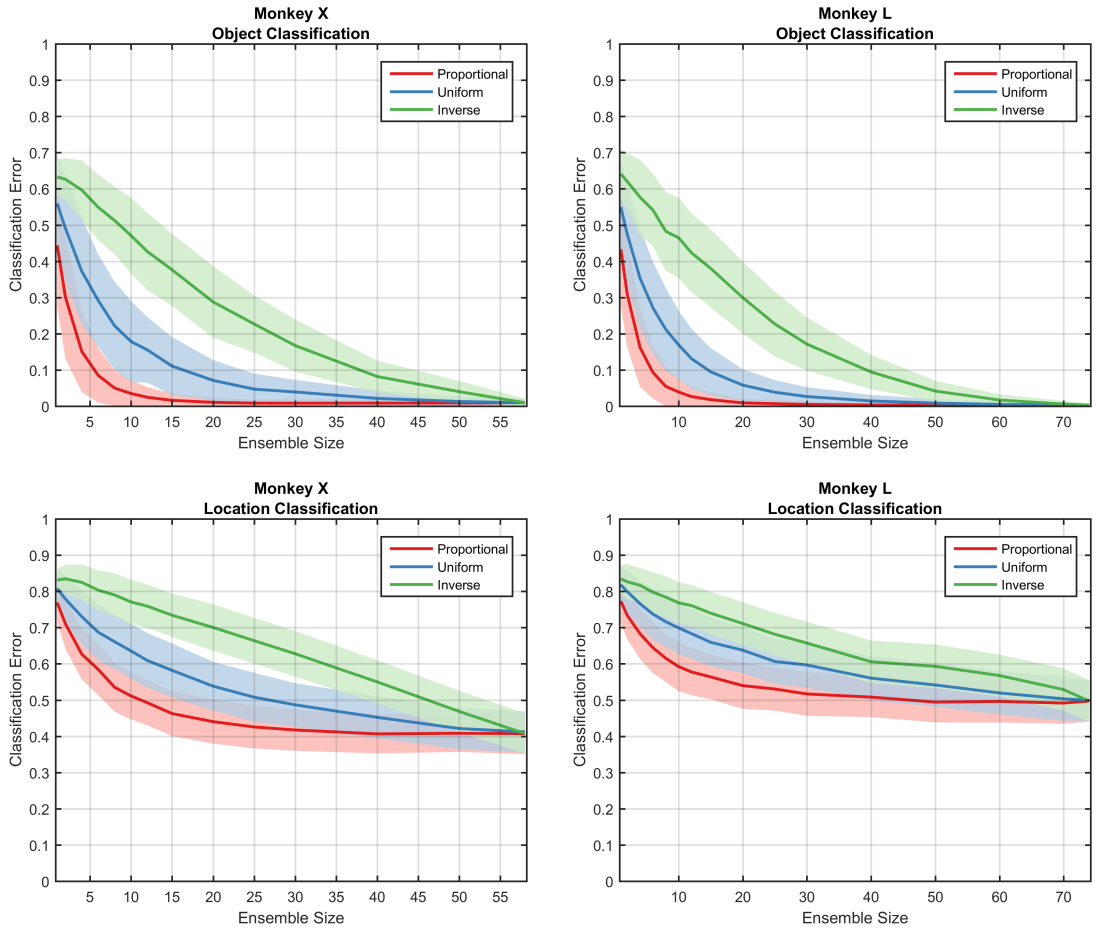

Figure 5.5: Classification performance for ensembles of units chosen based on similarity of natural clusters to trial labels. Each ensemble size and method was evaluated over 500 repetitions. Selected ensembles were then used to train naive bayes classifiers to classify trials according to object shape or reach location. Darker line shows average classification error versus ensemble size for each the three ensemble selection methods. Shaded region indicates 1 standard deviation of classification error for each method.

5.3.4 Inter-unit partition similarity

In order to explore pairwise similarity in partitioning among units, we calculated the NMI between the partitions for each pair of units. Pairs or groups of units with comparatively high inter-unit NMI might be indicative of having a common source of

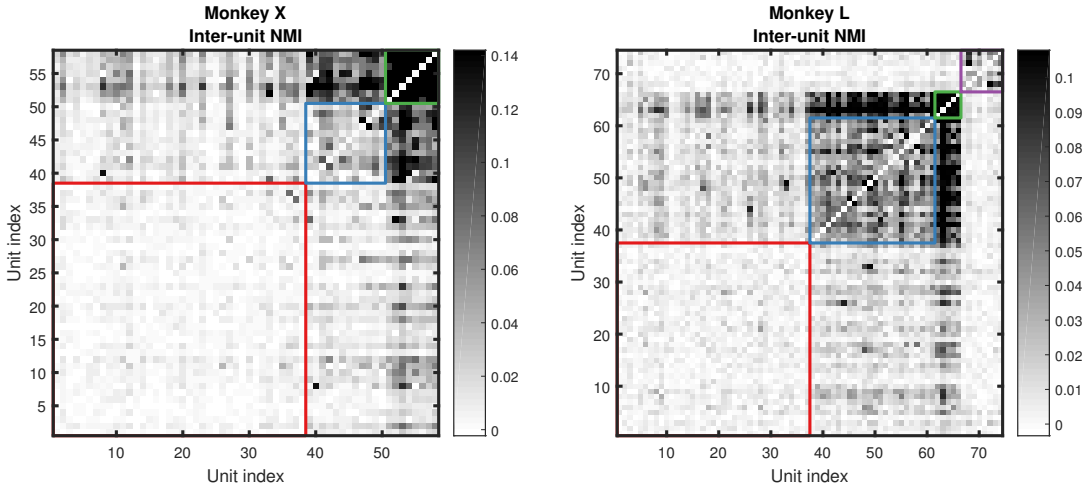

Figure 5.6: Clustering of units based on similarity of single trial partitions. Cluster boundaries are indicated by white lines. The primary factor for clustering seems to be the degree to which trials were task modulated. Both monkeys indicated the presence of groups of units with high, moderate, and low task-related modularity. Interestingly, clustering of units in monkey L also indicated a group of units which modulate similarly across trials but do not appear to be related to the task.

modulation. We expect to see, for instance, that units with high unit-task similarity would also tend to have high inter-unit similarity. The pairwise inter-unit similarities for all units in each monkey are shown in Fig. 5.6.

We applied k-means analysis to this matrix to search for structure in the form of clusters. Empirically we discovered 3 clusters of units in monkey X and 4 clusters in monkey L. These clusters are indicated by color in Fig. 5.6.

Examination the relationship between inter-unit similarity and unit-task similarity suggests that the primary means of similarity between units was their degree of task-specificity. The scatter plot in Fig. 5.7 shows the relationship between each unit's clustering similarity to the 24 task conditions versus the maximal inter-unit similarity among all other units. In both monkeys we see that the two are correlated. We also

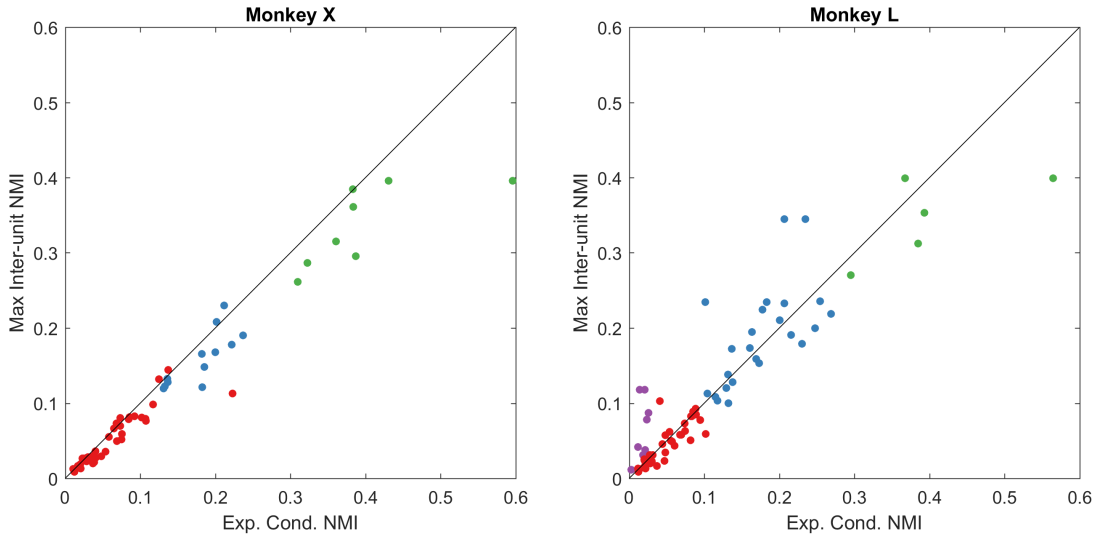

Figure 5.7: Comparison of partition similarity between experimental conditions versus other units. Each point represents an individual unit colored according to its cluster assignment based on inter-unit NMI. Displacement along the horizontal axis corresponds to similarity between partitions based on trial clustering and partitions based on experimental design. Displacement along the vertical axis corresponds to the maximum of the similarity of partitions based on trial clustering between the given unit and all other units. Diagonal line represents identity.

see that for most units, clustering assignments were more similar to the experimental condition groupings than they were to the clustering of any other unit.

One noticeable exception to this is the small cluster of units observed in Monkey L shown in purple in Fig. 5.4, Fig. 5.6, and Fig. 5.7. Units in this cluster all belong to the same array (G) and appear to have greater inter-unit similarity than unit-task similarity. This difference in similarity suggests that there may be some unobserved external variable that is causing these units to be coordinated and that this external variable is not directly linked to object type or reach location. Indeed, examination of the unit rasters, as shown for one of the units in Fig. 5.8 tends to show common temporal structure within clusters. However when these same units are examined

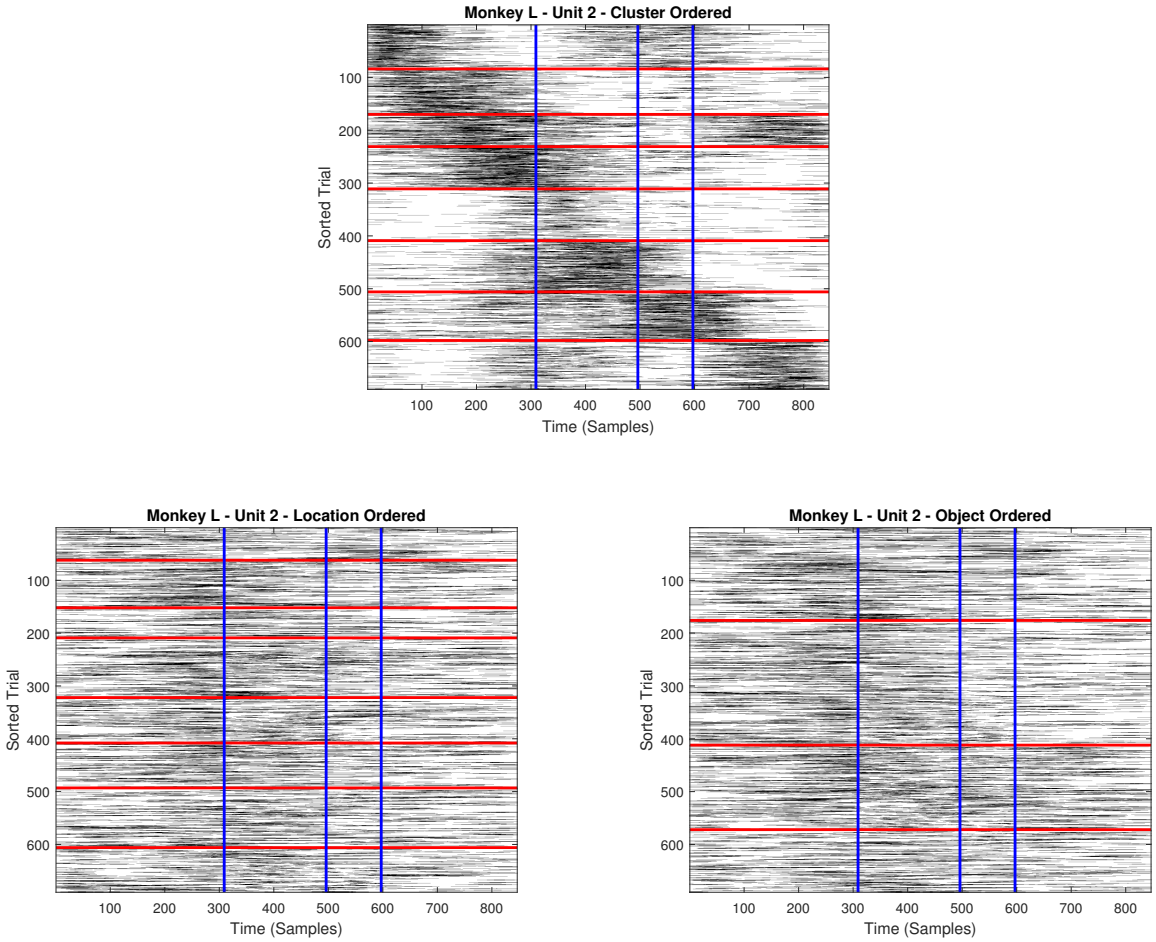

Figure 5.8: Raster of unit 2 in Monkey L, ordered by cluster, object, and location. Red horizontal lines indicate divisions between groups. Vertical blue lines indicate event boundaries after time rescaling (OM, SC, SH). Each plot shows the same firing rate activity where each row represents a trial. Trials are reordered based on group membership where groups are clusters (top), reach location (bottom left) or object type (bottom right). This unit located on Array G shows substantial structure when ordered by cluster assignment but no empirically apparent structure when organized by experimental condition.

for structure or modulation related to object type or location, there is less (if any)

structure apparent.

5.4 Discussion

In this chapter we applied a cluster analysis to the single trial responses of individual units that were simultaneously recorded during a reach to grasp and manipulate task. The cluster assignments for each trial for a given unit made up a specific partition. We compared this partition to other trial partitions determined by experimental conditions and observed that there seemed to be significant agreement between these partitions for many units. To investigate the utility behind these similarities, we performed a classification analysis that relied on stochastically chosen ensembles with each unit's probability of selection related to its partition similarity. We observed superior performance from ensembles that were preferentially made up of units whose spike-based partitions were similar to the task-based partitions. Similarly we observed below average performance from ensembles that were made up of units with low unit-task partition similarity. Finally we attempted to search for community structure among the units by examining inter-unit similarity. Though most of the discovered structure appeared to be related to the primary experimental variables, we found evidence for at least one community that appeared more likely to be modulated by some unobserved variable.

5.4.1 On Clustering

Our method is dependent upon finding meaningful clusters among a set of trials for individual units. Clustering in general is often difficult due to the challenge of finding a useful metric to define the relationship between elements of a set and also deciding on how clusters should be shaped [153]. A specific choice of metric may dramatically change the results and reveal clustered structures that other metrics would miss [116, 145].

When dealing with neuronal spike trains, commonly used distance measures include euclidean distance [91,140], correlation [131,132], cosine distance [128,147], and hamming distance [126,154]. Many of these distances may take on different properties depending on how the spike train is represented as in the case of conversion to firing rates by convolution with a kernel [133,155–159]. Other studies have avoided the need for convolution by using distance metrics based on edit-distance [116, 160–162]. An important point to note is that each of these distance metrics require some specification of a time scale. In nearly all cases, at least one free parameter must be chosen in order to represent the time-scale on which similarity will be observed. Smaller time-scales will emphasize synchrony while larger time-scales will place more emphasis on variation in mean firing rate. In general, there does not appear to be any distance measure which performs optimally under all conditions. Here we found general success with a gaussian kernel with standard deviation of 25 milliseconds, though different kernel widths may perform better for specific units.

The choice of clustering method is nearly as influential as the choice of distance metric. Here k-means was chosen for its simplicity as well as its suitability. K-means tends to find clusters that are compact, which in this case seemed reasonable to assume that firing rate vectors from a single experimental condition might form compact clusters around a prototypical centroid spike train. While k-means has been broadly applied [129], different results may be obtained from fuzzy k-means [128], hierarchical clustering [91, 140, 141, 163], spectral clustering [126, 131, 132, 154, 164–166], and other network methods [133, 167, 168]. For review on differences in clustering techniques and the various user choices involved, see [153].

Finally with regards to clustering, one must consider how to optimize over the various hyperparameters involved. These include the number of clusters to look for as well as the time-scale of similarity. We made a critical assumption that trials from each unit should form natural groups that reflect the block design of the experiment. Though k-means was performed on the units over many repetitions and many numbers of clusters, we ultimately selected the partitions that resulted in trial clusterings that aligned with the division among experimental conditions. This step is likely critical with regards to using the partitions for feature selection, but not necessarily for searching for structure in trials unrelated to the task. Different optimal partitions would likely have been selected had we used another metric such as the silhouette value or gap coefficient. It is unclear though how strongly this would have impacted our results, if at all.

5.4.2 Feature Selection for Classification

As we have demonstrated, our clustering approach may be used as a means to identify units that will provide good performance when included in a classifier. Within the domain of research related to brain computer interfaces, feature selection is a common topic [169–175]. In general, classifier performance can degrade when the number of features is large relative to the number of available samples. This phenomenon is often called the "curse of dimensionality" [176] and is generally related to a classifier's inability to properly learn generalizable relations among the high dimensional data. The task of feature selection generally involves measuring the relevance of each feature to the task and then selecting some subset of features with the most relevance. The most common approach is to identify task-relevant neurons by grouping trials according to a known experimental condition and then performing ANOVA analysis on the group-averaged firing activity. Other approaches learn a generative model to describe the firing for each group [169, 172, 175] and attempt to find neurons with significant task-related variation across models. A third approach involves analysis of classification performance when features are included or excluded from a classifier [171].

By comparison, our approach to feature selection is model-free and does not depend on explicit knowledge of the explicit differences between experimental conditions. Instead, our approach simply needs to know when different experimental conditions were occurring. Even then, in the absence of this knowledge, reasonable results

might be obtained by thoughtful construction of a synthetic partition of the trials by the researcher.

At its core, the clustering acts as a form of vector quantization (VQ). VQ serves to reduce the dimensionality of vectors or time-series by finding a low dimensional codebook and then encoding the vectors using these codes. In our case, fire rates of several hundred samples were reduced to one of 2 to 10 scalar values corresponding to the identity of their cluster assignment. After this quantization, each spike train could be thought of as realizations of draws from a random variable from a categorical distribution. The true trial labels themselves (reach location, object type, or experimental condition number) can similarly be thought of as observations of random variables from categorical distribution. With these assumptions, mutual information between the two variables is a natural approach to feature selection [177].

5.4.3 Identifying Latent Communities

An important benefit to our approach is the potential for detection of communities of units. Though several other clustering applications have shared a similar aim, our approach has an important fundamental difference in initial assumption. Many community detection approaches assume that units within a community have similar firing properties expressed in terms of synchrony in spiking or correlation at a wider time-scale [126, 131, 133, 154]. Our approach assumes instead that units may belong to a community where membership is based not on spiking similarity but in modu-

lating their firing activity in response to changes to some common external variable. Members of these co-modulated communities may be related through some common upstream source of stimulation.

Interestingly, cluster analysis revealed a small community of units in Monkey L that appeared to significantly coordinate across trials yet did not appear to provide substantially discriminative information about reach location or object. Additionally, empirical analysis of rasters of firing rate when ordered by experimental condition did not show apparent structure within conditions. However, when ordered by cluster, rasters and PETHs showed evidence of temporal structure and phasic activity. These units were all located on array G in Monkey L, which was located laterally along the M1 relative to arrays showing selectivity for reach location and object. This suggests this community may have been involved somehow in orbitofacial movements. This result in particular highlights the value of our approach. The multistage clustering revealed the presence of a potential neural assembly that would not have otherwise been found had investigation been limited to analysis of activity specifically related to reaching and grasping alone.

The clustering method described in this chapter proved to have significant utility for identifying groups of neurons with certain desirable properties such as task relevance. The approach makes no attempt, however, to model the actual relationship among neurons in a group. The nature and strength of these relationships may actually contain important information that accounts for observed spiking as well as

task-specific variations in spiking. In the next chapter I will describe a novel approach to modeling the task-specific interactions among groups of neurons. These models will be used both to better describe spiking activity among groups of neurons and improve the ability to read-out the behavior represented in spiking activity.

Chapter 6

Task-specific Ensembles

6.1 Introduction & Background

Neurons in motor and premotor cortices in nonhuman primates demonstrate variations in firing activity that correlate with parameters related to motor behavior [7, 44, 178]. Identification of how populations of neurons encode these parameters is of great importance to improving the usability of brain-controlled prosthetic devices and increasing understanding of the brain as a whole [20, 86]. Reaching and grasping motions require the activation and coordination of functional networks of neurons. Significant effort has been applied to investigating encoding of motor behavior by neuronal populations by focusing on how individual neurons in motor and premotor cortices independently encode motor behaviors [7, 37, 44, 69, 179]. As recording technologies improve and the number of simultaneously observable neurons grows [2], so

too grows the potential for discovering relevant encoding of behavior in the interactions between neurons.

Inspection of simultaneous recordings of neuronal activity often focuses upon the existence of apparent interaction among neurons through correlations in firing patterns. This functional (or effective) connectivity [180, 181] is widely incorporated in models of neuronal interactions and demonstrates effectiveness in accounting for spike time variability [40, 41, 54, 124, 182–188]. In some cases, inclusion of ensemble activity has even been shown to result in improved ability to decode sensory stimuli [41] and some motor behaviors [54]. These studies treat the interactions among neurons in the ensemble as being stationary with regard to changes in stimulus or behavior. Instead, the relationship between firing rate and changes in behavior or stimuli are relegated to a tuning function or stimulus filter. Instead, improvements to decoding performance due to inclusion of the ensemble terms are relegated to accounting for shared inputs or common noise [54].

Dynamic interactions among neurons in an ensemble may contain important information about a stimulus or behavior that complements the information contained in direct variations in firing rate alone [189, 190]. A cartoon of this concept is depicted in Fig. 6.1. Changes in spike correlation between pairs of motor cortex neurons at short time scales (< 50 ms) have been observed to vary repeatably during motor tasks [190–192]. Other studies observed that short time scale correlations were shown to encode motor information beyond that coded through simple rate modula-

tion [189, 193]. Changes in firing rate covariance of small groups of neurons at longer time scales has been observed during performance of arm movements [65], prehension [194], and motor planning [195,196]. Accounting for these task-related changes in functional connectivity could potentially improve both encoding and decoding models based of neuronal activity.

In this chapter I construct models of spiking activity that incorporate ensemble activity from other neurons through task-specific functional connections. Specifically, I investigate whether information about motor behaviors is available within the variation of functional connectivity in neuronal ensembles. I examine both the case where the ensemble weights are static across all grasp types as well as the case in which the ensemble weights are task-specific and assumed to vary with the task being performed. Specifically, I compare the performance of these models within the context of decoding the object being grasped by monkeys performing a reach-to-grasp task. Through this analysis I show that additional discriminative information about motor behavior may be found in variations in functional connectivity of a neuronal ensemble.

6.2 Methods

6.2.1 Encoding Models

The firing of each spiking unit was modeled as a discrete-time point process. Discrete-time point processes are random processes in discretized time with binary

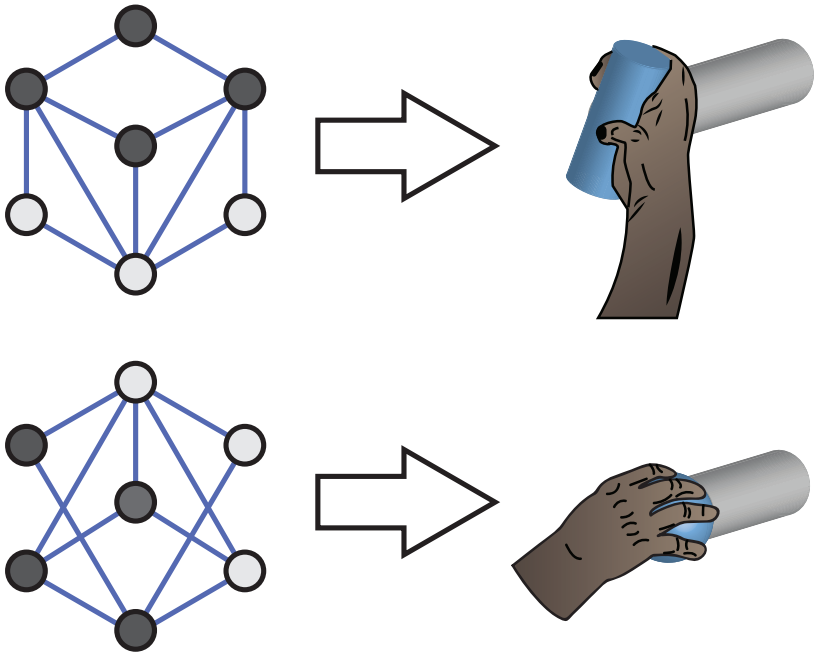

Figure 6.1: Conceptual image of task-specific ensembles. In this diagram, grasps for two different objects are shown alongside a conceptual diagram of a network of neurons. The colored circles represent individual neurons with variable firing rates corresponding to the grasp being performed (darker implies higher firing rate). Meanwhile the lines connecting the circles indicate functional connectivity between pairs of neurons. Here we can see that different grasps may cause neurons to modify their firing rate but may also be associated with a change in the overall network topology.

observations. Within this context, the spiking activity of a unit can be represented as a time-series with a value of 1 when spikes occur and a value of 0 otherwise. Models of point processes are fully characterized by a conditional intensity function (CIF), $\lambda(t)$, which describes the estimated instantaneous event rate at time t. To represent spiking as a discrete-time point process, I discretized spike trains from each unit to 1 ms bins such that at most one spike could occur in any time bin.

Following this discretization, a valid CIF for a given unit may be any function that

produces an estimate of the probability of a spike occurring in a given time bin. Here, I cast this as a binomial logistic regression problem [197], which is a specific formulation of a generalized linear model (GLM) [198]. Thorough derivations of this general approach as it applies to modeling spiking have been published previously [40, 199]. Under this model and the limitation of at most one spike occurring in any time bin, the likelihood of an observation in a single time bin t_k for a given CIF is provided by:

$$P(X_i(t_k)|\lambda(t_k)) = \exp\left\{\log \lambda_i(t_k)X_i(t_k) - \lambda_i(t_k)\right\} \tag{6.1}$$

where $\lambda_i(t_k)$ is the value of the estimated conditional intensity function for neuron i in time bin t_k and $X_i(t_k)$ is the (binary) spiking activity of neuron i in time bin t_k. This likelihood function may be extended to account for a sequence of spiking activity under a given CIF by treating the sequence as a collection of conditionally independent Bernoulli trials. For a collection of k sequential time bins, the likelihood of such a sequence given a CIF can be expressed as:

$$P(X_i(t_{1:k})|\lambda(t_{1:k})) = \prod_{k=1}^{K} P(X_i(t_k)|\lambda(t_k)) \tag{6.2}$$

Thus, the task of learning a encoding model can be reduced to providing a valid prototype function for $\lambda(t)$ and estimating the coefficients through maximum likelihood estimation.

The encoding models I examine here consist of two distinct components: a baseline

firing rate and a rate dependent on the recent activity of other neurons in the recorded ensemble. Following the convention applied in [40, 42, 200], I model the firing rate of a unit as consisting of a baseline firing rate combined with a multiplicative term that conditionally modifies the baseline rate. Our general form for the CIF is

$$\lambda(t|g, \mathcal{H}_t) = \lambda^B(t|g)\lambda^E(t|g, \mathcal{H}_t) \tag{6.3}$$

where $\lambda^B(t|g)$ represents the baseline firing rate dependent on the grasp, g, and $\lambda^E(t|g, \mathcal{H}_t)$ represents a variable gain function dependent on the grasp as well as the past spiking activity of other units in the ensemble, $\mathcal{H}_t$. Here, I propose three variations on this general form.

6.2.1.1 Baseline Model

The baseline model treats the spiking probability for each unit as constant within trials with a rate that is dependent upon the object being grasped.

$$\lambda_i^B(t|g) = \exp\{\beta_0(g)\} \tag{6.4}$$

where $\beta_0(g)$ is a functional parameter that represents the baseline firing rate as a function of the discrete grasp, g, being performed. In this case, other units in the observed ensemble make no contribution to the predicted spiking probability.

The functional baseline parameter $\beta_0(g)$ is intended to behave as a single coefficient

whose value is dependent on the grasp being performed. In this work, functional coefficients are used in conjunction with indicator functions as follows:

$$\beta_k(g) = \sum_{g\prime=1}^{G} \beta_{k,g\prime} \cdot \mathbb{I}(g = g\prime) \tag{6.5}$$

where $g\prime \in \{1, 2, ...G\}$ is a discrete value indicating one of G possible grasps, β is a model parameter and $\mathbb{I}(g = g\prime)$ is an indicator function that is identity during trials when grasp g is being performed and zero otherwise. Here k is a grouping subscript to indicate that the β_k parameters interact as a group with the k^{th} model covariate (or constant, for $k = 0$). Within the context of the baseline model, this functional parameter allows for variations in a unit's average firing rate depending on the grasp being performed.

6.2.1.2 Static Ensemble Model

The *static ensemble model* augments the baseline model with ensemble terms that modulate the baseline firing probability as a weighted combination of the firing rates of other units. Under this paradigm, the firing of each unit is modeled as:

$$\lambda_i(t|g, \mathcal{H}_t) = \lambda_i^B(t|g) \cdot \exp\left\{\sum_{j\neq i} \beta_j \cdot r_j(t)\right\} \tag{6.6}$$

where $r_j(t)$ is the observed number of spikes fired by unit j in the previous 100 ms and β_j is a ensemble coefficient representing the strength of influence of unit j upon

the firing of unit i. In this model the ensemble coefficients, β_j, are assumed to be constant and not conditional upon the grasp performed. In other words, the influence of spiking from other units is assumed to be stationary with respect to both time and behavior.

6.2.1.3 Task-specific Ensemble Model

The *task-specific ensemble model* further extends the baseline and static ensemble models by adding the flexibility to allow for ensemble weights that are conditional upon the task being performed. This model is expressed as:

$$\lambda_i(t|g, \mathcal{H}_t) = \lambda_i^B(t|g) \cdot \exp\left\{\sum_{j \neq i} \beta_j(g) \cdot r_j(t)\right\} \tag{6.7}$$

where $\beta_j(g)$ indicates the task-specific influence of recent spikes from the j^{th} unit. In this paradigm, the ensemble coefficients, $\beta_j(g)$ are assumed to vary with the task and can be expanded as described in equation (6.5). Here the functional ensemble coefficients vary with the grasp being performed and allow modeling of task-specific influence from other neurons. In both the static and task-ensemble models, ensemble effects were captured in a single 100 ms history window. This was chosen to incorporate relevant time periods identified in the literature [37, 40, 54, 187] while minimizing the total number of parameters in our final model. Self-history effects were excluded in order to better isolate the role of ensemble effects on encoding and

decoding performance.

These three models represent different assumptions about the underlying behavior of neurons and provide varying degrees of model flexibility. An example of the encoding performance of each of these three models for an individual unit is shown in Fig. 6.2. Each of the three models incorporates a task-dependent baseline component that allows for variation in average firing rate due to the task. Beyond this point the three models diverge. The static and task-specific ensemble models incorporate influence from the firing rate of other neurons. Each other unit's firing rate may be thought of simply as a time-varying signal. The static model assumes that the influence of these time-varying signals is fixed while the task-specific model allows for this variation to depend on the task. As Fig. 6.2 shows, these assumptions and model prototypes result in very different model behavior.

6.2.2 Model Fitting

Estimates for model parameters were obtained using weighted maximum likelihood estimation. This approach follows the same procedure of the standard maximum likelihood estimation procedure for point process GLM models as described in [40] with the exception that each sample in the training data was assigned a weight to account for differences in trial duration. Variations in experimental conditions resulted in trials of different lengths as can be seen in Fig. 3.4. For instance, trials to the right side of the workspace took longer on average than trials to the left. This results in trials

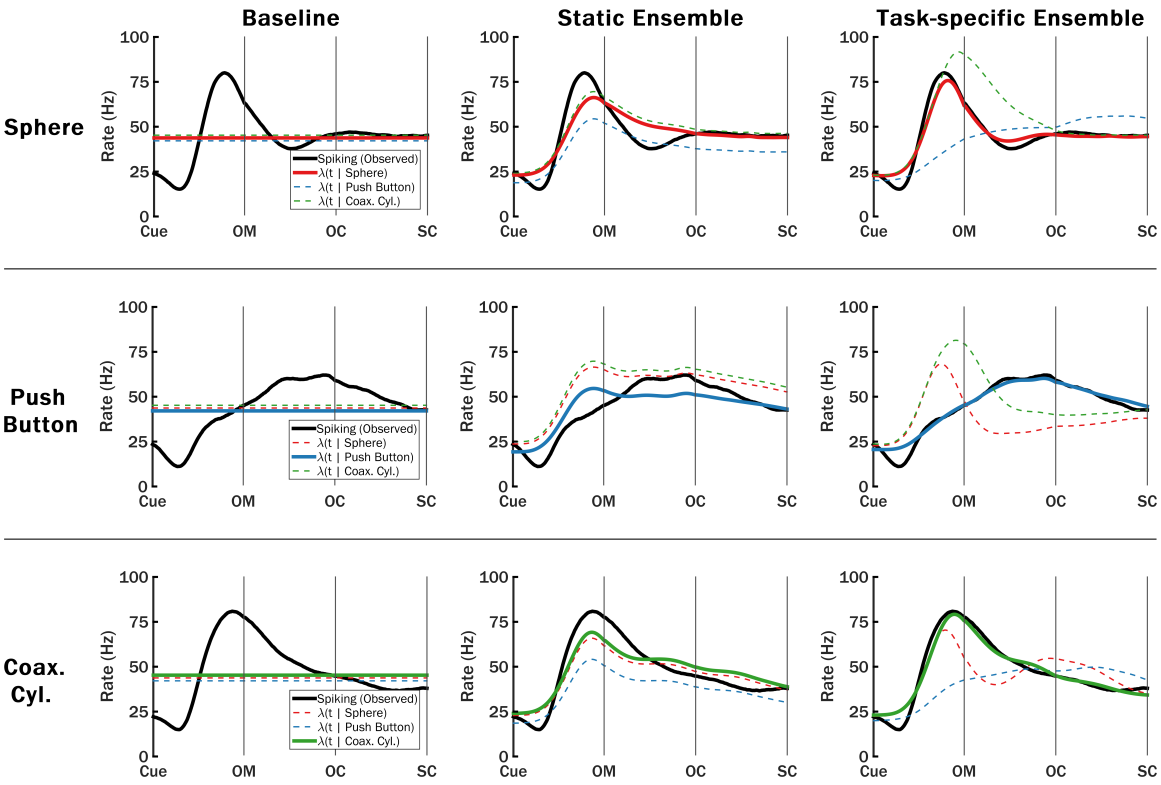

Figure 6.2: Example of trial-averaged predicted spiking activity for an individual unit versus observed spiking activity under each of the object conditioned model paradigms. The black trace shows the trial-averaged observed firing rate for all trial repetitions of a particular object type. The colored traces show the predicted firing rates ($\lambda(t|\cdot)$) that were predicted by each of the models under different assumptions regarding the object being grasped. In each row, the predicted firing corresponding to a match between the assumed object being grasp and the actual object being grasped is indicated as a solid colored trace. Predicted firing rates for a mismatch between model assumptions and actual object are shown with dashed traces. For illustrative purposes, both observed and predicted spiking activity were convolved with a gaussian kernel (std. dev. 25 ms) before averaging. Trials were time-normalized within each experimental epoch before averaging. Vertical traces indicated alignment points for event times of cue, onset of movement (OM), switch closure (SC) and static hold (SH).

to the right contributing more data samples to the training set than trials to the left.

As a result of this imbalance, in regular maximum likelihood, samples from experimental conditions with longer trials on average could contribute a disproportionately

large amount to the total likelihood. The weighted maximum likelihood approach compensates for these potential biases by assigning lower weights to samples from experimental conditions that were longer than average and higher weights to samples from experimental conditions that tended to be shorter than average.

Encoding performance of each model for each unit was assessed in terms of spike timing predictability (STP). This measure compares the predictive performance of a proposed encoding model against an uninformed *null model* of spiking [41,54,124,143]. The null model is an uninformed model that predicts the unit's firing probability as being constant regardless of experimental conditions or other factors. This probability is equivalent to the unit's overall average firing rate across all trials. STP is defined as

$$\mathrm{STP}(\lambda) = \mathbb{E}\left[\log \mathcal{L}(x|\lambda)\right] - \mathbb{E}\left[\log \mathcal{L}(x|\lambda_0)\right] \tag{6.8}$$

where $\mathbb{E}\left[\log \mathcal{L}(x|\lambda)\right]$ is the expected log likelihood of some spiking sequence x under the proposed model and $\mathbb{E}\left[\log \mathcal{L}(x|\lambda_0)\right]$ is the expected log likelihood evaluated under the null model. This measure was calculated in $\log_2$ and normalized over time to return a value in bits per second. As described in [124, 150] this value represents the expected number of bits per second saved by a model representing the observed sequence with some additional knowledge such as the grasp being performed or the activity of other neurons. A positive STP indicates that the alternative model's prediction of spiking tends to better match observed spiking than the uninformed null model. A negative STP indicates that the alternative model tends to be less efficient

at describing the observed spiking than the null model. In general one expects that adding informative covariates to the model would result in increased STP whereas adding non-informative covariates would result in either no change or a decrease to the STP.

6.2.3 Decoding

After encoding models were fit for each unit, the models were applied to the task of decoding the grasp on each trial given observed spiking activity. Using the definition for the probability of a particular sequence conditioned on a grasp type described in equations (6.1) and (6.2), the posterior probability over grasp postures can be evaluated using Bayes' Rule. The posterior density over grasps can be expressed as follows:

$$P(g|X_i(t_{1:k}), \lambda(t_{1:k})) = \frac{P(X_i(t_{1:k})|\lambda(t_{1:k}), g)P(g)}{\sum_G P(X_i(t_{1:k})|\lambda(t_{1:k}), g)P(g)} \tag{6.9}$$

where $P(g|X_i(t_{1:k}), \lambda(t_{1:k}))$ is the posterior likelihood of the grasp being performed given the set of models and the observed population spiking activity, $P(X_i(t_{1:k})|\lambda(t_{1:k}), g)$ is the likelihood of spiking under some hypothesized task and $P(g)$ is the prior distribution over task probabilities. The prior distribution over tasks was taken as uniform since there is no reason to expect a priori that any one behavior in this experiment is more likely than the others. Given this estimate of the posterior density, decoding can be performed by identifying the grasp type that has the maximum probability

under the posterior.

This decoding approach was applied in a synchronous manner in that the decoder had knowledge of when a trial was initiated. Since the likelihood of a sequence of spiking activity evolves as the number of observations increases, so too does the estimate of the posterior density over grasps. In general, one expects that the posterior density is uniform over all grasps at the beginning of a trial and becomes more peaked around one or more grasp types as additional data is observed. Applying the decoder synchronously allows us to examine the evolution of decoder performance over the time-course of a trial.

The decoding approach described so far applies to so-called *individual unit decoding* as the decoder output is determined by the spiking of an individual unit. Note, however, that the output of the CIF may depend on observed spiking of other neurons. In practice, individual unit outputs are combined within the context of population decoder to overcome the low signal to noise ratio of individual unit spike trains. To extend decoding to incorporate the population activity as a whole, I applied a simple majority voting rule. At each time bin during a trial, each observed unit supplied a vote for the grasp with the maximum probability according to the posterior distribution. The grasp receiving the most votes was chosen as the output of the classifier.

The posterior likelihood generated by our decoder provides the added benefit of a measure of certainty or confidence in the prediction. Thus, decoding performance was

compared in terms of classification accuracy as well as confidence in the prediction as measured by the posterior distribution over grasps. The evaluated model types were compared using a multinomial selection procedure (MSP) to assess differences in decoding performance for each spiking unit [201,202]. Rather than just accounting for classification accuracy, the MSP takes into account the posterior probability associated with each model's prediction. In the case where models have similar decoding accuracy, we would generally prefer a classifier that assigns a higher confidence to its prediction. The MSP procedure reflects this preference. Under the MSP approach, the predictions from each model in a set are evaluated against known labeled data. For each sample data point, the model that assigns the highest posterior probability to the correct class is chosen as a winner. This step in particular helps to disambiguate between models that may have similar classification accuracy. Across all samples, the percentage of times each model one is calculated. The two models with the highest win percentages are identified and a two proportion Z Test is performed to assess statistical significance.

6.3 Results

The analysis was performed on a single session of recorded data from each of two monkeys. The sessions consist of neural recordings made during repetitions of unilateral center-out reach-to-grasp trials to four objects across eight locations as shown

in Fig. 3.1b. The number of trials performed by each monkey under each experimental condition is summarized in Table 3.1. To account for potential imbalances in the sampled experimental conditions, data from each session was subdivided into two subsets for analysis. Subset 1 consisted of the sphere, push button, and pull trials each at locations 1, 2, 3, and 4 (0°, 22.5°, 45°, 67.5°) and consisted of 377 and 376 trials for monkey X and L, respectively. Subset 2 consisted of push button, pull, and mallet trials each at locations 3, 4, 5, and 6 (45°, 67.5°, 90°, 112.5°) and consisted of 340 trials for each monkey. Trials at locations 7 and 8 (135°and 157.5°) were excluded from the analysis since only two different objects were ever grasped at these locations, whereas other locations included grasps of at least three different objects.

Each subset of trials was analyzed independently. Analysis was isolated to the time period between cue presentation and completion of object manipulation indicated by closure of the associated microswitch. This period had an average duration of 0.79 seconds per trial in monkey X and 0.65 seconds per trial in monkey L. Within each of the subsets, a stratified 5-fold cross-validation approach was used to divide trials into mutually exclusive groups for training and testing. In each fold of cross-validation, 20% of trials from each experimental condition included in the subset were held out for testing. The remaining 80% of trials were used to estimate the parameters of the encoding models. The encoding and decoding performance of these models was evaluated using the trials in the test group. Each of the trials within a data subset was included in the testing group once across all five cross-validation folds.

Firing rate models were estimated only for units with average firing rates greater than 3 Hz. This selection lessened the chance of model overfitting on units with very sparse firing activity. This resulted in inclusion of 58 of 112 units in monkey X and 74 of 104 units in monkey L. For monkey X, of the 58 units with firing rates greater than 3 Hz, there were 2 definite and 17 definite or probable single units. The SNR was 2.8 $\pm$ 1.2 (mean $\pm$ standard deviation) for the remaining 39 multi units. For monkey L, of the 74 units with firing rates greater than 3 Hz, there were 14 definite and 29 definite or probable single units. The SNR was 2.8 $\pm$ 1.0 for the remaining 31 multi units. The included units had mean firing rates of 12.0 Hz and 14.9 Hz for monkey X and monkey L, respectively.

6.3.1 Encoding Performance

For each unit in the ensemble, I estimated three encoding models: a baseline model, a static-ensemble model, and a task-specific ensemble model. An example of the trial-averaged firing rates predicted by each of these models for an individual unit is shown in Fig. 6.2. This figure compares the trial averaged observed firing rate for the indicated unit as well as the trial averaged conditional predicted firing rate under each grasp type and each model type. As shown in Fig. 6.2, the three model variations exhibit very different predictions for spiking behavior. The predicted firing activity from the baseline models has an average rate that varies across task conditions but is otherwise constant in time. The static ensemble model allows for

some temporal variation that better matches the observed spiking activity. However, because ensemble weights are assumed to be constant across object types, grasp-specific variations in predicted firing rate are limited to changes in offset and the overall shape of the predicted firing rate profile has a similar shape regardless of the grasp the model is conditioned on. Finally, the task-specific model demonstrates greater overall temporal variability in the predicted firing rate as well as object-specific temporal variations in the predicted firing activity.

Model encoding performance was assessed by evaluating how well each model's predicted firing activity compared to observed firing activity. I examined the spike timing predictability (STP) of each model [124], which is the ratio of the expected log-likelihood of spiking activity under the proposed model compared to a null model based on average spiking across all trials. The null model is a constant-rate model representing the average firing rate across all trials irrespective of experimental condition. STP has units of bits per second and positive values correspond to a more descriptive encoding model. The average encoding and decoding performance of each unit is shown in Fig. 6.3

The baseline model significantly improved upon the STP of the null model in 52% of neurons in monkey X and 55% of neurons in monkey L (t-test, $p < 0.01$). The mean STP score of the baseline model was 0.48 ± 0.17 bits per second in monkey X and 0.42 ± 0.15 bits per second in monkey L. These results confirm that accounting for grasp-specific changes to the baseline firing rate often improves the performance

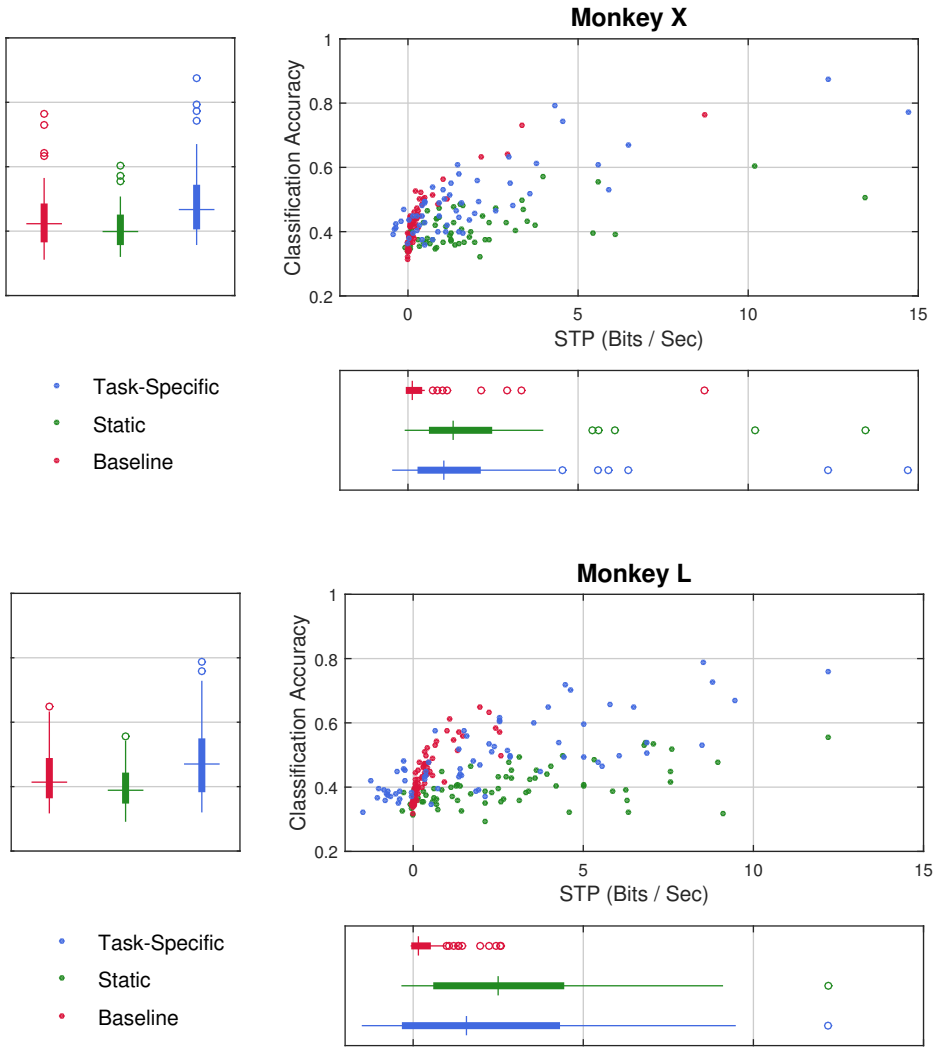

Figure 6.3: Relationship between spike timing predictability and accuracy. STP is plotted against average individual unit classification accuracy (main panel) for each unit. Values represent the average across both data subsets. The marginal distribution of classification accuracy (left panel) and STP (bottom panel) of these units are shown as box plots. In the box plots, the tick mark corresponds to the median and the thicker region of each colored trace indicates inter-quartile range.

of a model in predicting whether or not a spike is going to occur.

The addition of static ensemble terms improved the STP compared to the baseline model. Static ensemble models had higher STP scores compared to baseline models

in 83% of units in monkey X and 74% of units in monkey L (paired t-test, $p < 0.01$). The mean STP among units under the static ensemble model was 2.29 $\pm$ 0.42 bits per second in monkey X and 3.67 $\pm$ 0.56 bits per second in monkey L.

Task-specific ensemble models tended to have superior encoding performance compared to the baseline model but did not generally outperform static ensemble models. Task-specific ensemble models improved upon baseline models in 62% (57%) of units and improved upon static ensemble models in 10% (8%) of units in monkey X (monkey L) ($p < 0.01$). The mean STP under the task-specific ensemble models was 2.18 $\pm$ 0.49 bits per second in monkey X and 3.16 $\pm$ 0.62 bits per second in monkey L. The STP for each unit under the static and task-specific ensembles was strongly correlated in both monkeys (Pearson's r of 0.997 in monkey X, 0.991 in monkey L).

The average STP scores for each model type were aggregated across all units and a Friedman test with post hoc analysis was applied to compare encoding performance for each of the model types. In both monkeys, task-specific and static ensemble models had higher STP than baseline models ($p < 0.01$) and the static ensemble model had higher STP than the task-specific ensemble model ($p < 0.01$).

6.3.2 Decoding Performance

Decoding was performed by synchronously evaluating the maximum likelihood estimate of grasp shape using the learned encoding models. Decoding performance was evaluated using both classification accuracy as well as prediction confidence as

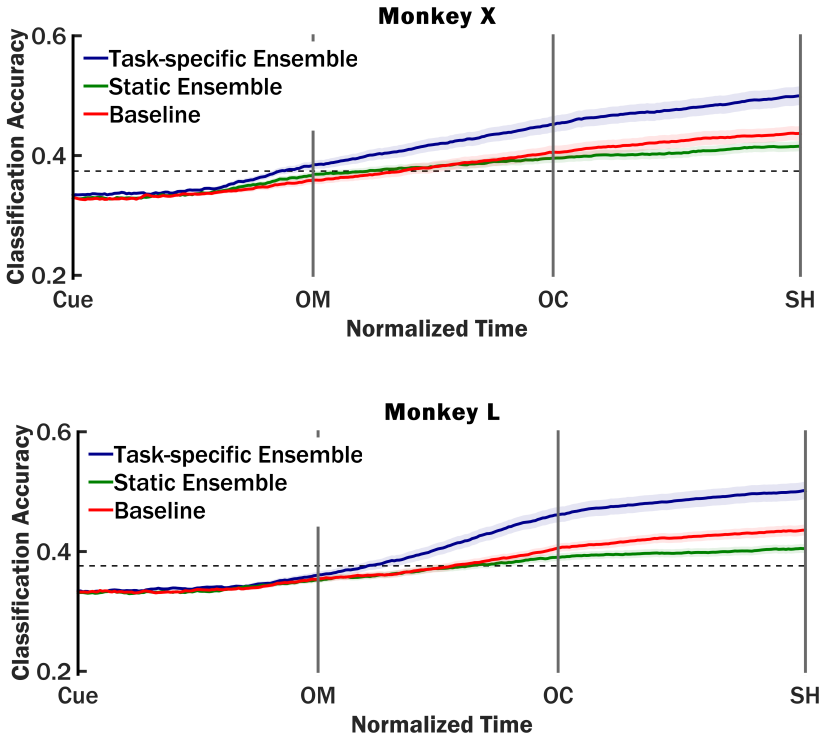

Figure 6.4: Trial averaged classification accuracy for individual unit decoding across all trials for both monkeys averaged across both subsets. Classification accuracy averaged across units is indicated for each of the three model types. Shaded region denotes standard error. Classification at each time step was performed by selecting the class corresponding to the maximum under the posterior distribution given observations prior to that time step. Vertical lines indicate cue presentation (Cue), onset of movement (OM), object contact (OC), and static hold (SH). Decoder output was time-normalized within each epoch (Cue to OM, OM to OC, OC to SH) before averaging. The horizontal dashed line indicates threshold for chance decoding performance at p = 0.05 significance level.

accounted for by the use of the posterior distribution in the multinomial selection procedure. Each trial was evaluated sequentially, allowing the predicted class estimate to be updated with each time step. The evolution of average individual unit accuracy over the time course of a trial is shown in Fig. 6.4.

Differences in individual unit decoding performance for individual units was evaluated using the multinomial selection procedure (MSP), which is based on the posterior

distribution of the classifier rather than accuracy. Task-specific ensemble models exhibited superior decoding performance in 82% of units in both monkey X and monkey L (averaged over both data subsets, $p < 0.01$). Baseline models had the best classification accuracy in approximately 1% of units in each monkey. The remaining units did not have superior performance under any one model according to the MSP. Static ensemble models were never identified as having the best decoding performance.

Individual unit decoding performance was also assessed based on average classification accuracy at the end of each trial (switch closure). In monkey X (monkey L) individual units achieved a mean accuracy of 43.7% $\pm$ 1.2% (43.6% $\pm$ 0.9%) under the baseline model, 41.6% $\pm$ 0.9% (41.0% $\pm$ 0.7%) under the static ensemble model and 50.0% $\pm$ 1.6% (50.2% $\pm$ 1.5%) under the task-specific ensemble model. Overall individual unit classification accuracy under the three models were compared using a Friedman test with post hoc analysis. In both monkeys, individual unit classification accuracy was significantly higher for the task-specific ensemble model than both the static ensemble and baseline models ($p < 0.01$). The baseline model had higher classification accuracy than the static ensemble model in monkey L ($p < 0.01$), but not in monkey X ($p > 0.05$).

Within a model type, units showed a strong correlation between STP and individual unit classification accuracy. In monkey X (monkey L), the Pearson's correlation between the mean STP and mean individual unit decoding performance for each unit had a value of 0.66 (0.58) for the baseline model, 0.79 (0.80) for the static ensemble,

and 0.80 (0.76) for the task-specific ensemble. This suggests that within a model type, units with better encoding performance relative to the population also tend to have better decoding performance.

Population decoding was performed using a simple majority vote during each step of a trial. Typical trial-averaged performance is shown in Fig. 6.5. Population classification accuracy was greatest for the task-specific ensemble models, though all three models performed significantly better than chance with average accuracy of at least 75% by the time of switch closure. In monkey X (monkey L) the final mean population classification accuracy was 79.6% ± 2.8% (87.8% ± 1.1%) for the baseline model, 77.3% ± 1.3% (75.8% ± 1.6%) for the static ensemble model and 95.4% ± 1.5% (96.6% ± 0.6%) for the task-specific ensemble model. In both monkeys, classification accuracy for population decoding was significantly higher for the task-specific ensemble model than both the static ensemble and baseline models ($p < 0.001$). Population decoding performance under the baseline model was significantly greater than the static model in monkey L ($p < 0.001$) but not in monkey X ($p > 0.05$).

6.4 Discussion

I examined the impact of modeling task-specific effective connectivity among an ensemble of simultaneously recorded cortical neurons in motor and premotor regions

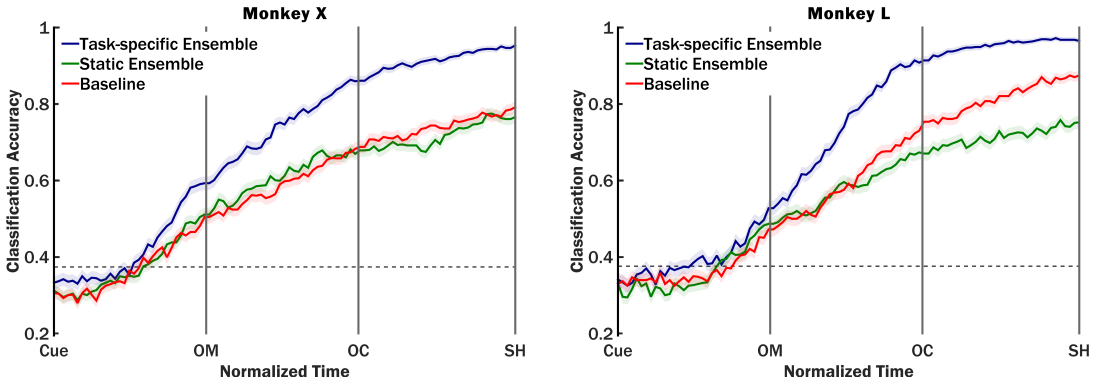

Figure 6.5: Trial averaged classification accuracy for population decoding across all trials for both monkeys averaged across both subsets. Average classification accuracy is indicated for each of the three model types. Shaded region denotes standard error. Classification at each time step was performed using a simple majority vote with each spiking unit contributing a single vote for the most likely grasp given the observations prior to that time point. Vertical lines indicate cue presentation (Cue), onset of movement (OM), object contact (OC), and static hold (SH). Decoder output was time-normalized within each epoch (Cue to OM, OM to OC, OC to SH) before averaging. The horizontal dashed line indicates threshold for chance classification performance at $p = 0.05$ significance level.

during performance of a motor task. Point process encoding models were constructed based on neuronal activity recorded from motor cortical areas of non-human primates during a reach to grasp and manipulate task. I evaluated and compared three different models of neuronal firing. A *baseline* model in which each neuron was modeled as having a baseline firing rate dependent on the object being grasped. A *static ensemble* model in which the baseline model was augmented with ensemble interaction terms that were fixed across all grasp types. Finally, a *task-specific ensemble* model in which the influence of the ensemble interaction varied with the grasp performed. Model performance was assessed both in terms of the ability to predict spiking activity (encoding) as well as the ability to discriminate between different grasp types

(decoding).

The relative encoding and decoding performance of the three model types was consistent in both data subsets in both monkeys. Inclusion of ensemble activity in both the static and task-specific ensemble models improved encoding performance compared to the baseline model as can be seen in Fig. 6.3. This result is consistent with several previous studies [40,41,54] that found ensemble interactions can be especially predictive of spiking activity given even a modestly-sized ensemble. Modeling task-specific ensemble interactions did not generally improve spike timing prediction beyond that achieved by static ensemble models. Decoding performance was significantly improved compared to baseline in task-specific ensemble models but not in static ensemble models. This difference in decoding performance was observed in the case of both individual unit and population decoding as shown in Fig. 6.4 and Fig. 6.5. The inclusion of ensemble activity generally improves prediction of spiking, but significant improvements in decoding performance due to ensemble activity require the model to account for task-specific variations in functional connectivity. Simply increasing the number of parameters in the model, as in the case of the static ensemble model compared to baseline, does not necessarily increase classification accuracy.

One might expect *a priori* that the task-specific ensemble model would outperform the static ensemble models in both encoding and decoding performance. The task-specific ensemble model did not generally outperform the static ensemble model in terms of encoding. This was likely due to a difference in model structure and the

availability of data. The task-specific ensemble model had three times as many ensemble parameters as the static ensemble model. Additionally, under the task-specific ensemble model, estimates of ensemble parameters corresponding to a particular object are improved only by observations of trials involving that object; e.g. trials involving the sphere object tell us nothing about the ensemble structure specific to the push button object. As a result, there is more uncertainty in the estimates of task-specific ensemble parameters compared to static ensemble parameters given the same amount of trials overall.

In the event that task-specific ensemble effects are small or zero, differences in precision of model parameter estimates could account for lower STP performance by the task-specific ensemble model compared to the static ensemble. If object-specific ensemble effects were sufficiently large, one would expect to see the task-specific model to have better encoding performance compared to a static ensemble model. This was the case for some units, but not the majority. However, if there were no variation in ensemble effects with object, one would expect to see no difference in *decoding* performance between the static and task-specific ensemble models. Task-specific ensemble models do improve decoding performance compared to baseline while the static ensemble models do not. These results suggest that there are potentially small but significant variations in functional connectivity across objects.

Decoding of grasping activity from neuronal data has been demonstrated previously with high classification accuracy [36, 82, 87–89, 91, 203]. Though precise com-

parison across studies involving decoding is difficult due to variations in experimental procedure, our approach achieved decoding performance consistent with these earlier efforts. Our underlying model is a generative model that continually assesses the likelihood of spiking activity in one millisecond time bins given recently observed activity from the neural ensemble. Though this approach makes the common assumption that the time of cue presentation was known, transitioning to purely asynchronous decoding could be facilitated through a separate state classifier or other heuristic to detect the onset of a new trial or intention to move [50, 67, 82, 105, 204]. Another advantage is that our method relies on modeling functional interactions with other neurons with time-varying behavior. This allows our model to account for significant task-specific temporal variability in firing rates without explicit modeling of a tuning function or state-transition models [67, 105, 106]. Finally, the underlying application of a generalized linear model to model firing facilitates introspection of the model and further investigation of the model behavior.

Accounting for task-specific ensemble behavior is not without its drawbacks. The number of parameters included in the task-specific model is determined by the product of the number of units in the ensemble, the number of time bins included in each ensemble interaction, and the total number of task conditions being modeled. As the number of simultaneously recorded neurons grows or the task expands in complexity, the amount of data required to adequately estimate model parameters grows quickly. The risk of overfitting may be mitigated by limiting the number of ensemble interac-

tions through neuron selection or by incorporating regularization during the process of fitting the model itself, as in [183, 197, 199]. Modification of the cost function during regularization provides the added benefit of tuning the model to emphasize encoding performance, model sparsity, or decoding performance. In this study I opted for an unbiased maximum likelihood approach and reduced the risk of overfitting by excluding neurons with low firing rates.

The findings suggest task-specific functional interactions between neuronal spike trains recorded from motor-related cortical regions may provide information about motor behavior. By using point process models of spiking, these interactions are modeled and compared against traditional assumptions of independent variation of firing rate with motor behaviors. Both static and task-specific ensemble interactions explained significant amount of spiking behavior in many neurons. Task-specific variations in ensemble interactions, though small, carried a significant amount of discriminative information about the grasp being performed.

Chapter 7

Conclusions and Future Directions

7.1 Summary

The work presented here represents a significant contribution to the field of neuroscience as well as brain machine interfaces through the development and application of methods related to the encoding of motor behaviors by networks of neurons in motor and premotor cortices in primates. Understanding the representation of motor behaviors by the brain is of vital importance to neuroscience as well as the effectiveness and performance of BMIs. Traditional approaches to learning this representation were largely developed with a focus on individual units acting in isolation. This approach is suitable for applications when only a small number of neurons are available. Continued developments in recording technologies, however, have resulted in the ability to from hundreds of individual neurons simultaneously. Taking full advantage of

these observed populations requires new techniques for analyzing the encoding of information in these populations as well as new models for representing this encoding.

The first part of this thesis presented a number of techniques for exploratory analysis of neuronal activity during the performance of a complex motor task. The exploratory analysis consisted of initial dimensionality reduction techniques to better understand the overall neuronal population activity during the performance of a task that involved simultaneous reaching and grasping. This analysis revealed temporally complex trajectories that showed structured organization in population activity across movement types. Classifiers were built to examine the concept of temporal generalization both at the population level and at the individual unit level. Results of temporal generalization analysis indicated the presence of temporally and spatially dynamic coding of reaching and grasping by neurons in motor and premotor cortices.

The second aim consists of applying semi-supervised clustering techniques to trial responses of individual spiking units in order to find natural variations in spiking activity across a number of experimental conditions. This technique can be extended to serve as a neuron selection procedure for identifying relevant subsets of neurons to include in classification-based decoders. Additionally this same technique may be used to identify groups of neurons with common external drivers, even when the source of that drive is unknown. When applied to the reach-to-grasp experiment, this technique readily identified different subsets of neurons that offered higher than average performance in decoding of reach and decoding of grasp. Similarly this tech-

nique was also used to intentionally identify subsets of neurons with below average classification performance.

The third and final aim developed the idea of task-specific neuronal ensembles for use in encoding and decoding applications. The core model introduced here is built on the premise that members of a large ensemble of neurons will form a functional network through apparent statistical interactions and that the structure of this network is dependent on the task being performed. Task-specific ensemble models had good overall decoding performance and superior decoding performance to traditional models that assume only variations in baseline firing rate. These results indicate that ensemble interactions may be used to great benefit when modeling the behavior of individual units for the purposes of motor decoding. As larger ensembles are observed, these models will become more powerful as units have a larger universe of potential signals to incorporate.

7.2 Future Directions

Evidence suggests that neural data is trending toward larger and larger volumes [2]. Today, studies regularly report recording from several hundred units simultaneously [3] and at least one group reported recording from as many as 1,800 units at once [4]. This same study forecast that current technology could soon be used to record from more than 5,000 units simultaneously. In order to utilize these large

populations, a number of broad changes to methodology will likely occur including careful consideration of the relationship between feature dimensionality and algorithmic complexity. Very likely, methods assessing neuronal importance [169–175] will become of increasing importance as a means to perform feature selection as a preprocessing step. Recording from so many neurons will have many practical implications requiring dramatic changes to the way data is analyzed. While traditional approaches to data analysis born in the early days of single unit recording are unlikely to be abandoned, they will perhaps become less relevant as data grows increasingly larger. While this thesis presented a number of tools useful to addressing these changes, the results suggest a number of avenues for further research.

7.2.1 Honing Co-modulated Communities

The combination of knowledge about experimental design with clustering single-trial activity of individual units proved to be a powerful approach to neuron selection and an effective means for identifying groups of units for further analysis. The inspiration behind this approach was driven two factors:

1. Neurons should have similar responses across repetitions of the same stimulus or behavior

2. Neurons may coordinate as part of a group without having correlated firing activity

The first point leads to a question of how similarity between spike trains is defined. In the present work, similarity was gauged by cosine similarity of two trials following firing rate smoothing and time rescaling. The role of time in assessing similarity is important, however, as different neurons may have different intrinsic time scales for representation or may have different degrees of stochasticity to responses across multiple repetitions. As presented, the methodology assumed that this time scale was fixed and identical across all observed neurons. Different results might be achieved by extending the similarity measure to include optimization over multiple timescales [126, 155, 161].

The second point above gave rise to the idea of co-modulated communities. Neurons may be linked by a common upstream driver or ancestor. Selection of neurons for inclusion in a classifier was performed by comparing similarity of each neuron's trial clustering to known variation in blocked experimental variables. A similar concept may be employed to determine whether units are potentially modulated by other observed experimental variables. In the same way that neurons should have similar responses over repeated trials, other variables such as joint angles, endpoint kinematics, and electromyographic signals may should also express similar behavior over repeated trials. The described clustering method may be applied to each of these variables in turn. Resulting partitions may then be compared to partitions for each of the neurons. Similarity of partitions between a neuron and one of these external covariates may indicate presence of a functional interaction. This method could

potentially be used, for example, to identify groups of neurons modulated by muscle activity versus groups modulated by endpoint kinematics without requiring the nature of the encoding be specified.

Finally, the classification technique described in the earlier chapter is not directly translatable for usage in online brain-computer interfaces. The presented classifier relied on finding the nearest cluster for a newly observed spike train. Under the presented methods, calculating this cluster assignment required knowledge of the timing of behavioral events in order to properly perform time rescaling. In the scenario of online decoding in a BMI, the timing of behavioral events would be unknown. A suitable replacement for online control may be found by learning a spiking trajectory model associated with each cluster. These trajectory models may be approximated as hidden markov models [105, 106, 205] or switching linear dynamical systems [206]. Such trajectory models would largely eliminate the need for knowledge of precise timing but may result in poorer classifier performance due to the decrease in certainty of cluster assignment. Though in a closed-loop BMI setting, these differences may be mitigated by through mechanisms of feedback and adaptation.

7.2.2 Extensions to Task-Specific Ensembles

Encoding models incorporating task-specific interactions among neurons were shown to have several desirable properties including good encoding and decoding performance without requiring the specification of a motor-specific tuning function.

However, two particular assumptions made in this analysis could be examined more closely in future investigations to expand the basic model and potentially improve performance.

One assumption is that ensemble structures are static over the time course of a trial. We are may observe, however, that ensemble structure is dependent on both the type of movement as well as the overall movement state. Temporal variation in the observed ensemble structure is especially likely in the scenario where recordings are produced from different functional regions such as motor cortex, premotor cortex, and parietal cortex. We would expect to see network structure change across these areas as the subject transitions from observation to planning to movement. In light of the results from the analysis of dynamic coding of these same cells, we may observe temporal variations in ensemble structure even if the ensemble is recorded entirely from a single region. A simple solution to adding temporal structure to the task-specific ensemble model could be achieved through combination of the presented model with a separate model performing state estimation such as a hidden markov model [105, 106] or linear discriminant classifier [82].

In addition to temporal stationarity, the examined neuronal ensemble connections were assumed to be dependent upon grasp. Similar task-dependent ensemble structures may also be present during reaching. In the case of reaching however, the ensemble structure is more likely to vary continuously as a function of reach angle than switch between a finite set of states. If the ensemble of neurons is imagined

to form a fully connected network, the strength of connection between any pair of neurons may be modeled as a function of the reach direction. The task-specific ensemble models presented earlier may be viewed as a varying coefficient model [112] where each model coefficient varied as a function of grasp. In the case of grasping, the coefficient function was specified to be an indicator function. To extend this idea to reach direction, the indicator function may be replaced by a number of overlapping epanechnikov kernels with support over the domain of possible reach angles. The resultant model could then describe the expected spiking activity for reaches over a continuous range of values rather than only specific increments.

Bibliography

[1] S. P. Wise, D. Boussaoud, P. B. Johnson, and R. Caminiti, "Premotor and parietal cortex: Corticocortical connectivity and combinatorial computations," *Annual review of neuroscience*, vol. 20, no. 1, pp. 25–42, 1997.

[2] I. H. Stevenson and K. P. Kording, "How advances in neural recording affect data analysis," *Nature neuroscience*, vol. 14, no. 2, pp. 139–142, 2011.

[3] P. J. Ifft, S. Shokur, Z. Li, M. A. Lebedev, and M. A. Nicolelis, "A brain-machine interface enables bimanual arm movements in monkeys," *Science translational medicine*, vol. 5, no. 210, pp. 210ra154–210ra154, 2013.

[4] D. A. Schwarz, M. A. Lebedev, T. L. Hanson, D. F. Dimitrov, G. Lehew, J. Meloy, S. Rajangam, V. Subramanian, P. J. Ifft, Z. Li *et al.*, "Chronic, wireless recordings of large-scale brain activity in freely moving rhesus monkeys," *Nature methods*, vol. 11, no. 6, pp. 670–676, 2014.

[5] M. B. Ahrens, M. B. Orger, D. N. Robson, J. M. Li, and P. J. Keller, "Whole-

brain functional imaging at cellular resolution using light-sheet microscopy," *Nature methods*, vol. 10, no. 5, pp. 413–420, 2013.

[6] E. E. Fetz, "Operant conditioning of cortical unit activity," *Science*, vol. 163, no. 3870, pp. 955–958, 1969.

[7] A. P. Georgopoulos, J. F. Kalaska, R. Caminiti, and J. T. Massey, "On the relations between the direction of two-dimensional arm movements and cell discharge in primate motor cortex," *The Journal of Neuroscience*, vol. 2, no. 11, pp. 1527–1537, 1982.

[8] A. P. Georgopoulos, A. B. Schwartz, and R. E. Kettner, "Neuronal population coding of movement direction," *Science*, vol. 233, no. 4771, pp. 1416–1419, 1986.

[9] J. K. Chapin, K. A. Moxon, R. S. Markowitz, and M. A. Nicolelis, "Real-time control of a robot arm using simultaneously recorded neurons in the motor cortex," *Nature neuroscience*, vol. 2, no. 7, pp. 664–670, 1999.

[10] J. Wessberg, C. R. Stambaugh, J. D. Kralik, P. D. Beck, M. Laubach, J. K. Chapin, J. Kim, S. J. Biggs, M. A. Srinivasan, and M. A. Nicolelis, "Real-time prediction of hand trajectory by ensembles of cortical neurons in primates," *Nature*, vol. 408, no. 6810, pp. 361–365, 2000.

[11] V. Gilja, P. Nuyujukian, C. A. Chestek, J. P. Cunningham, M. Y. Byron, J. M. Fan, M. M. Churchland, M. T. Kaufman, J. C. Kao, S. I. Ryu *et al.*, "A high-

performance neural prosthesis enabled by control algorithm design," *Nature neuroscience*, vol. 15, no. 12, pp. 1752–1757, 2012.

[12] J. M. Fan, P. Nuyujukian, J. C. Kao, C. A. Chestek, S. I. Ryu, and K. V. Shenoy, "Intention estimation in brain–machine interfaces," *J. Neural Eng*, vol. 11, no. 016004, p. 016004, 2014.

[13] S. Koyama, S. M. Chase, A. S. Whitford, M. Velliste, A. B. Schwartz, and R. E. Kass, "Comparison of brain–computer interface decoding algorithms in open-loop and closed-loop control," *Journal of computational neuroscience*, vol. 29, no. 1-2, pp. 73–87, 2010.

[14] K. Ganguly and J. M. Carmena, "Emergence of a stable cortical map for neuroprosthetic control," *PLoS biology*, vol. 7, no. 7, p. 1508, 2009.

[15] M. D. Serruya, N. G. Hatsopoulos, L. Paninski, M. R. Fellows, and J. P. Donoghue, "Brain-machine interface: Instant neural control of a movement signal," *Nature*, vol. 416, no. 6877, pp. 141–142, 2002.

[16] D. M. Taylor, S. I. H. Tillery, and A. B. Schwartz, "Direct cortical control of 3d neuroprosthetic devices," *Science*, vol. 296, no. 5574, pp. 1829–1832, 2002.

[17] J. M. Carmena, M. A. Lebedev, R. E. Crist, J. E. O'Doherty, D. M. Santucci, D. F. Dimitrov, P. G. Patil, C. S. Henriquez, and M. A. L. Nicolelis, "Learning

to control a brainmachine interface for reaching and grasping by primates," *PLoS Biol*, vol. 1, no. 2, pp. 193–208, 10 2003.

[18] L. R. Hochberg, M. D. Serruya, G. M. Friehs, J. A. Mukand, M. Saleh, A. H. Caplan, A. Branner, D. Chen, R. D. Penn, and J. P. Donoghue, "Neuronal ensemble control of prosthetic devices by a human with tetraplegia," *Nature*, vol. 442, no. 7099, pp. 164–171, 2006.

[19] J. Simeral, S.-P. Kim, M. Black, J. Donoghue, and L. Hochberg, "Neural control of cursor trajectory and click by a human with tetraplegia 1000 days after implant of an intracortical microelectrode array," *Journal of neural engineering*, vol. 8, no. 2, p. 025027, 2011.

[20] J. L. Collinger, B. Wodlinger, J. E. Downey, W. Wang, E. C. Tyler-Kabara, D. J. Weber, A. J. McMorland, M. Velliste, M. L. Boninger, and A. B. Schwartz, "High-performance neuroprosthetic control by an individual with tetraplegia," *The Lancet*, vol. 381, no. 9866, pp. 557–564, 2013.

[21] K. Brodmann, *Brodmann's: Localisation in the cerebral cortex*. Springer Science & Business Media, 2007.

[22] C. A. Buneo and R. A. Andersen, "The posterior parietal cortex: sensorimotor interface for the planning and online control of visually guided movements," *Neuropsychologia*, vol. 44, no. 13, pp. 2594–2606, 2006.

[23] W. Penfield and E. Boldrey, "Somatic motor and sensory representation in the cerebral cortex of man as studied by electrical stimulation." *Brain: A journal of neurology*, 1937.

[24] W. Penfield and T. Rasmussen, "The cerebral cortex of man; a clinical study of localization of function." 1950.

[25] C. N. Woolsey, P. H. Settlage, D. R. MEYER, W. Sencer, H. T. Pinto, and A. M. Travis, "Patterns of localization in precentral and" supplementary" motor areas and their relation to the concept of a premotor area." *Research publications-Association for Research in Nervous and Mental Disease*, vol. 30, pp. 238–264, 1951.

[26] S. T. Grafton, "The cognitive neuroscience of prehension: recent developments," *Experimental brain research*, vol. 204, no. 4, pp. 475–491, 2010.

[27] M. Davare, A. Kraskov, J. C. Rothwell, and R. N. Lemon, "Interactions between areas of the cortical grasping network," *Current opinion in neurobiology*, vol. 21, no. 4, pp. 565–570, 2011.

[28] L. Turella and A. Lingnau, "Neural correlates of grasping," *Frontiers in human neuroscience*, vol. 8, 2014.

[29] M. Jeannerod, M. A. Arbib, G. Rizzolatti, and H. Sakata, "Grasping ob-

jects: the cortical mechanisms of visuomotor transformation," *Trends in neurosciences*, vol. 18, no. 7, pp. 314–320, 1995.

[30] M. Davare, M. Andres, G. Cosnard, J.-L. Thonnard, and E. Olivier, "Dissociating the role of ventral and dorsal premotor cortex in precision grasping," *The Journal of Neuroscience*, vol. 26, no. 8, pp. 2260–2268, 2006.

[31] A. L. Hodgkin and A. F. Huxley, "A quantitative description of membrane current and its application to conduction and excitation in nerve," *The Journal of physiology*, vol. 117, no. 4, pp. 500–544, 1952.

[32] D. H. Hubel *et al.*, "Tungsten microelectrode for recording from single units," *Science*, vol. 125, no. 3247, pp. 549–550, 1957.

[33] D. H. Hubel, "Single unit activity in striate cortex of unrestrained cats," *The Journal of physiology*, vol. 147, no. 2, pp. 226–238, 1959.

[34] D. H. Hubel and T. N. Wiesel, "Receptive fields of single neurones in the cat's striate cortex," *The Journal of physiology*, vol. 148, no. 3, pp. 574–591, 1959.

[35] M. A. Nicolelis, D. Dimitrov, J. M. Carmena, R. Crist, G. Lehew, J. D. Kralik, and S. P. Wise, "Chronic, multisite, multielectrode recordings in macaque monkeys," *Proceedings of the National Academy of Sciences*, vol. 100, no. 19, pp. 11 041–11 046, 2003.

[36] M. Mollazadeh, V. Aggarwal, A. G. Davidson, A. J. Law, N. V. Thakor, and

M. H. Schieber, "Spatiotemporal variation of multiple neurophysiological signals in the primary motor cortex during dexterous reach-to-grasp movements," *The Journal of Neuroscience*, vol. 31, no. 43, pp. 15 531–15 543, 2011.

[37] M. Saleh, K. Takahashi, Y. Amit, and N. G. Hatsopoulos, "Encoding of coordinated grasp trajectories in primary motor cortex," *The Journal of Neuroscience*, vol. 30, no. 50, pp. 17 079–17 090, 2010.

[38] D. J. Tolhurst, J. A. Movshon, and A. Dean, "The statistical reliability of signals in single neurons in cat and monkey visual cortex," *Vision research*, vol. 23, no. 8, pp. 775–785, 1983.

[39] D. R. Brillinger, "Maximum likelihood analysis of spike trains of interacting nerve cells," *Biological Cybernetics*, vol. 59, no. 3, pp. 189–200, 1988.

[40] W. Truccolo, U. T. Eden, M. R. Fellows, J. P. Donoghue, and E. N. Brown, "A point process framework for relating neural spiking activity to spiking history, neural ensemble, and extrinsic covariate effects," *Journal of neurophysiology*, vol. 93, no. 2, pp. 1074–1089, 2005.

[41] J. W. Pillow, J. Shlens, L. Paninski, A. Sher, A. M. Litke, E. Chichilnisky, and E. P. Simoncelli, "Spatio-temporal correlations and visual signalling in a complete neuronal population," *Nature*, vol. 454, no. 7207, pp. 995–999, 2008.

[42] S. V. Sarma, U. T. Eden, M. L. Cheng, Z. M. Williams, R. Hu, E. Eskandar, and

E. N. Brown, "Using point process models to compare neural spiking activity in the subthalamic nucleus of parkinson's patients and a healthy primate," *IEEE Trans. Biomed. Eng.*, vol. 57, no. 6, pp. 1297–1305, 2010.

[43] E. Stark, R. Drori, I. Asher, Y. Ben-Shaul, and M. Abeles, "Distinct movement parameters are represented by different neurons in the motor cortex," *European Journal of Neuroscience*, vol. 26, no. 4, pp. 1055–1066, 2007.

[44] Q. Fu, D. Flament, J. Coltz, and T. Ebner, "Temporal encoding of movement kinematics in the discharge of primate primary motor and premotor neurons," *J. Neurophysiol.*, vol. 73, no. 2, pp. 836–854, 1995.

[45] L. Paninski, M. R. Fellows, N. G. Hatsopoulos, and J. P. Donoghue, "Spatiotemporal tuning of motor cortical neurons for hand position and velocity," *Journal of neurophysiology*, vol. 91, no. 1, pp. 515–532, 2004.

[46] D. Lee, N. L. Port, W. Kruse, and A. P. Georgopoulos, "Variability and correlated noise in the discharge of neurons in motor and parietal areas of the primate cortex," *The Journal of neuroscience*, vol. 18, no. 3, pp. 1161–1170, 1998.

[47] M. N. Shadlen and W. T. Newsome, "The variable discharge of cortical neurons: implications for connectivity, computation, and information coding," *The Journal of neuroscience*, vol. 18, no. 10, pp. 3870–3896, 1998.

[48] T. M. Pearce and D. W. Moran, "Strategy-dependent encoding of planned arm movements in the dorsal premotor cortex," *Science*, vol. 337, no. 6097, pp. 984–988, 2012.

[49] M. M. Shanechi, R. C. Hu, M. Powers, G. W. Wornell, E. N. Brown, and Z. M. Williams, "Neural population partitioning and a concurrent brain-machine interface for sequential motor function," *Nature neuroscience*, vol. 15, no. 12, pp. 1715–1722, 2012.

[50] V. Aggarwal, S. Acharya, F. Tenore, H.-C. Shin, R. Etienne-Cummings, M. H. Schieber, and N. V. Thakor, "Asynchronous decoding of dexterous finger movements using m1 neurons," *Neural Systems and Rehabilitation Engineering, IEEE Transactions on*, vol. 16, no. 1, pp. 3–14, 2008.

[51] S. Nishimoto, A. T. Vu, T. Naselaris, Y. Benjamini, B. Yu, and J. L. Gallant, "Reconstructing visual experiences from brain activity evoked by natural movies," *Current Biology*, vol. 21, no. 19, pp. 1641–1646, 2011.

[52] M. H. Schieber and A. V. Poliakov, "Partial inactivation of the primary motor cortex hand area: effects on individuated finger movements," *The Journal of neuroscience*, vol. 18, no. 21, pp. 9038–9054, 1998.

[53] P. H. Thakur, A. J. Bastian, and S. S. Hsiao, "Multidigit movement synergies of the human hand in an unconstrained haptic exploration task," *The Journal of neuroscience*, vol. 28, no. 6, pp. 1271–1281, 2008.

[54] I. H. Stevenson, B. M. London, E. R. Oby, N. A. Sachs, J. Reimer, B. Englitz, S. V. David, S. A. Shamma, T. J. Blanche, K. Mizuseki *et al.*, "Functional connectivity and tuning curves in populations of simultaneously recorded neurons," *PLoS computational biology*, vol. 8, no. 11, p. e1002775, 2012.

[55] E. Salinas and L. Abbott, "Vector reconstruction from firing rates," *Journal of computational neuroscience*, vol. 1, no. 1, pp. 89–107, 1994.

[56] M. Velliste, S. Perel, M. C. Spalding, A. S. Whitford, and A. B. Schwartz, "Cortical control of a prosthetic arm for self-feeding," *Nature*, vol. 453, no. 7198, pp. 1098–1101, 2008.

[57] N. Hatsopoulos, J. Joshi, and J. G. O'Leary, "Decoding continuous and discrete motor behaviors using motor and premotor cortical ensembles," *Journal of neurophysiology*, vol. 92, no. 2, pp. 1165–1174, 2004.

[58] A. Brockwell, A. Rojas, and R. Kass, "Recursive bayesian decoding of motor cortical signals by particle filtering," *Journal of Neurophysiology*, vol. 91, no. 4, pp. 1899–1907, 2004.

[59] W. Wu, M. J. Black, D. Mumford, Y. Gao, E. Bienenstock, and J. P. Donoghue, "Modeling and decoding motor cortical activity using a switching kalman filter," *Biomedical Engineering, IEEE Transactions on*, vol. 51, no. 6, pp. 933–942, 2004.

[60] W. Wu, Y. Gao, E. Bienenstock, J. P. Donoghue, and M. J. Black, "Bayesian population decoding of motor cortical activity using a kalman filter," *Neural computation*, vol. 18, no. 1, pp. 80–118, 2006.

[61] M. Hauschild, G. H. Mulliken, I. Fineman, G. E. Loeb, and R. A. Andersen, "Cognitive signals for brain–machine interfaces in posterior parietal cortex include continuous 3d trajectory commands," *Proceedings of the National Academy of Sciences*, vol. 109, no. 42, pp. 17 075–17 080, 2012.

[62] U. Eden, L. Frank, R. Barbieri, V. Solo, and E. Brown, "Dynamic analysis of neural encoding by point process adaptive filtering," *Neural Computation*, vol. 16, no. 5, pp. 971–998, 2004.

[63] S. Koyama, U. T. Eden, E. N. Brown, and R. E. Kass, "Bayesian decoding of neural spike trains," *Annals of the Institute of Statistical Mathematics*, vol. 62, no. 1, pp. 37–59, 2010.

[64] K. Xu, Y. Wang, F. Wang, Y. Liao, Q. Zhang, H. Li, and X. Zheng, "Neural decoding using a parallel sequential monte carlo method on point processes with ensemble effect," *Biomed Res. Int.*, vol. 2014, 2014.

[65] E. Maynard, N. Hatsopoulos, C. Ojakangas, B. Acuna, J. Sanes, R. Normann, and J. Donoghue, "Neuronal interactions improve cortical population coding of movement direction," *The journal of Neuroscience*, vol. 19, no. 18, pp. 8083–8093, 1999.

[66] B. B. Averbeck and D. Lee, "Neural noise and movement-related codes in the macaque supplementary motor area," *The Journal of neuroscience*, vol. 23, no. 20, pp. 7630–7641, 2003.

[67] K. V. Shenoy, D. Meeker, S. Cao, S. A. Kureshi, B. Pesaran, C. A. Buneo, A. P. Batista, P. P. Mitra, J. W. Burdick, and R. A. Andersen, "Neural prosthetic control signals from plan activity," *Neuroreport*, vol. 14, no. 4, pp. 591–596, 2003.

[68] G. Santhanam, S. I. Ryu, M. Y. Byron, A. Afshar, and K. V. Shenoy, "A high-performance brain–computer interface," *nature*, vol. 442, no. 7099, pp. 195–198, 2006.

[69] E. Stark and M. Abeles, "Predicting movement from multiunit activity," *The Journal of neuroscience*, vol. 27, no. 31, pp. 8387–8394, 2007.

[70] J. P. Cunningham, M. Y. Byron, V. Gilja, S. I. Ryu, and K. V. Shenoy, "Toward optimal target placement for neural prosthetic devices," *Journal of neurophysiology*, vol. 100, no. 6, pp. 3445–3457, 2008.

[71] J. Rickert, A. Riehle, A. Aertsen, S. Rotter, and M. P. Nawrot, "Dynamic encoding of movement direction in motor cortical neurons," *The Journal of Neuroscience*, vol. 29, no. 44, pp. 13 870–13 882, 2009.

[72] R. A. Andersen, G. K. Essick, and R. M. Siegel, "Encoding of spatial location by posterior parietal neurons," *Science*, vol. 230, no. 4724, pp. 456–458, 1985.

[73] S. Musallam, B. Corneil, B. Greger, H. Scherberger, and R. Andersen, "Cognitive control signals for neural prosthetics," *Science*, vol. 305, no. 5681, pp. 258–262, 2004.

[74] G. H. Mulliken, S. Musallam, and R. A. Andersen, "Decoding trajectories from posterior parietal cortex ensembles," *the Journal of Neuroscience*, vol. 28, no. 48, pp. 12 913–12 926, 2008.

[75] M. D. Golub, M. Y. Byron, A. B. Schwartz, and S. M. Chase, "Motor cortical control of movement speed with implications for brain-machine interface control," *Journal of neurophysiology*, vol. 112, no. 2, pp. 411–429, 2014.

[76] C. Kemere, K. V. Shenoy, and T. H. Meng, "Model-based neural decoding of reaching movements: a maximum likelihood approach," *Biomedical Engineering, IEEE Transactions on*, vol. 51, no. 6, pp. 925–932, 2004.

[77] L. Srinivasan, U. T. Eden, S. K. Mitter, and E. N. Brown, "General-purpose filter design for neural prosthetic devices," *Journal of neurophysiology*, vol. 98, no. 4, pp. 2456–2475, 2007.

[78] B. Yu, C. Kemere, G. Santhanam, A. Afshar, S. Ryu, T. Meng, M. Sahani, and

K. Shenoy, "Mixture of trajectory models for neural decoding of goal-directed movements." *Journal of neurophysiology*, vol. 97, no. 5, pp. 3763–3780, 2007.

[79] M. M. Shanechi, Z. M. Williams, G. W. Wornell, R. C. Hu, M. Powers, and E. N. Brown, "A real-time brain-machine interface combining motor target and trajectory intent using an optimal feedback control design," *PloS one*, vol. 8, no. 4, p. e59049, 2013.

[80] D. P. McMullen, G. Hotson, K. D. Katyal, B. Wester, M. S. Fifer, T. G. McGee, A. Harris, M. S. Johannes, R. J. Vogelstein, A. D. Ravitz *et al.*, "Demonstration of a semi-autonomous hybrid brain–machine interface using human intracranial eeg, eye tracking, and computer vision to control a robotic upper limb prosthetic," *Neural Systems and Rehabilitation Engineering, IEEE Transactions on*, vol. 22, no. 4, pp. 784–796, 2014.

[81] M. H. Schieber, "Individuated finger movements of rhesus monkeys: a means of quantifying the independence of the digits," *Journal of neurophysiology*, vol. 65, no. 6, pp. 1381–1391, 1991.

[82] V. Aggarwal, M. Mollazadeh, A. G. Davidson, M. H. Schieber, and N. V. Thakor, "State-based decoding of hand and finger kinematics using neuronal ensemble and lfp activity during dexterous reach-to-grasp movements," *Journal of neurophysiology*, vol. 109, no. 12, pp. 3067–3081, 2013.

[83] R. Vinjamuri, D. J. Weber, Z.-H. Mao, J. L. Collinger, A. D. Degenhart, J. W.

Kelly, M. L. Boninger, E. C. Tyler-Kabara, and W. Wang, "Toward synergy-based brain-machine interfaces," *Information Technology in Biomedicine, IEEE Transactions on*, vol. 15, no. 5, pp. 726–736, 2011.

[84] M. Mollazadeh, V. Aggarwal, N. V. Thakor, and M. H. Schieber, "Principal components of hand kinematics and neurophysiological signals in motor cortex during reach to grasp movements," *Journal of neurophysiology*, vol. 112, no. 8, pp. 1857–1870, 2014.

[85] R. Vinjamuri, V. Patel, M. Powell, Z.-H. Mao, and N. Crone, "Candidates for synergies: linear discriminants versus principal components," *Computational intelligence and neuroscience*, vol. 2014, p. 9, 2014.

[86] L. R. Hochberg, D. Bacher, B. Jarosiewicz, N. Y. Masse, J. D. Simeral, J. Vogel, S. Haddadin, J. Liu, S. S. Cash, P. van der Smagt *et al.*, "Reach and grasp by people with tetraplegia using a neurally controlled robotic arm," *Nature*, vol. 485, no. 7398, pp. 372–375, 2012.

[87] B. R. Townsend, E. Subasi, and H. Scherberger, "Grasp movement decoding from premotor and parietal cortex," *The Journal of Neuroscience*, vol. 31, no. 40, pp. 14 386–14 398, 2011.

[88] S. Schaffelhofer, A. Agudelo-Toro, and H. Scherberger, "Decoding a wide range of hand configurations from macaque motor, premotor, and parietal cortices," *The Journal of Neuroscience*, vol. 35, no. 3, pp. 1068–1081, 2015.

[89] J. Carpaneto, M. Umilta, L. Fogassi, A. Murata, V. Gallese, S. Micera, and V. Raos, "Decoding the activity of grasping neurons recorded from the ventral premotor area f5 of the macaque monkey," *Neuroscience*, vol. 188, pp. 80–94, 2011.

[90] J. Carpaneto, V. Raos, M. A. Umiltà, L. Fogassi, A. Murata, V. Gallese, S. Micera, W. Zhang, J. Johnston, M. Ross *et al.*, "Continuous decoding of grasping tasks for a prospective implantable cortical neuroprosthesis," *Journal of neuroengineering and rehabilitation*, vol. 9, no. 1, p. 84, 2012.

[91] Y. Hao, Q. Zhang, M. Controzzi, C. Cipriani, Y. Li, J. Li, S. Zhang, Y. Wang, W. Chen, M. C. Carrozza *et al.*, "Distinct neural patterns enable grasp types decoding in monkey dorsal premotor cortex," *Journal of neural engineering*, vol. 11, no. 6, p. 066011, 2014.

[92] H.-C. Shin, V. Aggarwal, S. Acharya, M. H. Schieber, and N. V. Thakor, "Neural decoding of finger movements using skellam-based maximum-likelihood decoding," *Biomedical Engineering, IEEE Transactions on*, vol. 57, no. 3, pp. 754–760, 2010.

[93] C. E. Vargas-Irwin, G. Shakhnarovich, P. Yadollahpour, J. M. Mislow, M. J. Black, and J. P. Donoghue, "Decoding complete reach and grasp actions from local primary motor cortex populations," *J. Neurosci.*, vol. 30, no. 29, pp. 9659–9669, 2010.

[94] A. K. Bansal, W. Truccolo, C. E. Vargas-Irwin, and J. P. Donoghue, "Decoding 3d reach and grasp from hybrid signals in motor and premotor cortices: spikes, multiunit activity, and local field potentials," *Journal of neurophysiology*, vol. 107, no. 5, pp. 1337–1355, 2012.

[95] D. N. Hill, S. B. Mehta, and D. Kleinfeld, "Quality metrics to accompany spike sorting of extracellular signals," *J. Neurosci.*, vol. 31, no. 24, pp. 8699–8705, 2011.

[96] R. Shadmehr and J. W. Krakauer, "A computational neuroanatomy for motor control," *Experimental Brain Research*, vol. 185, no. 3, pp. 359–381, 2008.

[97] M. Weinrich and S. P. Wise, "The premotor cortex of the monkey," *The Journal of Neuroscience*, vol. 2, no. 9, pp. 1329–1345, 1982.

[98] M. M. Churchland, M. Y. Byron, S. I. Ryu, G. Santhanam, and K. V. Shenoy, "Neural variability in premotor cortex provides a signature of motor preparation," *The Journal of neuroscience*, vol. 26, no. 14, pp. 3697–3712, 2006.

[99] D. A. Crowe, B. B. Averbeck, and M. V. Chafee, "Rapid sequences of population activity patterns dynamically encode task-critical spatial information in parietal cortex," *The Journal of Neuroscience*, vol. 30, no. 35, pp. 11 640–11 653, 2010.

[100] S. L. Brown, J. Joseph, and M. Stopfer, "Encoding a temporally structured

stimulus with a temporally structured neural representation," *Nature neuroscience*, vol. 8, no. 11, pp. 1568–1576, 2005.

[101] E. Seidemann, I. Meilijson, M. Abeles, H. Bergman, and E. Vaadia, "Simultaneously recorded single units in the frontal cortex go through sequences of discrete and stable states in monkeys performing a delayed localization task," *Journal of Neuroscience*, vol. 16, no. 2, pp. 752–768, 1996.

[102] J. Ashe and A. P. Georgopoulos, "Movement parameters and neural activity in motor cortex and area 5," *Cerebral Cortex*, vol. 4, no. 6, pp. 590–600, 1994.

[103] D. W. Moran and A. B. Schwartz, "Motor cortical representation of speed and direction during reaching," *Journal of Neurophysiology*, vol. 82, no. 5, pp. 2676–2692, 1999.

[104] M. M. Churchland and K. V. Shenoy, "Temporal complexity and heterogeneity of single-neuron activity in premotor and motor cortex," *Journal of neurophysiology*, vol. 97, no. 6, pp. 4235–4257, 2007.

[105] C. Kemere, G. Santhanam, M. Y. Byron, A. Afshar, S. I. Ryu, T. H. Meng, and K. V. Shenoy, "Detecting neural-state transitions using hidden markov models for motor cortical prostheses," *Journal of neurophysiology*, vol. 100, no. 4, pp. 2441–2452, 2008.

[106] X. Kang, S. V. Sarma, S. Santaniello, M. H. Schieber, and N. V. Thakor, "Task-

independent cognitive state transition detection from cortical neurons during 3d reach-to-grasp movements," *IEEE Trans. Neural Syst. Rehabil. Eng*, vol. 23, no. 4, pp. 672–682.

[107] T. Ball, A. Schulze-Bonhage, A. Aertsen, and C. Mehring, "Differential representation of arm movement direction in relation to cortical anatomy and function," *Journal of neural engineering*, vol. 6, no. 1, p. 016006, 2009.

[108] B. Yu, J. Cunningham, G. Santhanam, S. Ryu, K. Shenoy, and M. Sahani, "Gaussian-process factor analysis for low-dimensional single-trial analysis of neural population activity." *Journal of neurophysiology*, vol. 102, no. 1, pp. 614–635, 2009.

[109] B. R. Cowley, M. T. Kaufman, Z. S. Butler, M. M. Churchland, S. I. Ryu, K. V. Shenoy, and M. Y. Byron, "Datahigh: Graphical user interface for visualizing and interacting with high-dimensional neural activity," *Journal of neural engineering*, vol. 10, no. 6, p. 066012, 2013.

[110] J. B. Kruskal, "Multidimensional scaling by optimizing goodness of fit to a nonmetric hypothesis," *Psychometrika*, vol. 29, no. 1, pp. 1–27, 1964.

[111] J. P. Cunningham and M. Y. Byron, "Dimensionality reduction for large-scale neural recordings," *Nature neuroscience*, 2014.

[112] J. Friedman, T. Hastie, and R. Tibshirani, *The elements of statistical learning*. Springer series in statistics Springer, Berlin, 2001, vol. 1.

[113] J. King and S. Dehaene, "Characterizing the dynamics of mental representations: the temporal generalization method," *Trends in cognitive sciences*, vol. 18, no. 4, pp. 203–210, 2014.

[114] M. M. Churchland, J. P. Cunningham, M. T. Kaufman, J. D. Foster, P. Nuyujukian, S. I. Ryu, and K. V. Shenoy, "Neural population dynamics during reaching," *Nature*, vol. 487, no. 7405, pp. 51–56, 2012.

[115] J. C. Kao, P. Nuyujukian, S. I. Ryu, M. M. Churchland, J. P. Cunningham, and K. V. Shenoy, "Single-trial dynamics of motor cortex and their applications to brain-machine interfaces," *Nature communications*, vol. 6, 2015.

[116] C. E. Vargas-Irwin, D. M. Brandman, J. B. Zimmermann, J. P. Donoghue, and M. J. Black, "Spike train similarity space (ssims): A framework for single neuron and ensemble data analysis," 2014.

[117] A. G. Rouse and M. H. Schieber, "Spatiotemporal distribution of location and object effects in reach-to-grasp kinematics," *Journal of neurophysiology*, pp. jn–00 686, 2015.

[118] K. D. Harris, "Neural signatures of cell assembly organization," *Nature Reviews Neuroscience*, vol. 6, no. 5, pp. 399–407, 2005.

[119] E. Pastalkova, V. Itskov, A. Amarasingham, and G. Buzsáki, "Internally generated cell assembly sequences in the rat hippocampus," *Science*, vol. 321, no. 5894, pp. 1322–1327, 2008.

[120] D. R. Euston, M. Tatsuno, and B. L. McNaughton, "Fast-forward playback of recent memory sequences in prefrontal cortex during sleep," *science*, vol. 318, no. 5853, pp. 1147–1150, 2007.

[121] S. Fujisawa, A. Amarasingham, M. T. Harrison, and G. Buzsáki, "Behavior-dependent short-term assembly dynamics in the medial prefrontal cortex," *Nature neuroscience*, vol. 11, no. 7, pp. 823–833, 2008.

[122] C. D. Harvey, P. Coen, and D. W. Tank, "Choice-specific sequences in parietal cortex during a virtual-navigation decision task," *Nature*, vol. 484, no. 7392, pp. 62–68, 2012.

[123] D. O. Hebb, *The organization of behavior: A neuropsychological approach*. John Wiley & Sons, 1949.

[124] K. D. Harris, J. Csicsvari, H. Hirase, G. Dragoi, and G. Buzsáki, "Organization of cell assemblies in the hippocampus," *Nature*, vol. 424, no. 6948, pp. 552–556, 2003.

[125] G. Buzsáki, "Neural syntax: cell assemblies, synapsembles, and readers," *Neuron*, vol. 68, no. 3, pp. 362–385, 2010.

[126] M. D. Humphries, "Spike-train communities: finding groups of similar spike trains," *The Journal of Neuroscience*, vol. 31, no. 6, pp. 2321–2336, 2011.

[127] M. Shimono and J. M. Beggs, "Functional clusters, hubs, and communities in the cortical microconnectome," *Cerebral Cortex*, p. bhu252, 2014.

[128] J.-M. Fellous, P. H. Tiesinga, P. J. Thomas, and T. J. Sejnowski, "Discovering spike patterns in neuronal responses," *The Journal of Neuroscience*, vol. 24, no. 12, pp. 2989–3001, 2004.

[129] R. Paz, C. Natan, T. Boraud, H. Bergman, and E. Vaadia, "Emerging patterns of neuronal responses in supplementary and primary motor areas during sensorimotor adaptation," *The Journal of neuroscience*, vol. 25, no. 47, pp. 10 941–10 951, 2005.

[130] A. Peyrache, K. Benchenane, M. Khamassi, S. I. Wiener, and F. P. Battaglia, "Principal component analysis of ensemble recordings reveals cell assemblies at high temporal resolution," *Journal of computational neuroscience*, vol. 29, no. 1-2, pp. 309–325, 2010.

[131] V. Lopes-dos Santos, S. Conde-Ocazionez, M. A. Nicolelis, S. T. Ribeiro, and A. B. Tort, "Neuronal assembly detection and cell membership specification by principal component analysis," *PLoS One*, vol. 6, no. 6, p. e20996, 2011.

[132] V. Lopes-dos Santos, S. Ribeiro, and A. B. Tort, "Detecting cell assemblies in

large neuronal populations," *Journal of neuroscience methods*, vol. 220, no. 2, pp. 149–166, 2013.

[133] Y. N. Billeh, M. T. Schaub, C. A. Anastassiou, M. Barahona, and C. Koch, "Revealing cell assemblies at multiple levels of granularity," *Journal of neuroscience methods*, vol. 236, pp. 92–106, 2014.

[134] C. Mason, J. Gomez, and T. Ebner, "Hand synergies during reach-to-grasp," *Journal of Neurophysiology*, vol. 86, no. 6, pp. 2896–2910, 2001.

[135] M. Santello, M. Flanders, and J. F. Soechting, "Patterns of hand motion during grasping and the influence of sensory guidance," *The Journal of Neuroscience*, vol. 22, no. 4, pp. 1426–1435, 2002.

[136] R. Holdefer and L. Miller, "Primary motor cortical neurons encode functional muscle synergies," *Exp Brain Res*, vol. 146, pp. 233–243, 2002.

[137] A. d'Avella, P. Saltiel, and E. Bizzi, "Combinations of muscle synergies in the construction of a natural motor behavior," *Nature neuroscience*, vol. 6, no. 3, pp. 300–308, 2003.

[138] M. S. Graziano, C. S. Taylor, and T. Moore, "Complex movements evoked by microstimulation of precentral cortex," *Neuron*, vol. 34, no. 5, pp. 841–851, 2002.

[139] M. S. Graziano, T. N. Aflalo, and D. F. Cooke, "Arm movements evoked by

electrical stimulation in the motor cortex of monkeys," *Journal of Neurophysiology*, vol. 94, no. 6, pp. 4209–4223, 2005.

[140] A. V. Poliakov and M. H. Schieber, "Limited functional grouping of neurons in the motor cortex hand area during individuated finger movements: a cluster analysis," *Journal of neurophysiology*, vol. 82, no. 6, pp. 3488–3505, 1999.

[141] T. Brochier, R. L. Spinks, M. A. Umilta, and R. N. Lemon, "Patterns of muscle activity underlying object-specific grasp by the macaque monkey," *Journal of neurophysiology*, vol. 92, no. 3, pp. 1770–1782, 2004.

[142] M. Rigotti, O. Barak, M. R. Warden, X.-J. Wang, N. D. Daw, E. K. Miller, and S. Fusi, "The importance of mixed selectivity in complex cognitive tasks," *Nature*, vol. 497, no. 7451, pp. 585–590, 2013.

[143] L. Paninski, S. Shoham, M. R. Fellows, N. G. Hatsopoulos, and J. P. Donoghue, "Superlinear population encoding of dynamic hand trajectory in primary motor cortex," *The Journal of neuroscience*, vol. 24, no. 39, pp. 8551–8561, 2004.

[144] B. Petreska, M. Y. Byron, J. P. Cunningham, G. Santhanam, S. I. Ryu, K. V. Shenoy, and M. Sahani, "Dynamical segmentation of single trials from population neural data," in *Advances in neural information processing systems*, 2011, pp. 756–764.

[145] A. J. Brockmeier, J. S. Choi, E. G. Kriminger, J. T. Francis, and J. C.

Principe, "Neural decoding with kernel-based metric learning," *Neural computation*, vol. 26, no. 6, pp. 1080–1107, 2014.

[146] D. Arthur and S. Vassilvitskii, "k-means++: The advantages of careful seeding," in *Proceedings of the eighteenth annual ACM-SIAM symposium on Discrete algorithms*. Society for Industrial and Applied Mathematics, 2007, pp. 1027–1035.

[147] S. Schreiber, J. Fellous, D. Whitmer, P. Tiesinga, and T. J. Sejnowski, "A new correlation-based measure of spike timing reliability," *Neurocomputing*, vol. 52, pp. 925–931, 2003.

[148] L. Danon, A. Diaz-Guilera, J. Duch, and A. Arenas, "Comparing community structure identification," *Journal of Statistical Mechanics: Theory and Experiment*, vol. 2005, no. 09, p. P09008, 2005.

[149] S. Fortunato, "Community detection in graphs," *Physics Reports*, vol. 486, no. 3, pp. 75–174, 2010.

[150] T. M. Cover and J. A. Thomas, *Elements of information theory*. John Wiley & Sons, 2012.

[151] P. J. Rousseeuw, "Silhouettes: a graphical aid to the interpretation and validation of cluster analysis," *Journal of computational and applied mathematics*, vol. 20, pp. 53–65, 1987.

[152] R. Tibshirani, G. Walther, and T. Hastie, "Estimating the number of clusters in a data set via the gap statistic," *Journal of the Royal Statistical Society: Series B (Statistical Methodology)*, vol. 63, no. 2, pp. 411–423, 2001.

[153] A. K. Jain, "Data clustering: 50 years beyond k-means," *Pattern recognition letters*, vol. 31, no. 8, pp. 651–666, 2010.

[154] G. I. Newman, V. Aggarwal, M. H. Schieber, and N. V. Thakor, "Identifying neuron communities during a reach and grasp task using an unsupervised clustering analysis," in *Engineering in Medicine and Biology Society, EMBC, 2011 Annual International Conference of the IEEE*. IEEE, 2011, pp. 6401–6404.

[155] M. van Rossum, "A novel spike distance." *Neural computation*, vol. 13, no. 4, p. 751, 2001.

[156] C. Houghton and J. Victor, "Measuring representational distances–the spike-train metrics approach," *Visual Population Codes–Toward a Common Multivariate Framework for Cell Recording and Functional Imaging*, pp. 391–416, 2010.

[157] A. R. Paiva, I. Park, and J. C. Príncipe, "A comparison of binless spike train measures," *Neural Computing and Applications*, vol. 19, no. 3, pp. 405–419, 2010.

[158] D. Chicharro, T. Kreuz, and R. G. Andrzejak, "What can spike train distances

tell us about the neural code?" *Journal of neuroscience methods*, vol. 199, no. 1, pp. 146–165, 2011.

[159] I. M. Park, S. Seth, A. Paiva, L. Li, and J. Principe, "Kernel methods on spike train space for neuroscience: A tutorial," *Signal Processing Magazine, IEEE*, vol. 30, no. 4, pp. 149–160, 2013.

[160] J. D. Victor and K. P. Purpura, "Nature and precision of temporal coding in visual cortex: a metric-space analysis," *Journal of neurophysiology*, vol. 76, no. 2, pp. 1310–1326, 1996.

[161] J. D. Victor and K. P. Purpura, "Metric-space analysis of spike trains: theory, algorithms and application," *Network: computation in neural systems*, vol. 8, no. 2, pp. 127–164, 1997.

[162] D. Aronov, "Fast algorithm for the metric-space analysis of simultaneous responses of multiple single neurons," *Journal of neuroscience methods*, vol. 124, no. 2, pp. 175–179, 2003.

[163] S. Feldt, J. Waddell, V. Hetrick, J. Berke, and M. Żochowski, "Functional clustering algorithm for the analysis of dynamic network data," *Physical Review E*, vol. 79, no. 5, p. 056104, 2009.

[164] A. Y. Ng, M. I. Jordan, Y. Weiss *et al.*, "On spectral clustering: Analysis and

an algorithm," *Advances in neural information processing systems*, vol. 2, pp. 849–856, 2002.

[165] S. White and P. Smyth, "A spectral clustering approach to finding communities in graph." in *SDM*, vol. 5. SIAM, 2005, pp. 76–84.

[166] U. Von Luxburg, "A tutorial on spectral clustering," *Statistics and computing*, vol. 17, no. 4, pp. 395–416, 2007.

[167] M. E. Newman, "Fast algorithm for detecting community structure in networks," *Physical review E*, vol. 69, no. 6, p. 066133, 2004.

[168] M. E. Newman and M. Girvan, "Finding and evaluating community structure in networks," *Physical review E*, vol. 69, no. 2, p. 026113, 2004.

[169] J. C. Sanchez, J. M. Carmena, M. Lebedev, M. A. Nicolelis, J. G. Harris, J. C. Principe *et al.*, "Ascertaining the importance of neurons to develop better brain-machine interfaces," *Biomedical Engineering, IEEE Transactions on*, vol. 51, no. 6, pp. 943–953, 2004.

[170] R. Wahnoun, J. He, and S. I. H. Tillery, "Selection and parameterization of cortical neurons for neuroprosthetic control," *Journal of neural engineering*, vol. 3, no. 2, p. 162, 2006.

[171] G. Singhal, V. Aggarwal, S. Acharya, J. Aguayo, J. He, and N. Thakor, "Ensemble fractional sensitivity: a quantitative approach to neuron selection for

decoding motor tasks," *Computational intelligence and neuroscience*, vol. 2010, p. 6, 2010.

[172] K. Kahn, M. Sheiber, N. Thakor, and S. V. Sarma, "Neuron selection for decoding dexterous finger movements," in *Engineering in Medicine and Biology Society, EMBC, 2011 Annual International Conference of the IEEE*. IEEE, 2011, pp. 4605–4608.

[173] H.-N. Kim, Y.-H. Kim, H.-C. Shin, V. Aggarwal, M. H. Schieber, and N. V. Thakor, "Neuron selection by relative importance for neural decoding of dexterous finger prosthesis control application," *Biomedical signal processing and control*, vol. 7, no. 6, pp. 632–639, 2012.

[174] K. Xu, Y. Wang, Y. Wang, F. Wang, Y. Hao, S. Zhang, Q. Zhang, W. Chen, and X. Zheng, "Local-learning-based neuron selection for grasping gesture prediction in motor brain machine interfaces," *Journal of Neural Engineering*, vol. 10, no. 2, pp. 26 008–26 020, 2013.

[175] K. Kahn, S. Saxena, E. Eskandar, N. Thakor, M. Schieber, J. T. Gale, B. Averbeck, U. Eden, and S. V. Sarma, "A systematic approach to selecting task relevant neurons," *Journal of neuroscience methods*, vol. 245, pp. 156–168, 2015.

[176] J. H. Friedman, "On bias, variance, 0/1loss, and the curse-of-dimensionality," *Data mining and knowledge discovery*, vol. 1, no. 1, pp. 55–77, 1997.

[177] I. Guyon and A. Elisseeff, "An introduction to variable and feature selection," *The Journal of Machine Learning Research*, vol. 3, pp. 1157–1182, 2003.

[178] J. Kalaska, "From intention to action: Motor cortex and the control of reaching movements," in *Progress in Motor Control*, ser. Advances in Experimental Medicine and Biology. Springer US, 2009, vol. 629, pp. 139–178.

[179] A. P. Georgopoulos, G. Pellizzer, A. V. Poliakov, and M. H. Schieber, "Neural coding of finger and wrist movements," *J. Comput. Neurosci.*, vol. 6, no. 3, pp. 279–288, 1999.

[180] D. H. Perkel, G. L. Gerstein, and G. P. Moore, "Neuronal spike trains and stochastic point processes: Ii. simultaneous spike trains," *Biophys. J.*, vol. 7, no. 4, pp. 419–440, 1967.

[181] A. Aertsen, G. Gerstein, M. Habib, and G. Palm, "Dynamics of neuronal firing correlation: modulation of "effective connectivity"," *J. Neurophysiol.*, vol. 61, no. 5, pp. 900–917, 1989.

[182] R. Kelly, M. Smith, R. Kass, and T. S. Lee, "Accounting for network effects in neuronal responses using l1 regularized point process models," in *Advances in neural information processing systems*, 2010, pp. 1099–1107.

[183] M. Okatan, M. A. Wilson, and E. N. Brown, "Analyzing functional connectivity

using a network likelihood model of ensemble neural spiking activity," *Neural computation*, vol. 17, no. 9, pp. 1927–1961, 2005.

[184] D. F. Putrino, Z. Chen, S. Ghosh, and E. N. Brown, "Motor cortical networks for skilled movements have dynamic properties that are related to accurate reaching," *Neural Plast.*, vol. 2011, 2011.

[185] E. Schneidman, M. J. Berry, R. Segev, and W. Bialek, "Weak pairwise correlations imply strongly correlated network states in a neural population," *Nature*, vol. 440, no. 7087, pp. 1007–1012, 2006.

[186] I. H. Stevenson, J. M. Rebesco, N. G. Hatsopoulos, Z. Haga, L. E. Miller, and K. P. Kording, "Bayesian inference of functional connectivity and network structure from spikes," *Neural Systems and Rehabilitation Engineering, IEEE Transactions on*, vol. 17, no. 3, pp. 203–213, 2009.

[187] W. Truccolo, L. R. Hochberg, and J. P. Donoghue, "Collective dynamics in human and monkey sensorimotor cortex: predicting single neuron spikes," *Nature neuroscience*, vol. 13, no. 1, pp. 105–111, 2009.

[188] F. Gerhard, G. Pipa, B. Lima, S. Neuenschwander, and W. Gerstner, "Extraction of network topology from multi-electrode recordings: is there a small-world effect?" *Frontiers in Computational Neuroscience*, vol. 5, p. 4, 2011.

[189] A. Riehle, S. Grün, M. Diesmann, and A. Aertsen, "Spike synchronization and

rate modulation differentially involved in motor cortical function," *Science*, vol. 278, no. 5345, pp. 1950–1953, 1997.

[190] N. G. Hatsopoulos, C. L. Ojakangas, L. Paninski, and J. P. Donoghue, "Information about movement direction obtained from synchronous activity of motor cortical neurons," *Proceedings of the National Academy of Sciences*, vol. 95, no. 26, pp. 15 706–15 711, 1998.

[191] E. Vaadia, I. Haalman, M. Abeles, H. Bergman, Y. Prut, H. Slovin, and A. Aertsen, "Dynamics of neuronal interactions in monkey cortex in relation to behavioural events," *Nature*, vol. 373, no. 6514, pp. 515–518, 1995.

[192] S. Baker, R. Spinks, A. Jackson, and R. Lemon, "Synchronization in monkey motor cortex during a precision grip task. i. task-dependent modulation in single-unit synchrony," *J. Neurophysiol.*, vol. 85, no. 2, pp. 869–885, 2001.

[193] M. R. Cohen and W. T. Newsome, "Context-dependent changes in functional circuitry in visual area mt," *Neuron*, vol. 60, no. 1, pp. 162–173, 2008.

[194] E. Stark, A. Globerson, I. Asher, and M. Abeles, "Correlations between groups of premotor neurons carry information about prehension," *J. Neurosci.*, vol. 28, no. 42, pp. 10 618–10 630, 2008.

[195] N. G. Hatsopoulos, L. Paninski, and J. P. Donoghue, "Sequential movement

representations based on correlated neuronal activity," *Exp. Brain Res.*, vol. 149, no. 4, pp. 478–486, 2003.

[196] M. Zhao, A. Batista, J. P. Cunningham, C. Chestek, Z. Rivera-Alvidrez, R. Kalmar, S. Ryu, K. Shenoy, and S. Iyengar, "An l 1-regularized logistic model for detecting short-term neuronal interactions," *Journal of computational neuroscience*, vol. 32, no. 3, pp. 479–497, 2012.

[197] Z. Chen, D. F. Putrino, S. Ghosh, R. Barbieri, and E. N. Brown, "Statistical inference for assessing functional connectivity of neuronal ensembles with sparse spiking data," *Neural Systems and Rehabilitation Engineering, IEEE Transactions on*, vol. 19, no. 2, pp. 121–135, 2011.

[198] P. McCullagh and J. A. Nelder, *Generalized Linear Models*, 2nd ed. Boca Raton, FL: Chapman & Hall/CRC, 1989.

[199] L. Paninski, "Maximum likelihood estimation of cascade point-process neural encoding models," *Network: Computation in Neural Systems*, vol. 15, no. 4, pp. 243–262, 2004.

[200] R. Kass and V. Ventura, "A spike-train probability model," *Neural Comput.*, vol. 13, no. 8, pp. 1713–1720, 2001.

[201] S. G. Alsing, K. W. Bauer Jr, and J. O. Miller, "A multinomial selection pro-

cedure for evaluating pattern recognition algorithms," *Pattern Recogn.*, vol. 35, no. 11, pp. 2397–2412, 2002.

[202] L. I. Kuncheva, *Combining pattern classifiers: methods and algorithms.* John Wiley & Sons, 2004.

[203] C. E. Vargas-Irwin, L. Franquemont, M. J. Black, and J. P. Donoghue, "Linking objects to actions: Encoding of target object and grasping strategy in primate ventral premotor cortex," *J. Neurosci.*, vol. 35, no. 30, pp. 10 888–10 897, 2015.

[204] M. Velliste, S. D. Kennedy, A. B. Schwartz, A. S. Whitford, J.-W. Sohn, and A. J. McMorland, "Motor cortical correlates of arm resting in the context of a reaching task and implications for prosthetic control," *The Journal of Neuroscience*, vol. 34, no. 17, pp. 6011–6022, 2014.

[205] L. R. Rabiner, "A tutorial on hidden markov models and selected applications in speech recognition," *Proceedings of the IEEE*, vol. 77, no. 2, pp. 257–286, 1989.

[206] Y. Bar-Shalom, X. R. Li, and T. Kirubarajan, *Estimation with applications to tracking and navigation: theory algorithms and software.* John Wiley & Sons, 2004.

Vita

Ryan J. Smith was born in 1984 in Niceville, Florida. Ryan attended Niceville High School where he was named a National Merit Scholar and graduated as valedictorian. In 2002 he joined the University of Florida where he was a member of the inaugural class of Lombardi Scholars. He received a B.S. in Electrical Engineering from the University of Florida in 2006. In 2007 he enrolled with Johns Hopkins University and subsequently received a M.S.E. in Biomedical Engineering in 2009. He matriculated into the Ph.D. program in Biomedical Engineering at Johns Hopkins University that same year.

In March 2016, Ryan will join McKinsey & Company in Boston, MA as a data scientist on the People Insights team in the Organizational Solutions group.